Engineering Nanotechnologies to Improve Immune Responses to Cancer Vaccines

By

Carcia S. Carson

Dissertation

Submitted to the Faculty of the

Graduate School of Vanderbilt University

in partial fulfillment of the requirements

for the degree of

DOCTOR OF PHILOSOPHY

in

Biomedical Engineering

May 13, 2022

Nashville, Tennessee

Approved:

John T. Wilson, Ph.D.

Craig L. Duvall, Ph.D.

Marjan Rafat, Ph.D.

Michael R. King, Ph.D.

Justin M. Balko, Pharm.D., Ph.D.

DEDICATION

This work is dedicated to my late grandmother, Mary Lucille Wade. Even though she did not have formal education beyond the 8th grade, she never stopped sharing her wisdom and praying for my prosperity in education.

ACKNOWLEDGEMENTS

This journey in graduate school has been an enlightening, challenging, and enriching experience and it would not have been possible without the support and guidance from a multitude of people. First, I would like to thank my Lord and Savior, Jesus Christ, for giving me life, purpose, favor, and strength to see this journey to the end. I count this victory as a testimony to Your greatness.

None of this could have been possible without the love of my family. To my parents and long-standing supporters, Nicole and Chris Coleman. I can't even begin to express the depth of my gratitude for your unwavering support, unconditional love, and countless sacrifices. Thank you for providing all of my needs and most of my wants and giving me the best life possible. I am blessed to have two fathers and so would also like to thank my dad, Daryl Carson for your support. I also want to thank both sides of my extended family for their love and support, especially my Aunt Bunny and Aunt Neicey. You both have always believed in me, cheered me on, and prayed for my success in life. Thank you to my sisters, Bri Lewis and Crissi Coleman, for always being my ride-or-die and for the countless heart-to-heart conversations that gave me the strength to get through each day. I love you both deeply. Thank you to my best friend, confidante and hype-man, Dr. Kevin Santiago. You always can calm me down in my moments of stress and your unwavering love has given me the strength to see this work through.

To my advisor, Dr. John T. Wilson, thank you for being an exceptional mentor. I truly admire your passion for science, dedication to the Immunoengineering Lab, and tireless effort to secure funding to maintain the lab. I would not be the scientist I am today without your patience, guidance, motivation, and immense knowledge. I am also thankful to my committee members, Professors Dr. Craig Duvall, Dr. Marjan Rafat, Dr. Michael King, and Dr. Justin Balko, for lending their expertise and challenging me to become a better scientist.

I would like to thank past and present members of the Wilson lab: Dr. Sema Sevimli, Dr. Dan Shae, Dr. Max Jacobson, Dr. Frances Knight, Kyle Becker, Dr. Kyle Garland, Christian Palmer, Dr. Moe Wehbe, Dr. Lihong Bishop, Jessalyn Baljon, Lucinda Pastora, Taylor Sheehy, Dr. Karan Arora, Hayden Pagendarm, Payton Stone, Dr. Youn Jae Jung, Dr. Blaise Kimmel, and honorary lab member Bonnie Walton. Each of you played a vital role in my academic success and helping maintain a supportive and enjoyable working environment. To my undergraduate mentee,

Lorena Cruz, it has been a pleasure being your mentor and a privilege to be a small part of your early research career.

I would like to thank the Fisk-Vanderbilt Masters-to-PhD Program for affording me and many other underrepresented minorities the opportunity to pursue and earn higher level degrees. There were many in the Bridge program who took a great deal of time to mentor and educate me, particularly, I would like to thank Dr. Dina Stroud. Your belief in me as evidenced by your mentorship, advice, support, advocacy, and investment in my personal development as a scientist has helped me in more ways than one.

I would like to thank the many mentors who have supported and guided me throughout my academic career. Thank you, Dr. Quinton Williams, for engaging my curiosity and encouraging me to pursue my dream of becoming a scientist. Thank you, Dr. Julian Vernon, for teaching me how to effectively communicate my research and encouraging me to keep going. Thank you, Dr. Renã Robinson, for the strategy sessions to help map out bringing my PhD to an end and being a great role model. Thank you, Dr. Jamaal James, for taking the time to offer insightful suggestions to strengthen my research.

I am also thankful to the many friends who have supported me during the last six years. Thank you to Sarah Coulter, Brittanie Moore, Dr. ReAnna Roby, and Erica Tross for the love, support, and sister-hood. You ladies made permanent space for me to cry, laugh, and vent which I am forever thankful for. Thanks also to my roommates and frequent house guest, Candace Grisham (and her Mom), Arlene Garcia, AJ Sermarini, Mason Alford, Varun Menon, and Yinan Zheng, for the many laughs and for making my final two years of graduate school fun and exciting (less exciting than our neighbors but nonetheless still exciting!!)

I have a network of supporters, allies, friends, and family that have impacted my life but not enough space to name you all. I do want to honor the prayers, conversations, well-wishes, emails, and messages. I am grateful to you all!

Finally, I would like to acknowledge the National Science Foundation (1445197 and 1937963) and the Vanderbilt Bridge Doctoral Fellowship for the funding of this work. I am especially grateful to be a recipient of the National Science Foundation Graduate Research Fellowship.

TABLE OF CONTENTS

Page

LIST OF TABLES

LIST OF FIGURES

Figure Page

CHAPTER 1

Introduction

1.1 Background and Significance

Despite efforts devoted to reducing the cancer burden, it remains one of the leading causes of deaths worldwide with an estimated 1.9 million new cancer cases and over 600,000 cancer related deaths this year in the US alone.[1] While conventional treatments have contributed to the overall decline of cancer related deaths, the rate of recurrence of many cancer types remains high and the number of new cancer cases diagnosed per year is expected to rise. To reduce the risk of cancer recurrence as well as improve the overall outcome of treatments, researchers are now turning to cancer immunotherapies. The main types of immunotherapies used to treat cancer include immune checkpoint inhibitors, cytokine therapy, targeted antibodies, adoptive cell transfer, and cancer vaccines.[2] These innovative approaches work by stimulating, altering, and/or amplifying the immune system to promote antitumor immune responses.[3] Thus far, immunotherapies have demonstrated efficacy in a select group of cancers and only a fraction of patients with those cancers have durable responses.[4] So, despite the success of immunotherapies for some cancers, there is a lot of work that needs to be done to improve immunotherapy outcomes.

A critical question thus arises: why do immunotherapies work for some cancer types but not others. Part of the question lies in the immunological composition of the tumor microenvironment (TME). It has been observed in many cases that the survival of patients with various forms of cancer is associated with increased presence of antigen-specific tumor infiltrating lymphocytes.[5-7] Cancer vaccines are a promising treatment strategy with potential to induce $CD8^+$ T cell infiltration in poorly immunogenic tumors (also referred to as “cold” tumors), potentially

converting them to “hot” tumors amenable to immunotherapies. Consequently, vaccine strategies for improving the therapeutic efficacy of immunotherapies will be the focus of this dissertation.

This chapter will provide an overview of cancer immunotherapies, as well as, cancer vaccine strategies that are being investigated to overcome the limitations of clinically relevant immune checkpoint blockade (ICB). It will also highlight the need to optimize cancer vaccine platforms to enhance anti-tumor T cell responses, which can ultimately lead to improved clinical outcomes.

1.1.1 Overview of Cancer Immunotherapy

Cancer is caused by gene mutations that lead to uncontrolled cell division.[8-10] In some cases, tumor cells can invade surrounding tissue and metastasize to other parts of the body, ultimately leading to organ damage, failure, and eventually death.[11] A variety of treatment approaches have been used, which largely rely on a combination of local excision of malignant tissue, regional radiation, and systemically delivered chemotherapeutics, all of which can damage surrounding healthy tissue and cause adverse side-effects. These techniques have also failed to improve local and metastatic tumor control for most types of cancer and many patients will experience tumor recurrence.[12]

To reduce the risk of treatment side-effects and prevent future recurrence as well as improve the overall survival of patients with metastatic cancer, researchers are now turning to the immune system to fight cancer. In principle, the immune system can detect and destroy abnormal cells without affecting normal cells, providing a natural and potentially less toxic way of eliminating cancer.[2,13] However, many tumors have developed strategies that enable them to evade the immune system, such as downregulation or loss of tumor antigens, up upregulation of negative regulatory pathways, altered major histocompatibility complex class I (MHC-I) expression, and

the recruitment of immunosuppressive cell populations, resulting in the abrogation of antitumor immune responses.[14]

Cancer immunotherapies, which were developed based on extensive studies of the mechanisms of immune evasion exploited by cancer cells, manipulate the inefficient or suppressed immune system to overcome the pathways leading to escape, ultimately restoring an effective antitumor immune response.[2] A range of cancer immunotherapy approaches have proven effective in many patients, including cytokine-based therapy, adoptive cell therapy, cancer vaccines, and monoclonal antibodies (i.e., immune checkpoint inhibitors).[3,4] Despite the clinical success of immunotherapies over traditional cancer treatments, these approaches have proven to only be effective in a fraction of patients with only the following cancer types: metastatic melanoma, metastatic Merkel cell carcinoma, small cell lung cancer, non-small cell lung cancer, triple-negative breast cancer, head and neck squamous cell carcinoma, classical Hodgkin's Lymphoma, and metastatic renal cell carcinoma,[15] whereas ICIs demonstrated limited efficacy in patients with pancreatic cancer,[16] prostate cancer,[17] and glioblastoma.[18] This has led to clinical investigations exploring the potential of combining immunotherapies with current clinical therapies in addition to other immunotherapy agents to activate immune responses, decrease immunosuppression, and target signaling and resistance pathways to offer a more durable response compared to single immunotherapy treatment regimens for cancers.[19,20] For example, cytokines such as, interleukin 2 (IL-2) and interferon alpha (IFN-α), have demonstrated clinical benefit and consequently were among the first immunotherapies to receive FDA approval for the treatment of several cancers.[21] Yet, despite clinical benefits, low response rates and severe toxicity impede further applications of these cytokines as monotherapies, and therefore are being investigated clinically in combination with other immunotherapies. Another main treatment modality in immunotherapy is adoptive cell

transfer therapy which broadly works by collecting T cells, genetically modifying them, expanding them *ex vivo*, and then infusing them into cancer patients where they can specifically target and eliminate cancer cells.[22,23] Notably, autologous anti-CD19 chimeric antigen receptor (CAR) T cell therapy is the only FDA approved adoptive cell therapy due to its impressive efficacy and durable responses in patients with mantel cell lymphoma, acute lymphoblastic leukemia, and diffuse large B-cell lymphoma.[24] However, this success is limited in solid tumors, partly due to the immunosuppressive tumor microenvironment (TME) that exhausts CAR T cells, leading to the investigation of combination strategies for improving CAR T cell functions against solid tumors.[22] In preclinical studies, combination therapy of CAR T cells and immune checkpoint inhibitors has improved efficacy compared to each treatment alone in several cancer types, supporting their combinatorial use in clinical studies.[22,25,26]

1.1.2 Immune Checkpoint Blockade in Cancer Therapy

One of the most successful approaches in cancer immunotherapy is the use of immune checkpoint inhibitors (ICIs), which have shown remarkable clinical benefits for many cancer types.[27,28] Immune checkpoints consist of coinhibitory signaling pathways that maintain self-tolerance, yet are often utilized by cancer cells to evade immune surveillance. ICIs are able to restore or augment antitumor immune responses by interrupting coinhibitory signaling pathways and promote immune-mediated elimination of cancer cells. The major inhibitory pathways that have been identified are cytotoxic T-lymphocyte–associated antigen 4 (CTLA-4) pathway and programmed death 1 (PD-1) pathway both which are initiated by ligand-receptor interactions. More specifically, activated DCs express costimulatory molecules, CD80 (B7-1) and CD86 (B7-2), that binds to either CD28 or CTLA-4 co-stimulatory proteins on T cells. CTLA-4 outcompetes CD28 for binding to CD80 and CD86 reducing IL-2 production and T cell activation. PD-1 is

expressed by activated T cells and downmodulates T cell effector functions upon binding to its ligand PD-L1, which is expressed by immune cells and a wide range of tumor cells. Tumor cells utilize these pathways to their advantage by preventing T cell activation ultimately establishing a tumor microenvironment that permits tumor growth. Immune checkpoint inhibitors against CTLA-4 and PD-1 can readily block these inhibitory pathways, thus restoring or augmenting an anti-tumor immune response.[29-31] Inhibition of these pathways led to the approval of several drugs, CTLA-4 inhibitor (ipilimumab), PD-1 inhibitors (pembrolizumab, nivolumab, cemiplimab), and PD-L1 inhibitors (atezolizumab, avelumab, durvalumab).[32] ICIs when administered as a monotherapy or in combination have demonstrated cases of complete tumor regression and improved survival benefits in unresectable and metastatic cancers,[33] with clinical trials reporting an objective response rate of ~50% in metastatic melanoma patients,[34,35] ~20% in non-small cell lung cancer patients,[36,37] and ~18% in metastatic triple negative breast cancer.[38] So, while ICIs have improved clinical outcomes, only a fraction of patients with a select group of cancers exhibit durable responses and complete tumor regression.

A variety of factors contribute to whether a response to ICI will occur. Research indicates that responses in several cancers (i.e., advanced melanoma,[39] non-small cell lung cancer,[40] and metastatic triple negative breast cancer[41]) are in part due to the TME. Patients who respond typically have an immunogenic ("hot") TME that has a high tumor mutation burden, high levels of tumor infiltrating antigen-specific T cells (primarily CD8+ T cells), and increased secretion of interferon gamma (IFN-γ) and other cytokines, while nonresponsive patients have a non-immunogenic ("cold") TME that lack significant T cell infiltration and instead contains high levels of immunosuppressive cells such as tumor associated macrophages (TAMs), myeloid derived suppressor cells (MDSCs), and regulatory T-cells (Tregs) that inhibit T cell activation, infiltration,

and survival.[42] For instance, in cases of checkpoint blockade for metastatic melanoma, multiple groups reported that lymphocyte infiltration correlated with improved survival in patients,[43-45] which are thought to represent a prognostic marker for identifying patients that benefit from checkpoint blockade.[42,46-48] Therefore, the idea of combining ICB with therapies that increase the number of infiltrating tumor-specific T cells has potential for improved outcomes.

1.1.3 Cancer Vaccines for Generating $CD8^+$ T cells

One way to increase the magnitude and breadth of tumor infiltrating antigen-specific T cells is the use of cancer vaccines, which work by stimulating T cells against antigens that derive from tumors (i.e., tumor-associated antigens (TAAs), tumor-specific antigens, or neoantigens).[49] The strength of the antigen-specific T cell response elicited by the vaccine is highly dependent on the nature of the antigens. Early therapeutic vaccines strategies targeting TAAs (i.e., self-antigens that are abnormally expressed by cancer cells) were proven to be unsuccessful in generating an effective antitumor immune response.[50] This is likely due to high-affinity T cells that recognize self-antigens being eliminated from the immune repertoire by central and peripheral tolerance mechanisms. Thus, cancer vaccines using TAAs must be potent enough to activate any remaining low affinity T cells. TAAs can also be expressed in normal tissue to some extent, which increases the risk of vaccine-induced autoimmune toxicities.[51] More recently, advances in whole-exome sequencing have enabled the identification of patient-specific "neoantigens", which arise from mutations that lead to changes in the amino acid sequence of proteins.[52] Identification of these neoantigens lead to the development of personalized vaccines based on peptides, mRNA, DNA, viral vectors, and dendritic cells.[53] Peptide neoantigen vaccines have been the focus in many recent clinical trials due to their translation advantages, including safety, modest cost, and rapid manufacturing.[54,55] **Table 1.1** summarizes the peptide-based cancer vaccines in completed and

ongoing clinical trials.[56] In phase-I clinical trials, peptide vaccines induced both $CD8^+$ and $CD4^+$ T cell antigen-specific responses, although a higher proportion of $CD4^+$ T cells were observed, despite immunization with high-affinity MHC-I binding epitopes.[57-59] These data suggest that peptide vaccines are limited in their capacity to generate neoantigen-specific, cytotoxic $CD8^+$ T cells, which are the primary effector cells of anti-tumor immunity in most cancers. It is important to note that $CD4^+$ T cells recognize tumor antigens bound to MHC class II molecules that are taken up into the endo-lysosomal compartment, while $CD8^+$ T cells also known as cytotoxic T lymphocytes (CTLs) recognize cytosolic derived antigens bound to MHC class I molecules (MHC-I). The process by which exogenous antigens are captured by DCs, processed and presented onto MHC-I molecules to CTLs is called cross-presentation. Thus, it is critical in cancer vaccine design to achieve cytosolic delivery of tumor antigens for cross-priming by DCs in order to activate an efficient $CD8^+$ T cell response. Also, there are three main signals commonly considered to be necessary for effective CTL activation in response to a cancer vaccine: (1) engagement of T cell receptor with peptide-MHC complex, (2) expression of co-stimulatory molecules, and (3) production of cytokines that promote differentiation of T cells to an effector phenotype.[51] More specifically, T cell activation depends on the initial tumor antigen-specific signal provided to the T cell receptors via the antigen-loaded MHC-I complex on DCs. Co-stimulatory molecules (CD80 and CD86) found on DCs bind to the ligands of the costimulatory molecules that are expressed on T cells providing a second signal to fine tune and enhance CTLs. The combination of T cell receptor engagement and expression of co-stimulatory molecules on activated DCs, leads to the production of proinflammatory cytokines that aid in survival, proliferation, and differentiation of T cells. While neoantigen peptide vaccines can be used to stimulate T cells against antigens promoting anti-tumor immunity, so far, they have demonstrated only a modest capacity to elicit a

tumor-specific T cell response. Consequently, much effort has been devoted to developing strategies to enhance the immunogenicity of peptide vaccines.

Table 1.1: Clinical trials of peptide-based therapeutic cancer vaccines in recent five years

Tumor	Target	Phase	Notes	Reference
Melanoma	Multiple	I/II	Montanide ISA-51-adjuvanted intervention plus ipilimumab	NCT02385669
	NY-ESO-1 MART-1	II	Montanide ISA-51- and Hiltonol®-adjuvanted intervention combined with DC vaccination	NCT02334735
	Multiple	I/II	Combined with pembrolizumab	NCT02515227
Prostate Cancer	PSA	I/II	Montanide ISA-51- or GM-CSF-adjuvanted intervention combined with imiquimod	NCT02452307
Lung Cancer	PPV	I	Hiltonol®-adjuvanted intervention combined with pembrolizumab	NCT03380871
Kidney Cancer	PPV	I	Hiltonol®-adjuvanted intervention combined with ipilimumab	NCT02950766
	Multiple	I/II	Adjuvanted with GM-CSF and Montanide ISA-51	NCT02429440
NSCLC	UCP2	I/II	Adjuvanted with Montanide ISA-51	NCT02818426
Leukemia	PPV	I	Hiltonol®-adjuvanted intervention combined with pembrolizumab	NCT03380871
	Multiple	I	Adjuvanted with GM-CSF- and Montanide ISA-51	NCT02240537
Bladder Carcinoma	PPV	I	Hiltonol®-adjuvanted intervention combined with atezolizumab	NCT03359239
Glioma	IDH1	I	Adjuvanted with Montanide ISA-51	NCT02454634
	WT1	II	Combined with bevacizumab	NCT03149003
Brain Tumors	Multiple	I	Hiltonol®-adjuvanted intervention combined with varlilumab	NCT02924038
Ovarian Cancer	FOLR1	II	Combined with durvalumab	NCT02764333
	FOLR1	II	Adjuvanted with GM-CSF	NCT02978222
Anal Cancer	Multiple	IV	Single adjuvanted agent	NCT03051516

1.1.4 Immunostimulatory Nucleic Acid Adjuvants

Immunogenicity of cancer vaccines can be enhanced by the addition of adjuvants to enhance and modulate signals 1, 2, and 3 (described above). More specifically, adjuvants are molecules or compounds that can be tailored for specific immunomodulatory effects to target and activate pattern recognition receptors (PRRs) on innate immune cells by mimicking pathogen-associated molecular patterns (PAMPs) found only on microbes. Activation of PRRs initiates downstream signaling pathways which lead to production of type I interferons (IFNs) and other pro-inflammatory cytokines that can shape and enhance the subsequent adaptive immune response. There are several families of PRRs known, and the major and most extensively studied are toll-like receptors (TLRs). TLRs are located on the cell surface or in endosomal compartments where they are able to detect a wide range of PAMPS, including lipopolysaccharide, flagellin, single-stranded bacterial DNA, double-stranded viral RNA, and diacylated peptides. TLRs (TLR3, TLR7, and TLR9) that recognize nucleic acids are located predominantly within endosomal compartments. RIG-I-like receptors (RLRs) located in the cytosol recognize pathogen-derived nucleic acids. The two major RLRs, retinoic acid-inducible gene I (RIG-I) and melanoma differentiation-associated gene 5 (MDA5), are known as cytosolic RNA sensors and activate the transcription factors IRF3 and NF-κB, leading to downstream production of type I IFNs and proinflammatory cytokines which help direct activation and differentiation of T cells.

The double-stranded RNA (dsRNA) analogue polyIC is a promising adjuvant for cancer vaccines because it is a potent inducer of type I IFNs and proinflammatory cytokines. PolyIC can act through two dsRNA sensing pathways, TLR3 in the endosome and MDA5 in the cytosol. Downstream activation of these pathways leads to the production of type I IFNs and other pro-inflammatory cytokines which help direct activation and differentiation of T cells. However, major

delivery barriers such as degradation by nucleases, systemic distribution that causes off-target inflammatory side effects, and poor delivery to and uptake by DCs can all prevent polyIC from reaching its intracellular targets. It is vital to achieve efficient delivery of polyIC in order to modulate the desired innate and adaptive immune response. In addition, several clinical trial studies are exploring the use of polyIC complexed with poly-L-lysine and carboxymethylcellulose (polyIC-LC) and administered with peptide antigens, prominently in the context to generate local and systemic inflammation to induce immune infiltration into tumors. Formulations employing polyIC-LC have progressed as far as phase II clinical testing, and so they hold promise as candidate adjuvants with potential immunomodulatory capabilities. Although poly-L-lysine and carboxymethylcellulose improve the stability of poly-IC and minimizes the extent of RNAse degradation, the protection is not complete and poly-L-lysine and carboxymethylcellulose themselves may be susceptible to enzymatic degradation and immune clearance. Therefore, there is a need for particulate formulations for the delivery of polyIC to maximize its adjuvant properties.

1.2 Innovation

1.2.1 Nanoparticle Platform for Improving Immunogenicity of Cancer Vaccines

Antigen specific tumor infiltrating $CD8^+$ T cells are critical to an effective antitumor immune response. Therefore, an important aspect of cancer vaccine design involves the design of formulations that enable delivery of antigens to the cytosolic MHC-I pathway. A number of investigators have engineered nanotechnologies designed to overcome the endo-lysosomal pathway for cytosolic delivery of therapeutics. One approach involves the use of pH-responsive cationic polymers, typically featuring a large number of tertiary amines, like PEI, poly(2-(dimethylamino)ethylmethacrylate) (DMAEMA), and related polymers that protonate at endo-lysosomal pH. These polymers are believed to facilitate endosomal antigen escape through the

hypothetical “proton sponge effect”, which is an osmosis-driven process triggered by the proton buffering capacity of the polymers within the endosome. As a consequence, a parallel influx of chloride ions accompanies the influx of protons, leading to an increase of the osmotic pressure inside the endosome and eventual rupture of the vesicle, allowing the escape of vaccine cargo.[60] Several groups, including ours, have investigated the use of amphiphilic diblock pH-responsive copolymers to form nanoparticles for cytosolic delivery of antigens and nucleic acid adjuvants. These stimuli responsive, or so-called “smart”, nanoparticles are composed of a hydrophilic corona to stabilize the micelles in aqueous solution and a hydrophobic core that can be switched to hydrophilic in response to small changes in pH. These nanoparticles have the ability to significantly enhance the cytosolic delivery of therapeutics by destabilizing the endosomal membrane. More specifically, after endosomal uptake, the endosome starts to acidify, causing the core to become protonated, which subsequently destabilizes the micellar conformation of the particle. The hydrophobic core becomes exposed and interacts with the endosomal membrane causing it to disrupt, allowing release of cargo into the cytosol. For example, the Duvall lab has designed amphiphilic diblock copolymers with a first block comprising a hydrophilic corona of either polyethylene glycol (PEG), poly(ethylene glycol) methyl ether methacrylate (PEGMA), or 2-methacryloyloxyethyl phosphorylcholine to improve stability and reduce toxicity of the NP. The second block contains a balanced ratio of cationic DMAEMA and hydrophobic butyl methacrylate (BMA) responsible for RNA complexation and cytosolic delivery.[61-63] The Stayton lab designed a polymeric carrier for subunit vaccines comprising antigens and nucleic acid adjuvants. These carriers were amphiphilic diblock copolymers composed of a cationic DMAEMA first block for electrostatic complexation of nucleic acid adjuvants and a small percentage of pyridyl disulfide ethyl methacrylate (PDSMA) for conjugation of thiol-bearing antigens (ovalbumin) via disulfide

exchange. The endosome destabilizing terpolymer second block was comprised of propylacrylic acid (PAA), DMAEMA, and BMA, referred to as D-PDB, that act cooperatively to mediate efficient cytosolic delivery.[64] The features of these polymers have the potential to deliver tumor antigens to the MHC-I pathway and enable activation of cytosolic nucleic acids sensors. It is well known that DCs play essential roles in linking together innate and adaptive immunity, so the ability to target cytosolic nucleic acid sensors in DCs (i.e., TLR3 and MDA-5), triggering signaling cascades, may offer unprecedented opportunity to control the immune response generated by a cancer vaccine.

Studies show that a physical mixture of adjuvants with antigens can result in their dissociation following injection limiting their immune activation effects. Whereas, co-delivery increases the probability that both antigen and nucleic acid adjuvant get internalized by the same DC, allowing antigen presentation to occur in an appropriate pro-inflammatory context and avoiding induction of T cell tolerance when only antigen is presented in the absence of signals required for APC maturation and T cell activation. Indeed, in a recent study, Seder and colleagues demonstrated that mixing tumor peptide antigens with polyICLC yielded a poor CD8+ T cell response when compared to a nanovaccine platform designed for co-delivery of antigen and TLR7/8 agonists.[65] Therefore, packaged co-delivery of antigen and polyIC may also be an important design criterion for maximizing cellular immunity in response to vaccination. A number of major pharmacological barriers, including rapid clearance, poor cellular uptake, and inefficient lymph node (LN) accumulation, limit the immunogenicity of protein and peptide antigens as well as the potency, and potentially tolerability and safety, of many promising nucleic acid adjuvants.[66,67] Several delivery systems have been developed to overcome these immunopharmacological barriers, such as lipid-based and polymeric nanoparticles. It is well

established that nanoparticles less than ~100 nm in diameter can enter lymphatics and enhance cargo accumulation in vaccine site draining lymph nodes.[66,68] Therefore, another critical aspect of cancer vaccine design is to engineer a nanoparticle carrier that enables co-delivery of antigen and adjuvant to the same DC in the lymph node to effectively prime antigen-specific $CD8^+$ T cells.

Here, we describe an amphiphilic diblock polymer that self-assembles into micellar nanoparticles of ~30 nm in diameter in aqueous solution. This versatile nanoparticle vaccine platform allows for facile co-loading and cytosolic co-delivery of antigens and polyIC as the adjuvant. It is designed with a PEG-rich corona that displays pyridyl disulfide (PDS) groups for covalent conjugation of thiol-containing antigens via thiol-disulfide exchange reactions, and a pH-responsive, endosomolytic core for electrostatic loading of immunostimulatory nucleic acids that also facilitates cytosolic delivery of both antigen and adjuvants. We evaluate whether the NP platform can efficiently co-load a model antigen, chicken ovalbumin (OVA), and polyIC and promote dual-delivery of OVA and polyIC to the cytosol. We further investigate whether the NP can enhance the immunostimulatory activity of polyIC via the MDA-5 pathway and promote MHC-I restricted antigen presentation by DCs. In the final aim of this work, we begin investigating the impact of coordinated innate immune activation via MDA-5 and MHC-I antigen presentation on enhancing the magnitude and functionality of the CD8+ T cell response. This lays the groundwork for further studies of the effects of NP vaccines formulated with any clinically relevant peptide antigen, as well as other nucleic acid adjuvants in combination with immune checkpoint inhibitors.

1.3 Specific Aims

Cytosolic antigen delivery is key for a vaccine to efficiently stimulate a CTL response; thus, an effective cancer vaccine should be designed to facilitate intracellular delivery of cargo. The innate immune response largely dictates the magnitude, functionality, and phenotype of the subsequent adaptive immune response. Therefore, the addition of immune agonists such as nucleic acid adjuvants that can activate the appropriate molecular cues in dendritic cells (DCs) that lead to the production of type I interferons (IFNs) and other pro-inflammatory cytokines is essential for inducing a strong CTL response. Additionally, co-delivery of antigens and nucleic acid adjuvants to the same DC is important for eliciting an enhanced anti-tumor immune response. The overall goal of this work is to employ a pH-responsive NP that allows for conjugation of antigens along with the complexation of nucleic acid adjuvant polyIC, a TLR3 and MDA-5 agonist, to facilitate co-delivery to DCs. Upon uptake, the NP responds to the decreased pH within endosomal compartments and disassembles allowing cargo to be released into the cytosol. We demonstrate that the pH-responsive, endosomolytic NP vaccine can enhance antigen-specific T cell priming by DCs through increased uptake and cytosolic delivery of cargo, resulting in protection from tumor formation and inhibition of the growth of established tumors in a mouse tumor model.

Aim 1: Develop a polymeric NP system designed to enhance intracellular co-delivery of antigens and nucleic acid adjuvants. To address limitations of traditional approaches to cancer vaccines, polymeric NPs were engineering to promote the cytosolic co-delivery of polyIC and protein antigen. This NP is designed with a PEG-rich corona that displays pyridyl disulfide (PDS) groups for covalent conjugation of thiol-containing antigens via thiol-disulfide exchange reactions, and a pH-responsive, endosomolytic core for electrostatic loading of immunostimulatory nucleic acids that also facilitates cytosolic delivery of both antigen and adjuvants. Upon intracellular

uptake and in response to the decrease in pH within endosomal compartments, the NP destabilizes to trigger endosomal escape of vaccine cargo to the cytosol, allowing antigen to be processed and presented on MHC-I molecules and polyIC to activate the MDA-5 pathway. We demonstrate that the NP platform can efficiently co-load a model antigen, chicken ovalbumin (OVA), and polyIC to promote dual-delivery of OVA and polyIC to the cytosol. Cytosolic delivery of antigen resulted in increased antigen presentation on MHC-I molecules, while endosomal escape of polyIC strongly increased its immunostimulatory potency via the MDA-5 pathway, resulting in proinflammatory cytokine production, costimulatory molecule upregulation, and IFN-I secretion by dendritic cells.

Aim 2: Evaluate the DC-mediated T cell response induced by the optimized NP vaccine. After this pH-responsive nanoparticle vaccine showed promise in promoting cytosolic delivery of antigen and endosomal escape of polyIC, we further investigated its effects *in vivo*. Owing to its nanoscale dimensions, the NP vaccine platform extended the injection site half-life of protein antigen and polyIC and increased their accumulation in vaccine site draining LNs. By overcoming intracellular and physiological delivery barriers, NPs co-loaded with antigen and polyIC stimulated a strong, multifunctional $CD8^+$ T cell response that conferred protection from tumor formation and inhibited the growth of established tumors in a mouse tumor model.

Collectively, these studies established the use of a versatile NP platform for the co-delivery of antigens and nucleic acid adjuvants while also demonstrating its ability to stimulate optimal $CD8^+$ T cells against tumor cells.

CHAPTER 2

A Nanoparticle Platform for Delivery of Diverse Antigens and Adjuvants

Text for Chapter 2 adapted from:

Carson CS, Becker KW, Garland KM, Pagendarm HM, Stone PT, Arora K, Wang-Bishop L, Baljon JJ, Cruz LD, Joyce S, Wilson JT. A Nanovaccine for Enhancing Cellular Immunity via Cytosolic Co-Delivery of Antigen and PolyIC RNA. *J. Control. Release.* Volume 345, 2022, Pages 354-370, ISSN 0168-3659, https://doi.org/10.1016/j.jconrel.2022.03.020.

2.1 Abstract

Cytosolic delivery of biological cargo is essential for therapeutic strategies that aim to induce $CD8^+$ T cell responses. Polymeric nanoparticles are ideal platforms for the cytosolic dual-delivery of nucleic acid adjuvants and protein antigens but are hindered by entrapment and subsequent degradation in acidic compartments of the endosomal-lysosomal pathway. Here, we describe a pH-responsive, endosomolytic nanoparticle (NP) vaccine platform for facile co-loading and dual-delivery of diverse antigens and nucleic acid adjuvants. The NP vaccine design is based on diblock copolymers comprising a poly(ethylene glycol)-rich first block that is functionalized with reactive moieties for covalent conjugation of antigen via disulfide linkages, and a pH-responsive second block for electrostatic packaging of nucleic acids that also facilitates endosomal escape of associated vaccine cargo to the cytosol. Using polyIC, a clinically-advanced nucleic acid adjuvant, we demonstrated that endosomolytic NPs promoted the cytosolic co-delivery of polyIC and protein antigen, which acted synergistically to enhance antigen cross-presentation, co-stimulatory molecule expression, and cytokine production by dendritic cells. Overall, these data suggest the NP platform has the potential to improve the therapeutic efficacy of nucleic acid adjuvants and enhance MHC-I antigen presentation, resulting in improved $CD8^+$ T cell responses.

2.2 Introduction

In recent years, several groups, including ours, have devised ways to deliver antigens and/or adjuvants to the cytosol of professional antigen presenting cells (APCs) such as dendritic cells (DCs) to promote MHC-I presentation via the cytosolic antigen processing pathway, resulting in enhanced $CD8^+$ T cell responses.[64,69-74] The cytosol is rich in targets for augmenting cellular immunity. A number of pattern recognition receptors (PRRs) that are important in the sensing of foreign nucleic acids, including melanoma differentiation-associated protein 5 (MDA-5), RIG-I, and cGAS, are located within the cytosol for immune surveillance against many intracellular pathogens.[75-78] Accordingly, nucleic acid agonists of cytosolic PRRs are promising candidates as adjuvants for cancer vaccines due to their capacity to induce type-I interferons (IFN-I) and other pro-inflammatory cytokines essential to generating a robust $CD8^+$ T cell response.[79-81] However, major delivery barriers have limited the adjuvant activity of nucleic acid agonists of cytosolic PRRs, including degradation by nucleases, rapid systemic distribution that can cause undesirable inflammatory side effects, low delivery to and uptake by APCs, and critically, negligible delivery to the cytosol where these PRRs are localized.[76,82,83] Hence, the development of delivery platforms that address these barriers will be critical to realizing the potential of this promising and expanding class of vaccine adjuvants.

The double-stranded RNA (dsRNA) analogue polyIC is one of the most clinically advanced nucleic acid adjuvants. PolyIC can act through two distinct dsRNA sensing pathways: Toll-like receptor 3 (TLR-3), which resides in the endosomal membrane, and melanoma differentiation-associated protein 5 (MDA5) in the cytosol.[84-87] To protect polyIC from RNAse degradation, several formulations have been developed based on electrostatic complexation with cationic polymers, such as polyethylenimine (PEI) or poly-L-lysine (PLL).[87,88] Most notably, polyIC complexed with PLL and further stabilized with carboxymethylcellulose (polyICLC; also

known as Hiltonol®) was evaluated in multiple clinical trials and has been shown to stimulate IFN-I production and/or enhance T cell responses in humans and non-human primates.[89-93] Interestingly, polyICLC activates MDA-5 more effectively than polyIC and, thereby, enhances IFN-I and other proinflammatory cytokine responses to increase adjuvant potency.[85] This has been attributed to the ability of PLL to promote endosomal escape of polyIC via the "proton sponge effect." Hence, cytosolic delivery of polyIC is an important design consideration for vaccine delivery technologies that aim to maximize its adjuvant properties.[94,95]

PolyICLC has recently been investigated as a promising adjuvant for enhancing responses to peptide-based cancer vaccines in patients. Results from clinical trials demonstrated the ability of polyICLC to promote antigen-specific T cell responses to co-administered tumor antigens.[53,89,92,96,97] In these clinical studies, however, antigens were mixed with polyICLC prior to vaccine administration. While translationally appealing, ample evidence show that simple mixing of antigen and adjuvant is less effective than co-delivering antigen and adjuvant on a common carrier.[64,69,98-102] Co-delivery increases the probability that both antigen and adjuvant are internalized by the same APC, allowing antigen presentation to occur in an appropriate pro-inflammatory context and avoiding induction of T cell tolerance when only antigen is presented in the absence of signals required for APC maturation and T cell activation.[103] Indeed, in a recent study, Seder and colleagues demonstrated that mixing tumor peptide antigens with polyICLC yielded a poor CD8+ T cell response when compared to a nanovaccine platform designed for co-delivery of antigen and TLR7/8 agonists.[65] Therefore, packaged co-delivery of antigen and polyIC may also be an important design criterion for maximizing cellular immunity in response to vaccination.

Here, we describe a versatile nanoparticle (NP) vaccine platform for facile co-loading and cytosolic co-delivery of antigens and polyinosinic:polycytidylic acid (polyIC), a dsRNA analog, as the adjuvant. This NP is designed with a PEG-rich corona that displays pyridyl disulfide (PDS) groups for covalent conjugation of thiol-containing antigens via thiol-disulfide exchange reactions, and a pH-responsive, endosomolytic core for electrostatic loading of immunostimulatory nucleic acids that also facilitates cytosolic delivery of both antigen and adjuvants. Upon intracellular uptake and in response to the decrease in pH within endosomal compartments, the NP destabilizes to trigger endosomal escape of vaccine cargo to the cytosol, allowing antigen to be processed and presented on MHC-I molecules and polyIC to activate the MDA-5 pathway. We demonstrate that the NP platform can efficiently co-load and deliver a model antigen, chicken ovalbumin (OVA), and polyIC to the cytosol of professional antigen presenting cells. Consequently, this enhances the immunostimulatory activity of polyIC via the MDA-5 pathway and promotes MHC-I restricted antigen presentation by APCs. Collectively, these data indicate that pH-responsive, endosomolytic polymeric platform is a promising and versatile platform for cytosolic delivery of antigen and nucleic acid adjuvants, and offers a promising strategy for enhancing CD8+ T cell responses.

2.3 Results and Discussion

Synthesis and characterization of polymeric carriers for dual-delivery of antigen and nucleic acid adjuvants

We synthesized a pH-responsive diblock copolymer designed to facilitate cytosolic delivery of vaccine cargo, which we expected would increase the immunostimulatory activity of polyIC by enhancing access to MDA-5 while also promoting antigen presentation on MHC-I, resulting in increased CD8+ T responses. The polymer is composed of two blocks synthesized by reversible addition−fragmentation chain transfer (RAFT) polymerization (**Figure 2.1A, Figure**

2.2, Table 2.1). The first block is primarily composed of the hydrophilic monomer poly(ethylene glycol) methacrylate (PEGMA) (MW 300 Da), to confer colloidal stability to the NP, and is copolymerized with a small percentage (10%) of pyridyl disulfide ethyl methacrylate (PDSMA) for conjugation of thiol-bearing protein or peptide antigens via thiol-disulfide exchange reaction. The first block is then chain extended with the second block which is composed of cationic, pH-responsive dimethylamino ethyl methacrylate (DMAEMA) and hydrophobic butyl methacrylate (BMA) at a 50:50 molar ratio, which we and others have previously demonstrated exhibits potent endosomal escape activity.[61,104,105] In aqueous solution, this amphiphilic diblock copolymer self-assembles into micellar nanoparticles of ~30 nm in diameter. After cellular uptake, the acidic endosomal environment protonates DMAEMA residues, triggering a micelle-to-unimer conversion that exposes hydrophobic BMA groups, which act cooperatively with DMAEMA residues to destabilize the endosomal membrane, allowing release of cargo into the cytosol (**Figure 2.1B**). This is distinct from the inefficient and still poorly understood and debated proton sponge mechanism harnessed by PLL, PEI, and several other cationic polymers, which relies on the buffering capacity of cationic polymers with ionizable amino groups to generate osmotic stress within endo/lysosomes.[60]

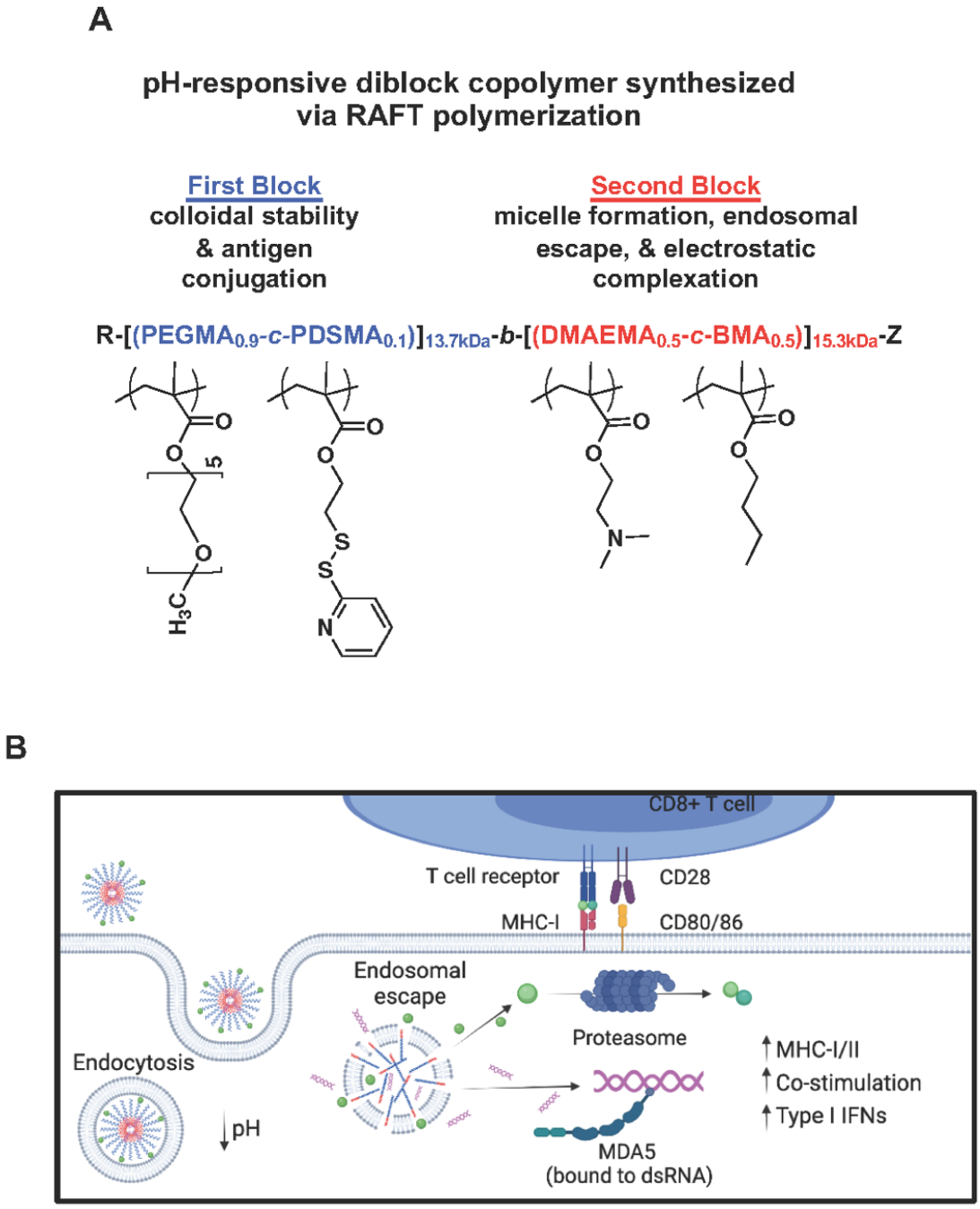

Figure 2.1: Fabrication of polymeric nanoparticle vaccine platform for cytosolic dual-delivery of antigen and nucleic acid adjuvants. (A) Chemical structure and composition of pH-responsive endosome-destabilizing poly[(PEGMA-co-PDSMA)-block-(DMAEMA-co-BMA)] diblock copolymer. **(B)** Schematic representation of polymeric nanoparticle promoting antigen and adjuvant (polyIC) delivery in the cytosol via endosomal escape, resulting in MHC-I antigen presentation and activation of innate immunity via MDA-5 signaling, which act synergistically to enhance antigen-specific $CD8^+$ T cell responses.

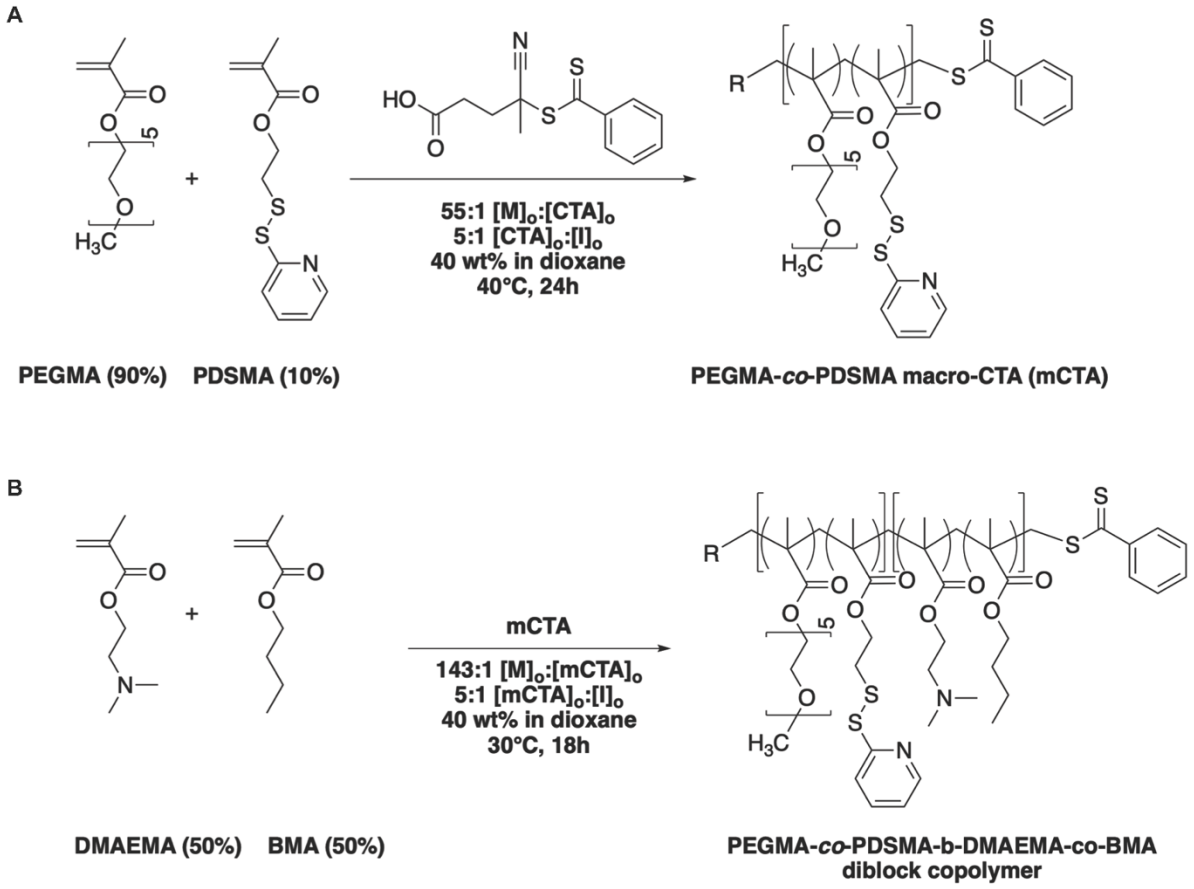

Figure 2.2: RAFT synthesis of pH-responsive for co-delivery of protein antigen and nucleic acid adjuvant. (A) Synthesis scheme and reaction conditions for PEGMA-co-PDSMA macro-chain transfer agent (mCTA). **(B)** Synthesis of pH-responsive diblock copolymer, (PEGMA-co-PDSMA)-block-(DMAEMA-co-BMA).

Table 2.2: Summary of polymer properties.

	pH-responsive polymer		
	1st block (mCTA)	**2nd block**	**Diblock copolymer**
Theoretical Molecular Weight (g/mol)	13,755	15,321	29,076

Nanoparticle vaccine formulation and characterization

The ability of the NP to co-load the model protein antigen ovalbumin (OVA) and the nucleic acid adjuvant polyIC was next assessed. To achieve this, and with an eye towards future translation, we devised a simple and scalable two-step formulation process that required no intermediate purification steps prior to administration. As shown in **Figure 2.3A**, micellar NPs in aqueous solution are first mixed with thiol-containing antigen (e.g., OVA) to covalently link antigen to the hydrophilic NP corona. The antigen-NP conjugates are then electrostatically complexed with polyIC at pH 4, followed by neutralization of the solution to pH 7.4 to yield NPs that are dual-loaded with antigen and nucleic acid adjuvant. To first investigate antigen conjugation, we thiolated AlexaFluor647-labeled OVA using Traut's reagent (3-5 thiols/OVA) and subsequently reacted it with PDSMA groups presented on the corona of the NP at various molar ratios of NP:OVA (2:1, 4:1, 6:1, 8:1, 10:1, 20:1) to form OVA-NP conjugates. To assess conjugation efficiency, we used SDS-polyacrylamide gel electrophoresis (SDS-PAGE) to monitor the band shift and disappearance of AF647-labeled OVA due to conjugation to NP. Complete conjugation was achieved at all tested ratios (**Figure 2.4**) demonstrating the potential to stoichiometrically tailor the antigen loading capacity. Following conjugation, negatively charged polyIC was electrostatically complexed to the tertiary amine groups on DMAEMA in the second block at various N:P charge ratios (i.e., the molar amount of protonatable amines (N = nitrogen) groups to the molar amount of phosphate (P) groups in the nucleic acid backbone). To achieve this, complexes were prepared at pH = 4, which is below the acid dissociation constant (pKa ~ 7) of DMAEMA, ensuring that the DMAEMA groups are predominantly protonated and positively charged, thus allowing for electrostatic complexation with negatively charged polyIC. Following complexation, the solution was further diluted in 100 mM phosphate buffer (pH 8) to a final pH

of 7.4 before use. N:P ratios of 1:1, 2:1, 4:1, 6:1, 8:1, 12:1, 20:1 were tested and agarose gel electrophoresis was used to evaluate polyIC complexation efficiency (**Figure 2.5**). It was determined that N:P ratios of 6:1 and greater enabled nearly complete complexation of polyIC, as demonstrated by the lack of migration of NP/polyIC complexes. A schematic representation of the formulations used in subsequent experiments is shown in **Figure 2.3B**.

We next assessed whether OVA and polyIC could be co-loaded on the same NP using SDS-PAGE and agarose gel electrophoresis. Using an NP:OVA molar ratio of 8:1 and charge ratio of 6:1 for polyIC complexation, it was determined that both species could be loaded onto NPs (**Figure 2.3C,D**). We further confirmed the assembly and evaluated the particle size of NP micelles, OVA-NP conjugates (8:1), NP/polyIC complexes (6:1), and NPs co-loaded with both OVA and polyIC (8:1 OVA-NP/polyIC 6:1) via dynamic light scattering (DLS) (**Figure 2.3E**). DLS analysis demonstrated that free NP micelles are ~30 nm in diameter and after co-loading OVA and polyIC the diameter increased to ~60 nm. A conjugation ratio of 8:1 and a complexation ratio of 6:1 were selected for all subsequent investigations in order to maximize the amount of antigen and adjuvant delivered per particle, while maintaining particle size and colloidal stability.

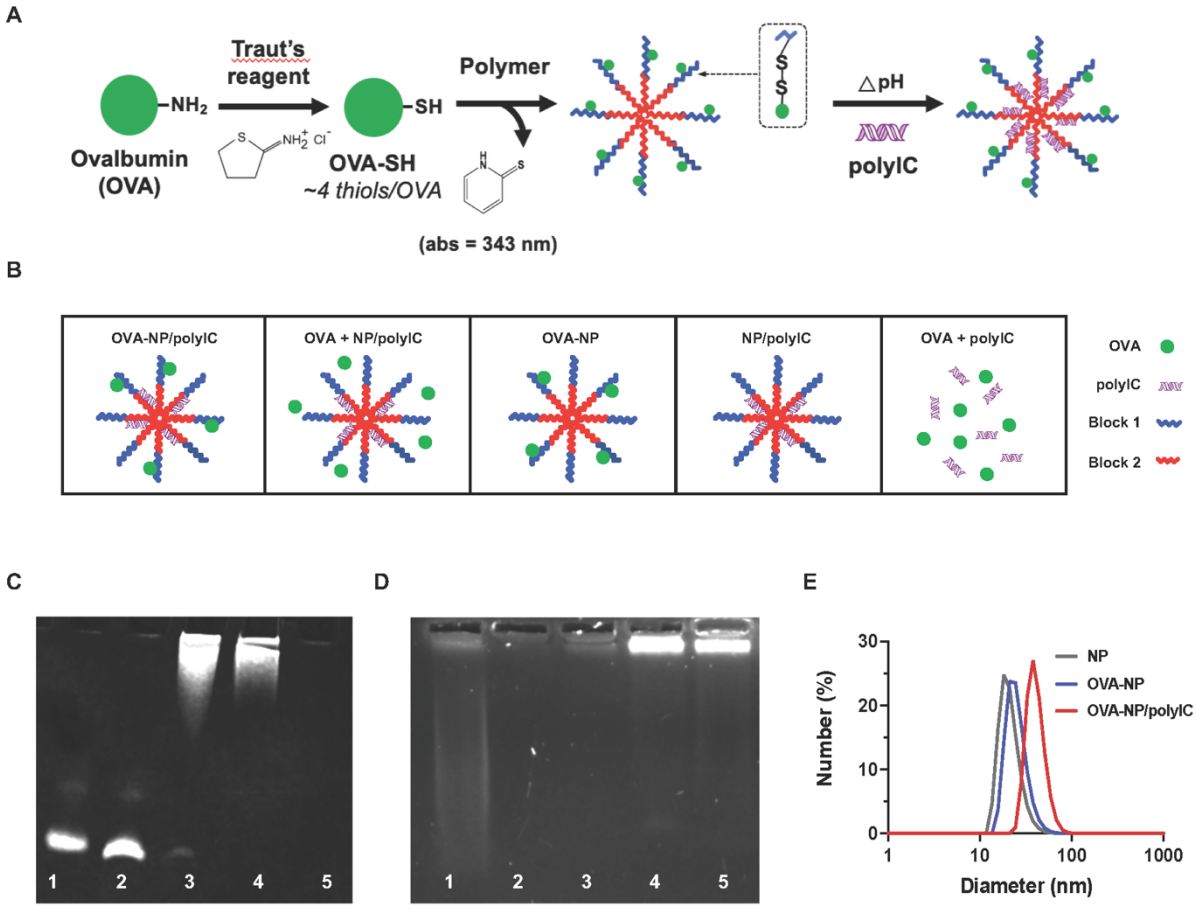

Figure 2.3: Nanoparticle vaccine formulation and characterization of loaded antigen and nucleic acid adjuvants. (A) Schematic representation of a rapid, facile, and scalable process for co-loading antigen and nucleic acid adjuvants via simple mixing of thiol containing antigen (OVA protein) and micellar nanoparticle, resulting in covalent linkage via disulfide bridge bond, followed by electrostatic complexation of polyIC to the cationic DMAEMA groups in the second block (core) of carrier. **(B)** Schematic of the experimental and control formulations evaluated. **(C)** Thiolated OVA protein labeled with Alexa Fluor 647 was reacted with NPs to form conjugates at a 6:1 molar ratio. SDS-PAGE was used to confirm antigen conjugation. Lane (1) free OVA protein; (2) OVA + NP/polyIC; (3) OVA-NP; (4) OVA-NP/polyIC; (5) NP alone (no OVA). Material loaded into each lane was normalized based on 2 μg OVA. **(D)** PolyIC was complexed with NP and conjugate (OVA-NP at 6:1 ratio) at a N:P (+/-) charge ratio of 4:1. Agarose gel electrophoresis was used to confirm polyIC complexation. Lane (1) free polyIC; (2) NP alone (no polyIC); (3) OVA-NP (no polyIC); (4) NP/polyIC; (5) OVA-NP/polyIC. Material loaded into each lane was normalized to 1 μg polyIC. **(E)** Representative number-average size distributions of NP alone, OVA-NP (6:1 molar ratio), and OVA-NP/polyIC (6:1 molar ratio, 4:1 charge ratio) as measured by dynamic light scattering.

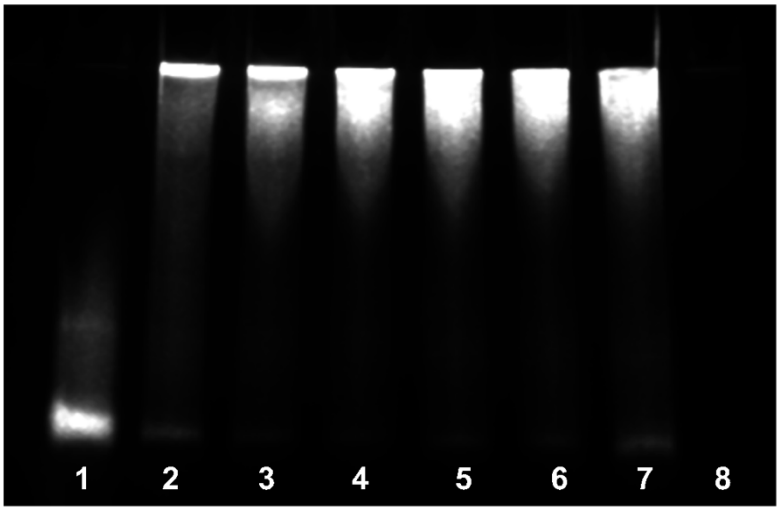

Figure 2.4: OVA-nanoparticle conjugation. Thiolated OVA protein labeled with Alexa Fluor 647 was reacted with NP to form conjugates at varying molar ratios of NP:OVA. SDS-PAGE was used to confirm antigen conjugation. Lane (1) free OVA protein; (2) OVA-NP (2:1); (3) OVA-NP (4:1); (4) OVA-NP (6:1); (5) OVA-NP (8:1); (6) OVA-NP (10:1); (7) OVA-NP (20:1); (8) NP. Material loaded into each lane was normalized to 2 μg OVA. Thiolated OVA was confirmed to conjugate at all molar ratios tested (lanes 2-7). The NP itself was not fluorescent (lane 8).

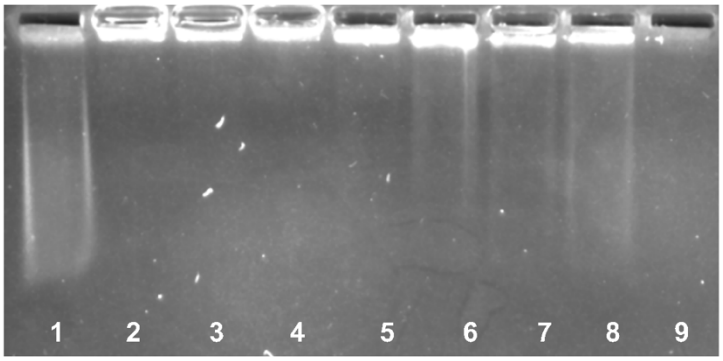

Figure 2.5: PolyIC complexation. PolyIC was complexed with NP at various charge ratios of NP:polyIC (+:-). Gel electrophoresis and SYBR safe staining were used to confirm adjuvant complexation. Lane (1) polyIC; (2) NP/polyIC (20:1); (3) NP/polyIC (12:1); (4) NP/polyIC (10:1); (5) NP/polyIC (8:1); (6) NP/polyIC (6:1); (7) NP/polyIC (4:1); (8) NP/polyIC (2:1); (9) NP. Material loaded into each lane was normalized to 1 μg polyIC. PolyIC complexed to NP at all ratios tested. NP did not show background staining from SYBR safe (lane 9).

Nanoparticle vaccine induces pH-dependent membrane disruption

Next, we assessed the capacity of the NPs alone and formulated with OVA and polyIC to induce pH-dependent disruption of lipid bilayer membranes using an erythrocyte hemolysis assay (**Figure 2.6A**), which is commonly used to predict the membrane-destabilizing activity of polymers.[106] Significant pH-dependent hemolytic activity was evident with the all of the formulations tested, with a slight decrease observed following complexation of polyIC, which may reflect reduced access of endosomolytic segments of the NP to erythrocyte membranes when complexed with the nucleic acid. To further validate the endosomolytic activity of the NP, we employed a Gal8-YFP reporter assay that directly measures endosomal disruption (**Figure 2.6B**).[107] This assay utilizes the fusion protein Gal8-YFP, which is a fusion between Galectin 8 (Gal8), an endogenous cytosolic protein that binds glycans, such as those found on the intraluminal membrane of endosomes, and yellow fluorescent protein (YFP). Following treatment with an endosomolytic agent, Gal8-YFP redistributes from the cytosol to the site of the ruptured endosomes to bind the newly exposed glycan. The degree of Gal8-YFP recruitment directly measures endosomal disruption, and has been shown to correlate with increased activity for cytosolic-acting nucleic acid drugs. In this study, we used a previously validated Gal8-YFP-expressing MDA-MB-231 breast cancer cell line (Gal8-MDA-MB-231).[107,108] Following treatment with 100 μg/mL of OVA-NP/polyIC, OVA-NP, NP/polyIC, empty NP, or PBS as a negative control, we quantified the integrated YFP fluorescence intensity of the puncta per cell, reflective of the quantity of bound Gal8-YFP molecules at the disrupted endosomes. Consistent with the hemolysis assay, all treatments significantly increased Gal8 recruitment compared to PBS, with empty NP inducing the most endosomal disruption, followed by NP/polyIC, OVA-NP/polyIC, and OVA-NP, though differences between the groups were not statistically significant

(**Figure 2.6C,D**). Collectively, these data demonstrate that our nanovaccine design strategy enables rapid, facile, and efficient co-loading of antigen and polyIC into sub-100 nm NPs that display potent endosomolytic activity.

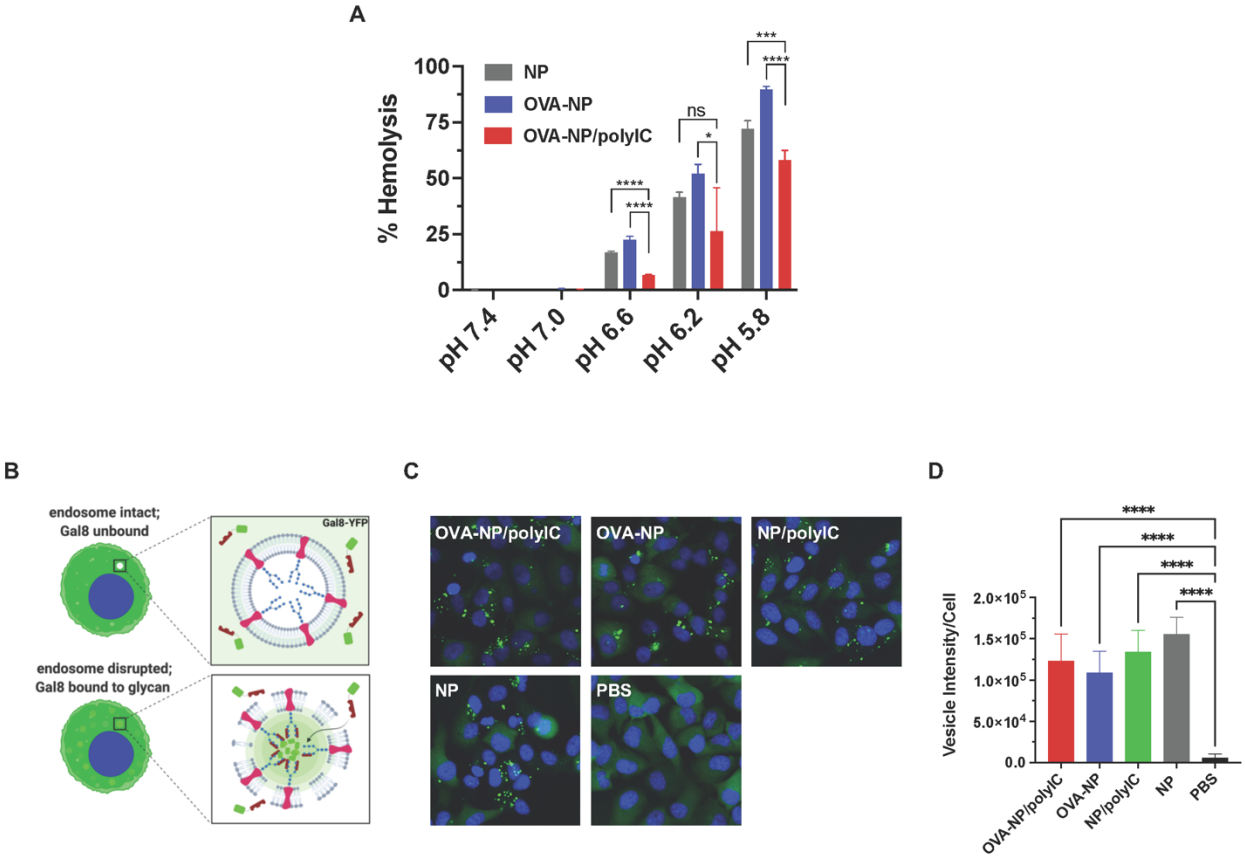

Figure 2.6: Nanoparticle vaccine induces pH-dependent endosomal escape. (A) Erythrocyte hemolysis assay demonstrating pH-dependent membrane destabilizing activity of the empty NP, nanoparticle OVA conjugate (OVA-NP), and conjugate complexed with polyIC (OVA-NP/polyIC). Concentrations are normalized to 5 μg/ml of polymer (mean ± SD; n = 4; statistical significance between OVA-NP/polyIC and all other formulations at each pH are shown; **P* <0.05, ***P* < 0.01, ****P* < 0.001, *****P* < 0.0001; one-way ANOVA with Dunnett's multiple comparisons test). **(B)** Schematic of Galectin 8 (Gal8) recruitment assay used to investigate endosomal escape of selected formulations. **(C)** Representative fluorescent images of MDA-MB-231 cells expressing Gal8-YFP fusion protein upon treatment with indicated nanovaccine formulations or controls. The fluorescent intensity of punctate increases significantly when YFP is recruited to the disrupted endosome. **(D)** Integrated Gal8-YFP intensity per cell for indicated formulations (mean ± SD; n = 6; statistical significance between all formulations vs. PBS are shown; **P* <0.05, ***P* < 0.01, ****P* < 0.001, *****P* < 0.0001; one-way ANOVA with Dunnett's multiple comparisons test).

Endosomolytic nanoparticles enhance activity of polyIC *in vitro*

Next, we evaluated the ability of the NP platform to enhance the immunostimulatory activity of polyIC using reporter cells that stably express an inducible reporter (Lucia Luciferase), which facilitates quantification of interferon-regulatory factor (IRF) pathway activation. THP1-Dual™ cells (human monocyte-like cell line), RAW-Dual™ cells (murine macrophage-like cell line), and A549-Dual™ cells (human lung epithelial cell line) were treated with OVA-NP/polyIC, NP/polyIC, empty NP, and free polyIC over a range of polyIC doses; PBS (vehicle) served as the negative control. After 24 h, cell culture supernatant was collected and the relative level of IFN-I production was quantified by luciferase luminescence assay. In all cell types, NPs complexed with polyIC led to a substantial increase in IFN-I production compared to free polyIC alone (**Figure 2.7A**), which exerted activity only at relatively high concentrations in vitro (>100 μg/mL).

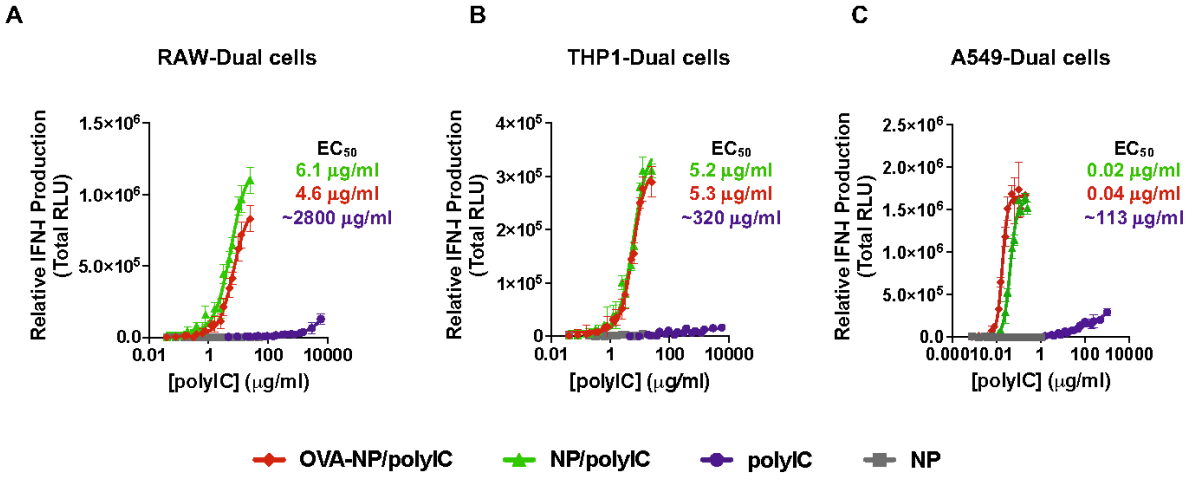

Figure 2.7: Nanoparticle vaccine enhances activity of polyIC. *In vitro* evaluation of TLR3 and MDA-5 activation in reporter cell lines **(A)** RAW-Dual cells **(B)** THP1-Dual cells **(C)** A549-Dual cells in response to stimulation with indicated formulations for 24 h.

Endosomolytic nanoparticles deliver polyIC to the cytosolic MDA-5 signaling pathway

Since polyIC is an agonist for both endosomal TLR3 and cytosolic MDA-5 signaling pathways, we directly assessed the contribution of MDA-5 in mediating this response by treating RAW-Lucia^{TM} ISG MDA-5-deficient reporter cell line (RAW-LuciaTM ISG KO MDA-5) and monitoring IRF-induced Lucia luciferase activity compared to RAW-Lucia^{TM} ISG cells that express endogenous MDA-5 (**Figure 2.8A,B**). IFN-I response was significantly diminished, though not fully abrogated, in the MDA-5 knockout cells, indicating that NPs facilitate delivery of polyIC to the cytosol and activate an MDA-5-dependent IFN-I response. Interestingly, the activity of polyIC delivered using the commercial transfection agent Lipofectamine 2000 was only slightly inhibited in the MDA-5 knockout cells, implicating the activation of other PRRs, likely TLR3, by polyIC, and further demonstrating the relative potency of the NPs to enhance cytosolic delivery of the adjuvant cargo. In this work we selected polyIC as a nucleic acid adjuvant due to its high translational relevance in immuno-oncology, but in principle the NP platform could be used to co-deliver antigen with virtually any nucleic acid adjuvant, including agonists of other cytosolic PRRs. For example, we have previously demonstrated that the immunostimulatory activity of 5'triphosphate RNA (3pRNA), an agonist of RIG-I, and interferon stimulatory DNA (ISD), a ligand for cGAS, can be dramatically enhanced when delivered using other endosomolytic carriers.[109,110] Hence, this nanovaccine platform may also open new opportunities for exploring other emerging adjuvants to maximize their in vivo activity.

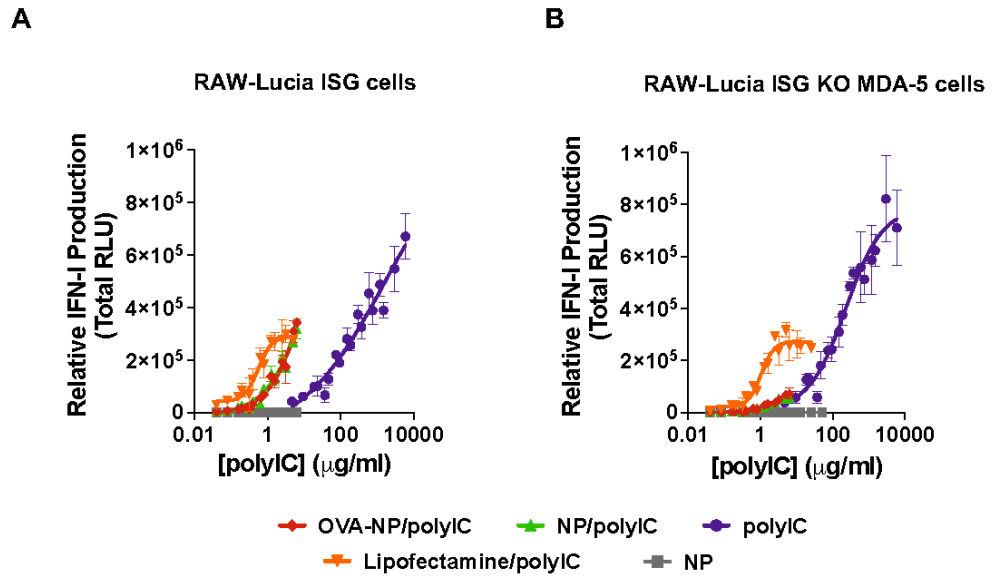

Figure 2.8: Nanoparticle vaccine delivers polyIC to cytosolic pathway. *In vitro* evaluation of the role of MDA-5 activation using **(A)** RAW-ISG Lucia vs. **(B)** RAW-ISG Lucia KO MDA-5 reporter cells to monitor the type-I interferon production in response to 24 h incubation with indicated formulations.

Nanoparticle Vaccine enhances DC activation and maturation *in vitro*

Consistent with their capacity to enhance polyIC activity, we also found that NP-mediated delivery of polyIC increased expression of the DC maturation markers MHC-II and co-stimulatory molecules CD80 and CD86 by murine bone marrow-derived dendritic cells (BMDCs) to a greater extent than free polyIC or NP formulations lacking polyIC (**Figure 2.9A**). Additionally, NPs complexed with polyIC significantly increased gene expression of *Ifnb1* and *Tnf* by BMDCs as measured by quantitative RT-PCR 6 h after treatment (**Figure 2.9B**). To further evaluate DC activation, we quantified cytokine and chemokine levels in the supernatant of BMDCs treated with NPs formulated with and without polyIC (**Figure 2.9C**). We observed that complexation of polyIC with NPs led to higher concentrations of secreted IFN-β1, an important cytokine for CD8+ T cell activation.[111] Interestingly, we also found that free polyIC induced a higher level of CXCL10,

TNFα, and IL-6 production than when complexed with the NP, potentially reflecting a differential cytokine response elicited by TLR-3 and MDA-5.[85,94,112] Additional studies, including a deeper analysis of the cytokine profiles induced by both free and NP-complexed polyIC, are necessary to further interrogate this possibility. The importance of IFN-I in generating $CD8^+$ T cell responses is notable and should be weighed against the potentially deleterious inflammatory side effects of IL-6 and TNFα that may limit vaccine tolerability, safety, and/or efficacy.[113,114] It should also be noted that endosomal escape is not a fully efficient event[115,116] and, therefore, it is likely that a fraction of internalized polyIC is retained within the endosome for activation of TLR-3. This raises the possibility that the cytokine profile can be tailored by controlling the relative activation of TLR3 and MDA5 pathways, which have been shown to act synergistically in some settings,[76,86,117] via delivery of polyIC with NPs of varying endosomolytic activity, a property we have demonstrated can be precisely tuned via control of polymer composition.[104] If true, this may also afford an opportunity to design NPs capable of leveraging, and optimizing, synergy between multiple nucleic acid adjuvants that engage both cytosolic (e.g., RIG-I, cGAS) and endosomal (e.g., TLR7, 9) PRRs.

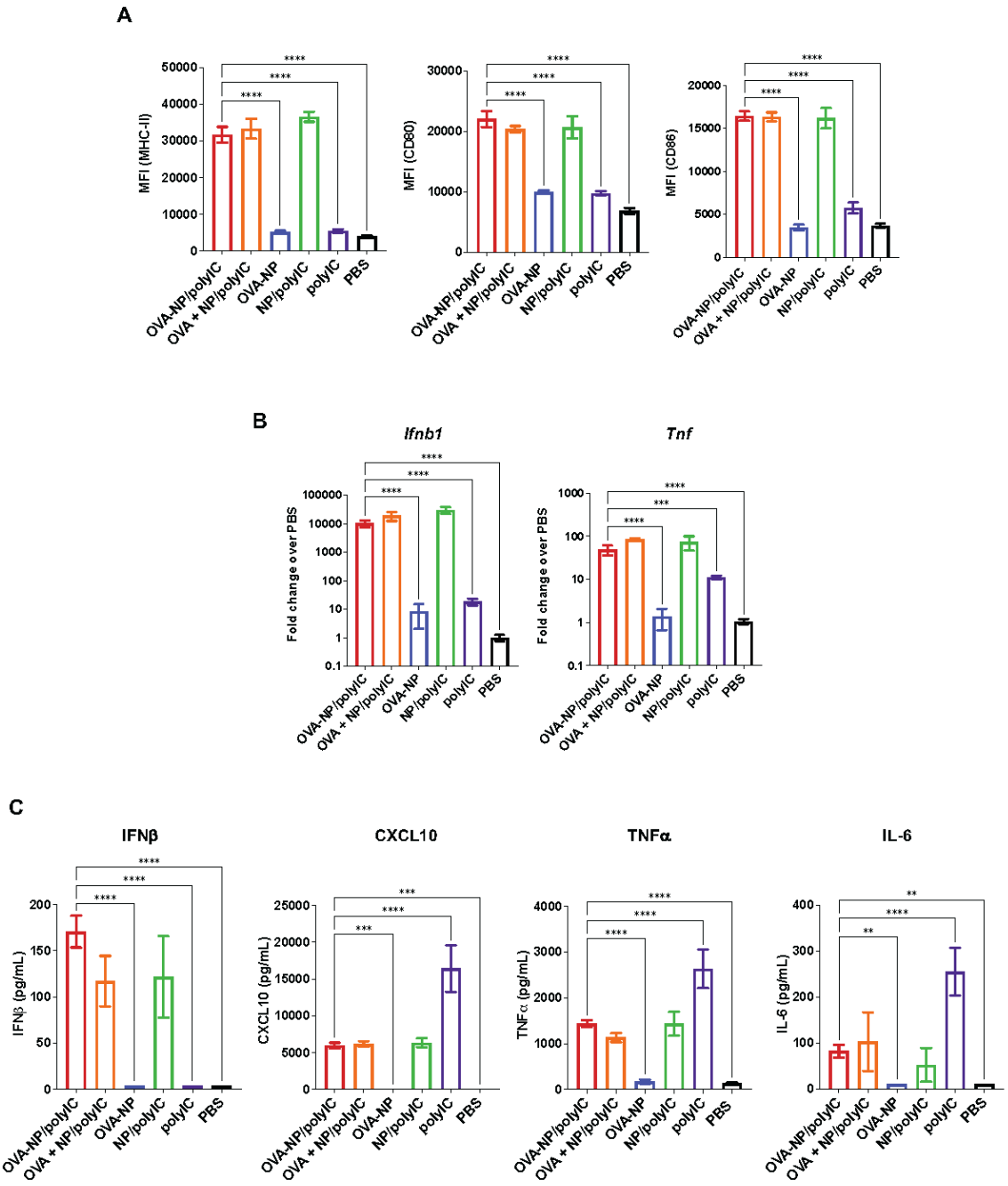

Figure 2.9: pH-responsive nanoparticles enhance delivery of polyIC to the cytosol to enhance dendritic cell activation in vitro. (A) Flow cytometric quantification of median fluorescence intensity (MFI) of CD80, CD86, MHC-II expression by BMDCs treated with indicated formulations. **(B)** Analysis of *Ifnb1* and *Tnf* gene-expression by qRT-PCR in BMDCs treated for 24 h as indicated. **(C)** Concentration of secreted cytokines by BMDCs treated with indicated formulations for 24 h. Statistical data are presented as mean ± SD; n = 4; statistical significance between OVA-NP/polyIC vs other indicated formulations are shown; *P <0.05, **P < 0.01, ***P < 0.001, ****P < 0.0001; one-way ANOVA with Tukey's multiple comparisons test.

Nanoparticle Vaccine enhances MHC-I antigen presentation *in vitro*

Finally, we evaluated the capacity of endosomolytic NPs to enhance MHC-I antigen presentation, using OVA as a model antigen. We treated DC2.4 dendritic cells with free OVA, OVA-NP, OVA-NP/polyIC, OVA + NP/polyIC, and OVA + polyIC, and $OVA_{257-264}$ (SIINFEKL) peptide. In vitro presentation of the immunodominant MHC-I restricted OVA epitope SIINFEKL was assessed by flow cytometry using a fluorescently-labeled antibody that recognizes H-2Kb-bound SIINFEKL (**Figure 2.10**). First, we found that covalent conjugation of OVA to NPs via a disulfide linker significantly enhanced SIINFEKL presentation on MHC-I compared to free OVA and a mixture of OVA and polyIC. This is consistent with our previous findings using other pH-responsive endosomolytic polymers that promote cytosolic antigen delivery.25-27,74 MHC-I presentation of SIINFEKL was further augmented upon complexation of OVA-NP conjugates with polyIC. Collectively, these results demonstrate that pH-responsive, endosomolytic NPs facilitate the cytosolic co-delivery of OVA and polyIC, resulting in DC activation, production of IFN-I, and enhanced class I antigen presentation, with the potential to enhance CD8+ T cell activation.

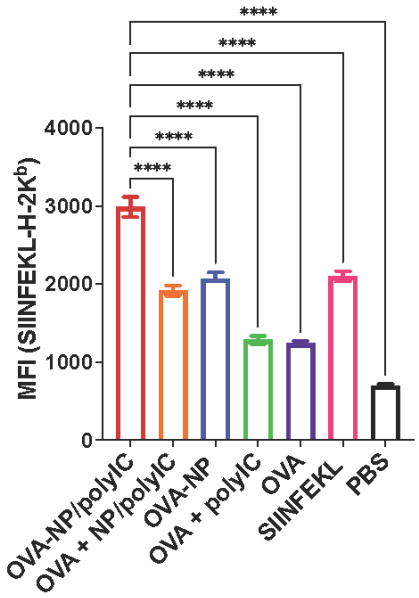

Figure 2.10: pH-responsive nanoparticles enhance dual-delivery of antigens and polyIC to the cytosol to enhance class I antigen presentation in vitro. Flow cytometric analysis of the median fluorescent intensity (MFI) of DC2.4 cells treated with indicated formulations and stained with PE-labeled anti SIINFEKL/H-2kb antibody (mean ± SD; n = 4; statistical significance between OVA-NP/polyIC vs other indicated formulations are shown; *P <0.05, **P < 0.01, ***P < 0.001, ****P < 0.0001; one-way ANOVA with Tukey's multiple comparisons test).

2.4 Conclusion

Efficient cytosolic delivery of protein antigens and nucleic acid adjuvants is essential for inducing a strong CD8+ T cell immune response. Many strategies using stimuli-responsive polymeric systems have been developed to deliver protein antigens to the cytosol and nucleic acid adjuvants to their intracellular targets to maximize antigen cross-presentation and DC activation. We utilized RAFT polymerization to synthesize a well-defined, multifunctional NP platform that enables co-loading of antigens and nucleic acid adjuvants and also harnesses a potent endosomal escape mechanism to facilitate cargo delivery into the cytosol. Taken together, our data shows that cytosolic delivery of antigen resulted in increased antigen presentation on MHC-I molecules, while endosomal escape of polyIC strongly increased its immunostimulatory potency via the MDA-5

pathway, resulting in proinflammatory cytokine production, costimulatory molecule upregulation, and IFN-I secretion by dendritic cells. Collectively, these data indicate that pH-responsive, endosomolytic polymeric platform is a promising and versatile platform for cytosolic delivery of antigen and nucleic acid adjuvants, and offers a promising strategy for enhancing CD8+ T cell responses, which is explored in more detail in the subsequent chapter.

2.5 Materials and Methods

Polymer synthesis and characterization

Reversible addition-fragmentation chain transfer (RAFT) was used to synthesize the amphiphilic diblock copolymer *poly*[(polyethylene glycol) methacrylate)$_{0.9}$-*co*-(pyridyl disulfide ethyl methacrylate)$_{0.1}$]$_{13.7kDa}$-*block*-[(dimethylamino ethyl methacrylate)$_{0.5}$-*co*-(butyl methacrylate)$_{0.5}$]$_{15.3kDa}$ (*p*[(PEGMA$_{0.9}$-*co*-PDSMA$_{0.1}$)]$_{13.7kDa}$-*b*-[(DMAEMA$_{0.5}$-*co*-BMA$_{0.5}$)]$_{15.3kDa}$. The chain transfer agent (CTA) used was 4-cyano-4-(phenyl-carbonothioylthio) pentanoic acid (Sigma-Aldrich) and the initiator used was 2,2′-azobis(4-methoxy-2,4 dimethylvaleronitrile) (V-70) (Wako Chemicals, Richmond, VA). Inhibitors were removed from monomer stocks by gravity filtration through an aluminum oxide column (activated, basic, Brockmann I; Sigma Aldrich).

For synthesis of the first block, filtered PEGMA (Mw = 300 Da, Sigma-Aldrich) and PDSMA (synthesized as previously described with minor modification) was allowed to react under a nitrogen atmosphere in dioxane (40 wt % monomer) at 40°C for 24 h in an oil bath. The initial molar ratio of DMAEMA to PDSMA was 90:10, and the initial monomer ($[M]_0$) to CTA ($[CTA]_0$) to initiator ($[I]_0$) ratio was 55:1:0.2. The resultant poly(PEGMA-co-PDSMA) macro-chain transfer agent (mCTA) was isolated by dialysis against pure acetone (3x) using a 3.5 kDa MWCO SnakeSkin™ membrane (Thermo Fisher Scientific), followed by half-acetone and half-deionized

water (2x), and pure deionized water (1x). Following dialysis, the purified mCTA was frozen at -80°C for 5 h and then lyophilized for 3 days.

For the second block, purified mCTA was used for block copolymerization of filtered DMAEMA (Sigma Aldrich) and BMA (Sigma Aldrich) to create a pH-responsive polymer. DMAEMA (50%) and BMA (50%) ($[M]_0/[mCTA]_0 = 143$) were added to the mCTA dissolved in dioxane (40 wt % monomer and mCTA) along with V-70 initiator ($[mCTA]_0/[I]_0 = 5$). The solution was sealed and purged with nitrogen gas for 30 minutes and then allowed to react for 18 h at 30°C in an oil bath. The resulting amphiphilic diblock copolymer was isolated by precipitation into 80:20 pentane/ether and dried under vacuum for 48 h and stored in solid form at 4°C.

^{1}H NMR ($CDCl_3$ with TMS; Bruker AV400 spectrometer) was used to calculate polymer composition, degree of polymerization, and theoretical molecular weight of both the mCTA and diblock copolymer (**Figure 2.11**).

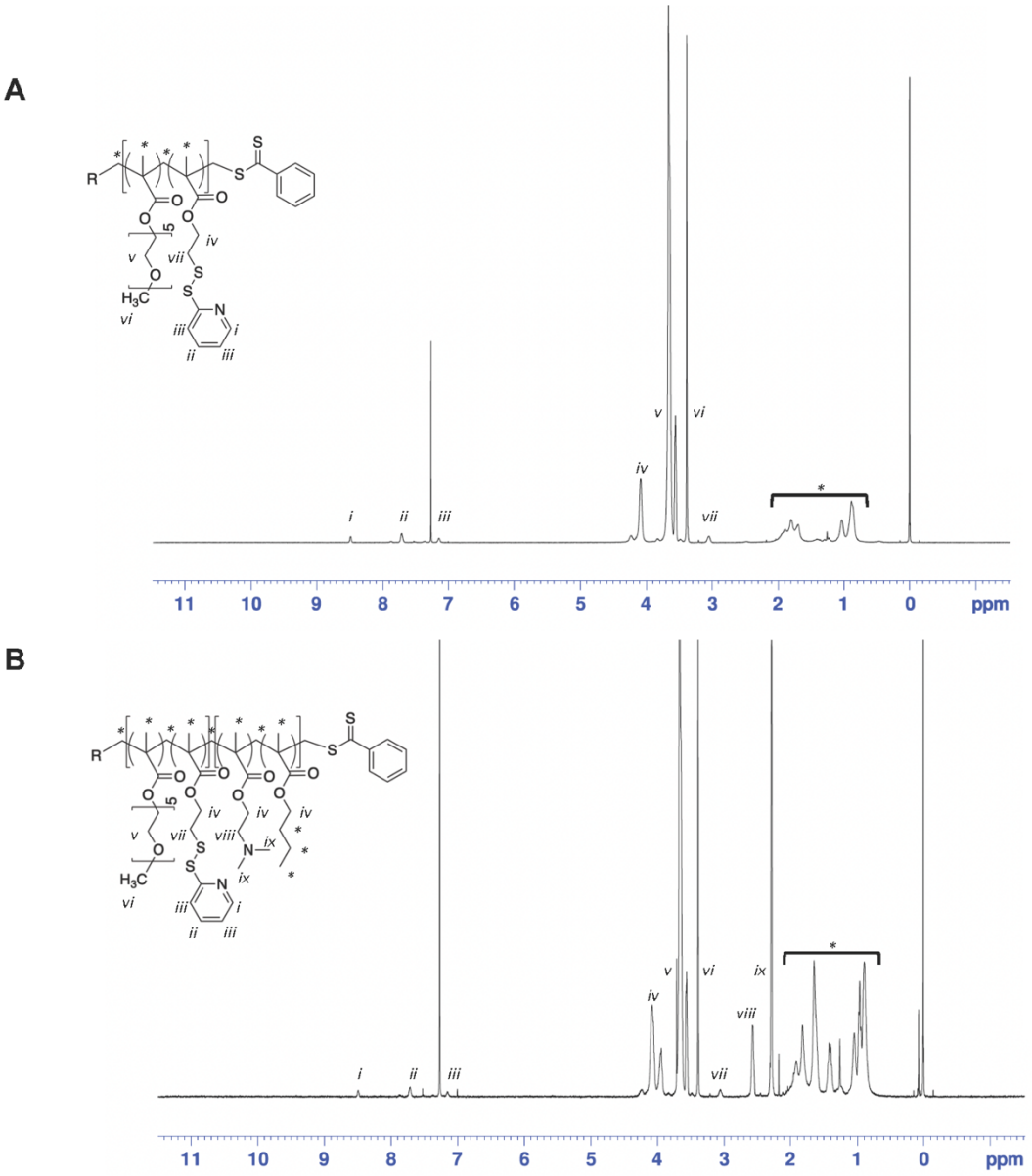

Figure 2.11: Polymer characterization. (A, B) Representative ^{1}H-NMR ($CDCl_3$) of **(A)** PEGMA-co-PDSMA macroCTA, and **(B)** (PEGMA-co-PDSMA)-block (DMAEMA-co-BMA) deblock copolymer.

Preparation and characterization of polymer nanoparticles

Self-assembled micellar nanoparticles (NPs) were formulated by dissolving lyophilized polymer in ethanol to 50 mg/mL, followed by rapidly pipetting aliquots into phosphate buffer (100 mM, pH 7) to a final concentration of 10 mg/mL. For in vivo studies, ethanol was removed by buffer exchange into PBS (pH 7.4) via three cycles of centrifugal dialysis (Amicon, 3 kDa MWCO, Millipore), and NP solutions were then passed through a 0.2 μm Whatman® Puradisc polyethersulfone sterile filter (MilliporeSigma). Final polymer concentration was determined by measuring absorbance at 300 nm using a conventional UV−vis spectrophotometer (Synergy H1 Multi-Mode Microplate Reader, BioTek). The hydrodynamic size and zeta potential of the NPs was measured by dynamic light scattering (DLS) using a Malvern Zetasizer (Malvern, USA) (**Figure 2.12**).

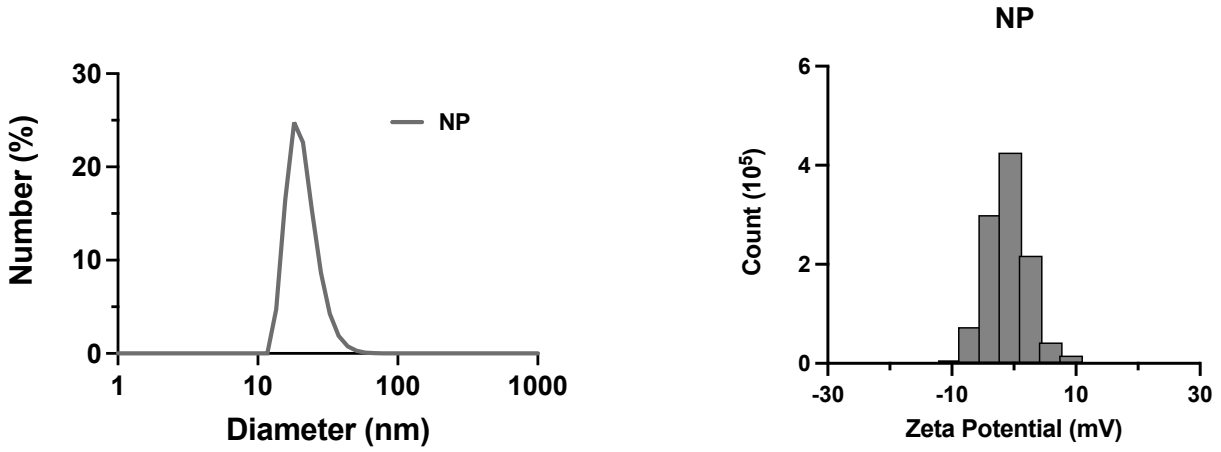

Figure 2.12: Characterization of nanoparticles. (A) Number average DLS trace indicating hydrodynamic diameter of nanoparticles. **(B)** Zeta potential of nanoparticles.

Preparation of antigen−nanoparticle conjugates

To covalently conjugate the model antigen, ovalbumin (OVA), to the pendant PDSMA groups on the NP via thiol−disulfide exchange reaction, free amines on the OVA protein were thiolated by incubation with ∼24 molar excess of 2-iminothiolane (Traut's Reagent, Thermo Fisher Scientific) in reaction buffer (100 mM phosphate buffer, pH 8, supplemented with 1 mM EDTA), as previously described.[118] The unreacted 2-iminothiolane was removed by buffer exchanging thiolated OVA into 1x PBS (pH 7.4) using Zeba Spin desalting columns (0.5 mL, 7 kDa MWCO, Thermo Fisher Scientific). For *in vivo* studies, thiolated OVA was sterilized via syringe filtration (0.2 μm, Millipore). The molar ratio of thiol groups to OVA protein was determined using Ellman's reagent (Thermo Fisher Scientific) according to the manufacturer's instructions and ∼3−5 thiols per OVA were incorporated. Thiolated OVA was then reacted with polymer NPs at various molar ratios of NP:OVA (4:1, 8:1, 10:1) in PBS to make OVA−NP conjugates. Conjugation was done overnight, in the dark, at room temperature, and under sterile conditions, as previously described.[70,118] Antigen conjugation was verified via nonreducing SDS-polyacrylamide gel electrophoresis (SDS-PAGE) using 4−20% Mini-Protean TGX Precast protein gels (Bio-Rad). Gels were run at 130 V for 1 h and imaged with a Gel Doc EZ System (Bio-Rad). A conjugation ratio of 8:1 was used for all *in vitro* and *in vivo* formulations in order to maximize the amount of antigen delivered while maintaining particle stability. OVA from chicken egg white (MilliporeSigma) was used for conjugation characterization, and Endotoxin-free (<1 EU/mg) EndoFit OVA (Invivogen) was used for *in vivo* studies. OVA labeled with Alexa Fluor 647-NHS ester (AF647; Thermo Fisher Scientific) at a 2:1 AF647:OVA molar ratio was used to evaluate conjugation efficiency via fluorescent imaging of SDS-PAGE gels and for tracking conjugates

after in vivo administration. DLS was used to measure the size of OVA−NP conjugates, as described above.

Formulation of nanoparticle/polyIC complexes

NP/polyIC complexes were formed by combining low molecular weight polyIC (Invivogen) with NP and OVA-NP in citric acid buffer (pH 4, 100 mM) at different theoretical charge ratios (+/-). After incubating at room temperature for 30 min, 2x volume 100 mM phosphate buffer (pH 8) supplemented with 2 mM NaOH was added and mixed rapidly to form NP/polyIC complexes. The charge ratio was defined as the molar ratio between protonated DMAEMA tertiary amines in the second block of the copolymer (positive charge; assuming 100% protonation at pH 4) and phosphate groups on polyIC backbone (negative charge). The charge ratios at which complete complexation of polyIC to the polymer occurred was determined via an agarose gel retardation assay. Free polyIC and complexes prepared at various charge ratios were loaded into lanes of a 2% agarose gel and run at 100 V for 1 h. Gels were stained with SYBR Safe (Invitrogen) for 1 h while protected from light and then imaged with a Gel Doc EZ system (Bio-Rad). A charge ratio of 6:1 was used for all *in vitro* and *in vivo* formulations in order to maximize the amount of polyIC delivered while maintaining stability of formulation. DLS was used to measure the size of the polyIC complexed with OVA-NP conjugates (OVA-NP/polyIC) formulation, as described above.

Erythrocyte lysis assay

The capacity of free polymer, ova polymer conjugates, and conjugate/polyIC complexes to induce pH-dependent disruption of lipid bilayer membranes was assessed via a red blood cell hemolysis assay as previously described.[106] Briefly, whole blood from de-identified patients was acquired from Vanderbilt Technologies for Advanced Genomics (VANTAGE) core. Blood was centrifuged to pellet erythrocytes, plasma was aspirated, and erythrocytes were resuspended in pH 7.4 PBS, and washed three times with PBS. After the final wash, erythrocytes were resuspended in 100 mM sodium phosphate buffer (supplemented with 150 mM NaCl) in the pH range of the endosomal processing pathway (pH 7.4, 7.0, 6.6, 6.2 and 5.8) and incubated with 10, 5, or 1 μg/mL polymer formulations (NP, OVA-NP, NP/polyIC, and OVA-NP/polyIC in a 96-well U-bottom plate for 1 h at 37°C. The extent of red blood cell lysis was determined using a UV−vis spectrophotometer (Synergy H1 Multi-Mode Microplate Reader, BioTek) by measuring the amount of hemoglobin released (abs = 541 nm) and normalized to a 100% lysis control (1%Triton X-100). Samples were run in quadruplicate.

Gal8 recruitment assay

Gal8 recruitment assay was performed as previously described with minor modifications.[107] Gal8-MDA-MB-231 cells were cultured and maintained in DMEM containing 4.5 g/L D-glucose and supplemented with 25 mM HEPES, 10% FBS, 100 U/mL penicillin, and 100 μg/mL streptomycin. Gal8-MDA-MB-231 cells were seeded in a 96 well cell culture microplate (Grenier) at a density of 5000 cells per well and allowed to adhere overnight. The following day, cells were treated with indicated nanoparticle formulations or PBS (Gibco). After a 16 h treatment, the media was aspirated and replaced with 100 μL of imaging media (FluoroBrite

DMEM supplemented with 25 mM HEPES, 10% FBS, 100 U/mL penicillin and 100 μg/mL streptomycin, and 4 μM Hoechst 33342 (ThermoFisher Scientific)). Cells were imaged using a 20x objective on an ImageXpress Micro XLS Widefield High-Content Analysis System. Four images were taken per well, and four wells were replicated per treatment, for a total of sixteen images per treatment (for PBS, twelve wells were replicated for a total of forty-eight images). Images were analyzed using the MetaXpress software Transfluor Application module to quantify the integrated YFP intensity and fluorescent nuclei per image, and integrated YFP intensity was normalized to the number of nuclei in each image. Statistics and graphing were then performed treating each image as an independent replicate.

Cell culture

The IRF and NF-κB reporter cell lines, human lung carcinoma A549-DualTM (Invivogen) and the murine macrophage cell line RAW-DualTM (Invivogen), were cultured in DMEM (Gibco) supplemented with 2 mM L-glutamine, 4.5 g/L D-glucose, 10% heat inactivated fetal bovine serum (HI FBS, Gibco), and 100 U/mL penicillin/100 μg/mL streptomycin (Gibco). The human monocyte cell line THP1-DualTM (Invivogen) was cultured in RPMI 1640 (Gibco) supplemented with 2 mM L-glutamine, 10% fetal bovine serum (FBS, Gibco), and 100 U/mL penicillin/100 μg/mL streptomycin (Gibco). The murine dendritic cell line DC2.4 was kindly provided by K. Rock (University of Massachusetts Medical School) and cultured in RPMI 1640 (Gibco) supplemented with 10% fetal bovine serum (HI FBS; Gibco), 2 mM L-glutamine, 100 U/mL penicillin/100 μg/mL streptomycin (Gibco), 50 μM 2-mercaptoethanol (Gibco), 1x nonessential amino acids (Cellgro), and 10mM HEPES (Invitrogen). Gal8-MDA-MB-231 cells were cultured and maintained in DMEM containing 4.5 g/L D-glucose and supplemented with 25 mM HEPES,

10% FBS, 100 U/mL penicillin, and 100 μg/mL streptomycin. All cell types were grown in a humidified atmosphere at 37 °C in 5% CO_2.

In vitro evaluation of polyIC activity

Reporter cell lines that allow the simultaneous detection of activated NF-κB pathways, quantified by monitoring SEAP activity, and the IRF pathway, assessed by secreted luciferase activity, were used to evaluate the biological activity of NP/polyIC. Briefly, murine RAW-Dual™ cells (macrophages; Invivogen) and human A549-Dual™ cells (lung epithelial; Invivogen) were plated at 5 x 10^4 cells/well in a 96-well plate, and allowed to adhere overnight. Human THP1-Dual™ cells (monocytes; Invivogen) are a suspension cell line so they were plated the same day as dosing at 1 x 10^5 cells/well. NP/polyIC was formulated as detailed above. A dose range was used to stimulate cells in the following groups: OVA-NP/polyIC, NP/polyIC, empty NP, free polyIC, or PBS for 24 h at 37°C with 5% CO_2. After incubation, cells were centrifuged at 1,500 rpm for 5 min; supernatant was collected and reporter proteins were measured using QUANTI-Blue™ (Invivogen), a SEAP detection reagent, and QUANT-Luc™ (Invivogen), a luciferase detection reagent by following the manufacturer's instructions. Luminescence from luciferase activity and absorbance of SEAP were measured using a spectrophotometer (Synergy H1 Multi-Mode Microplate Reader, BioTek). All measurements were normalized after baselining to the average value of the PBS-treated negative control group. Values for EC_{50} were extrapolated from dose-response curve fits using GraphPad Prism software.

In vitro evaluation of polyIC activity in MDA-5 deficient cells

RAW-Lucia™ ISG cells and RAW-Lucia™ ISG KO-MDA-5 cells were used to evaluate the role in MDA-5 in NP/polyIC function by monitoring interferon regulatory factor (IRF)-induced Lucia luciferase activity. Briefly, 5 x 10^4 cells/well in a 96-well plate were allowed to adhere overnight. A dose range of NP/polyIC formulated as above were used to treat cells in the following groups: OVA-NP/polyIC, NP/polyIC, empty NP, free polyIC, a physical mixture of Lipofectamine 2000 and polyIC, or PBS for 24 h at 37°C with 5% CO_2. Following incubation, cells were centrifuged for 5 min at 1,500 rpm and the levels of IRF-induced Lucia in the supernatant were measured using QUANTI-LucTM (Invivogen), a Lucia luciferase detection reagent as described above. All measurements were normalized to the average value of the PBS-treated negative control group.

In Vitro evaluation of BMDC activation and maturation

Bone marrow cells were harvested from femurs and tibias of 6-8 week-old female C57Bl/6J mice by flushing them with cold PBS. Cells were centrifuged for 5 minutes at 450 x g and resuspended in complete BMDC culture media (RPMI 1640 medium supplemented with 10% heat-inactivated FBS, 100 U/mL penicillin, 100 µg/mL streptomycin, 2 mM L-glutamine, 10 mM HEPES, 1 mM sodium pyruvate, 1x non-essential amino acids, 50 µM β-mercaptoethanol, and 20 ng/mL GM-CSF). The cell suspension was passed through a 70 µM cell strainer (FisherbrandTM; Thermo Fisher Scientific), and seeded in 100 x 15 mm non-tissue-culture-treated Petri dishes (Corning Inc.) in complete medium containing 20 ng/mL granulocyte-macrophage colony-stimulating factor (GM-CSF) to induce differentiation into BMDCs. Cell were cultivated in a humidified chamber maintained at 37°C with 5% CO2. Fresh complete BMDC culture medium

was added on days 3, 5, and 7. On day 8, the percentage of CD11c+ cells (i.e., BMDCs) was confirmed to be greater than 80% as measured by flow cytometry using anti-CD11c-FITC (clone N418; BioLegend) (**Figure 2.13**). BMDCs were seeded into wells of 12-well plates (Greiner Bio-One) at 6 x 105 cells/well. BMDCs were treated with OVA-NP/polyIC, OVA + NP/polyIC, OVA-NP, NP/polyIC, OVA + polyIC, free polyIC, MPLA (TLR-4 agonist; positive control), or PBS for 24 h at 37°C with 5% CO2. Following incubation, cells were scraped, washed with FACS buffer (PBS supplemented with 2% FBS), incubated with Fc-block (anti-CD16/CD32; clone 2.4G2; Tonbo) for 15 min at 4°C, and then stained with antibodies against the markers of DC activation: anti-CD80-PE/Cy5 (clone 16-10A1; BioLegend), anti-CD86-PE/Cy7 (clone GL-1; BioLegend) and anti-MHC-II-APC/Cy7 (clone M5.114.15.2; BioLegend) for 1 h at 4°C. Cells were then washed twice in FACS buffer, resuspended using FACS buffer supplemented with 1 µg/mL DAPI, and analyzed using an Luminex CellStream flow cytometer. Each treatment was performed with 3 technical replicates, and the experiment was conducted 3 times with similar results.

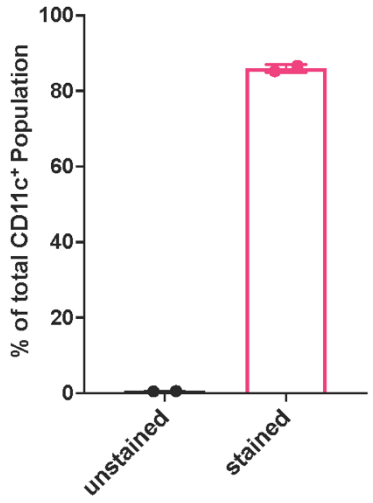

Figure 2.13: Confirmation of BMDC differentiation. Bone marrow cells were harvested and treated with GM-CSF to induce differentiation into BMDCs. The percentage of CD11c+ cells (i.e., BMDCs) was confirmed to be greater than 80% as measured with by flow cytometry using anti-CD11c-FITC.

For qRT-PCR analysis of gene expression, BMDCs were seeded in 12-well plates at 6 x 10^5 cells/well. BMDCs were treated as above for 6 h. Following incubation, cells were washed with PBS and 700 μL of RLT lysis buffer (Qiagen) was added to each well. Lysates were stored at -80°C until use. Messenger RNA (mRNA) was extracted from cell lysates using an RNA isolation kit (RNeasy mini kit, Qiagen). Complementary DNA (cDNA) was synthesized for each sample using a cDNA synthesis kit (iScript, Bio-Rad) and analyzed using qRT-PCR using Taqman kits (Thermo Fischer Scientific) and a CFX real-time PCR detection system (Bio-Rad) following the manufacturer's instructions. Taqman probes for mouse *Ifnb1* (Mm00439552_s1), *Tnf* (Mm00443258_m1), and *Hmbs* (Mm01143545_m1) were purchased from Thermo Fischer Scientific. Fold change was calculated using the $\Delta\Delta C_t$ method.

For analysis of secreted cytokines, supernatants were collected from BMDCs 24 h after treatment. A LEGENDplex Multi-Analyte Flow Assay Kit was used to measure secreted IFNβ, CXCL10, TNF-α, and IL-6 following the manufacturer's instructions using a V-bottom plate. Data were collected on an Amnis CellStream Luminex Flow Cytometer equipped with 405, 488, 561, and 642 nm lasers and analyzed with LEGENDplex Data Analysis software v8.0 (VigeneTech).

In Vitro dendritic cell antigen presentation assay

An antibody that recognizes the mouse MHC-I (H-2K^b)-bound SIINFEKL was used to determine the effect of pH-responsive, endosomolytic NPs on protein antigen cross-presentation. Briefly, DC2.4 cells were plated at 2 x 10^5 cells/well in a 12-well plate and allowed to adhere overnight. DC2.4 cells were treated with either OVA-NP/polyIC, OVA + NP/polyIC, OVA + polyIC, free OVA, PBS (negative control), or SIINFEKL peptide (positive control) for 24 h as described above. Following incubation, cells were treated with trypsin, washed, and resuspended

with FACs buffer, incubated with Fc-block (anti-CD16/CD32; clone 2.4G2; Tonbo) for 15 minutes at 4ºC, and then stained with PE/Dazzle 594-conjugated SIINFEKL/H-2K^b-reactive monoclonal antibody (clone 25.D1.16; Biolegend) for 1 h at 4°C. Cells were then washed 3x in FACS buffer, resuspended using FACS buffer supplemented with 1 μg/mL DAPI, and the relative levels of SIINFEKL/H-2K^b presentation was analyzed using an Amnis CellStream Luminex flow cytometer. Each treatment was performed with 3 technical replicates, and the experiment was conducted 3 times with similar results.

Statistical analysis

Significance for each experiment was determined as indicated in the corresponding figure captions. All analyses were done using GraphPad Prism software, version 9.3.1. Plotted values represent experimental means, and error bars represent S.E.M. unless otherwise noted in the figure captions. **** $P < 0.0001$, *** $P < 0.005$, **$P < 0.01$, * $P < 0.05$.

CHAPTER 3

Nanovaccine Enhances Cellular Immunity and Protects Against Murine Tumor Challenge

Text for Chapter 3 adapted from:

Carson CS, Becker KW, Garland KM, Pagendarm HM, Stone PT, Arora K, Wang-Bishop L, Baljon JJ, Cruz LD, Joyce S, Wilson JT. A Nanovaccine for Enhancing Cellular Immunity via Cytosolic Co-Delivery of Antigen and PolyIC RNA. *J. Control. Release.* Volume 345, 2022, Pages 354-370, ISSN 0168-3659, https://doi.org/10.1016/j.jconrel.2022.03.020.

3.1 Abstract

Traditional approaches to cancer vaccines elicit weak $CD8^+$ T cell responses and have largely failed to meet clinical expectations. This is in part due to inefficient antigen cross-presentation, inappropriate selection of adjuvant and its formulation, poor vaccine pharmacokinetics, and/or suboptimal coordination of antigen and adjuvant delivery. Here, we demonstrate that the nanovaccine platform increased the accumulation of antigen and polyIC in the local draining lymph nodes and increased expression of *Ifnb1*, *Cxcl10*, and *Tnfa*, critical mediators of antitumor $CD8^+$ T cell activation and recruitment. Consequently, dual-delivery of antigen and polyIC with endosomolytic nanoparticles significantly enhanced the magnitude and functionality of CD8+ T cell responses relative to a mixture of antigen and polyIC, resulting in inhibition of tumor growth in a mouse tumor model. Collectively, this work provides a proof-of-principle for a new cancer vaccine platform that strongly augments anti-tumor cellular immunity via cytosolic co-delivery of antigen and nucleic acid adjuvant.

3.2 Introduction

Cancer vaccines have recently re-emerged as a potentially powerful component of an expanding immunotherapy arsenal. Cancer vaccines aim to amplify preexisting antitumor CD8+ T cells, promote the generation of new tumor antigen-specific T cells, and/or promote CD8+ T cell infiltration into solid tumors. However, most cancer vaccines have demonstrated only a modest capacity to elicit a tumor-specific CD8+ T cell response in patients with limited therapeutic efficacy and disappointing clinical outcomes. These poor responses can be attributed, at least in part, to the relatively low immunogenicity of peptide and protein antigens, which suffer from several intertwined pharmacological shortcomings, including rapid degradation and/or clearance, low accumulation in secondary lymphoid organs (e.g., lymph nodes), and inefficient delivery of antigen to the major histocompatibility complex (MHC) class I (MHC-I) antigen processing pathway, which is essential for generating a CD8+ T cell response. To address these challenges, various approaches have been devised to increase the immunogenicity of cancer vaccine antigens, including the use of more potent adjuvants and/or particle-based delivery systems that promote uptake and cross-presentation of antigen on MHC-I by specific dendritic cell (DC) subsets. However, inefficient antigen cross-presentation, improper choice or delivery of adjuvant, poor vaccine pharmacokinetics, and/or suboptimal coordination of antigen and adjuvant delivery continue to limit the efficacy of many promising strategies.

Having optimized the nanovaccine platform using several *in vitro* techniques in chapter 2, the following will focus on extension of the nanovaccine platform to *in vivo* applications. In these studies, we delivered a model antigen, OVA, and immunostimulatory nucleic acid adjuvant, polyinosinic:polycytidylic acid (polyIC), with the nanovaccine platform. The vast majority of experimentation is performed in murine tumors established from the EG7.OVA cells (C57BL/6 mouse derived EL-4 thymoma line expressing OVA cDNA lymphoma cell line). We demonstrate

that the nanovaccine platform increased the accumulation of antigen and polyIC in the local draining lymph nodes. We further demonstrate that NP/polyIC complexes are significantly more potent than equivalent doses of free polyIC in eliciting pro-inflammatory responses in the lymph node. Consequently, dual-delivery of antigen and polyIC with endosomolytic nanoparticles significantly enhanced the magnitude and functionality of CD8+ T cell responses relative to a mixture of antigen and polyIC, resulting in inhibition of tumor growth in a mouse tumor model. Collectively, this work provides a proof-of-principle for a new cancer vaccine platform that strongly augments anti-tumor cellular immunity via cytosolic co-delivery of antigen and nucleic acid adjuvant.

3.3 Results and Discussion

NP delivery improves the pharmacological properties of antigen and polyIC in vivo

Rapid clearance, poor cellular uptake, and inefficient lymph node (LN) accumulation are major pharmacological barriers that limit the immunogenicity of protein and peptide antigens as well as the potency, and potentially tolerability and safety, of many promising nucleic acid adjuvants.[66,67] It is well-established that nanoparticles less than ~100 nm in diameter can exploit lymphatic drainage to enhance cargo accumulation in vaccine site draining lymph nodes.[66,68] Hence, we postulated that delivery of OVA and polyIC with NPs could address these barriers. To evaluate this, we first used intravital imaging to quantify injection site retention kinetics of AlexaFluor647-labeled OVA and rhodamine-labeled polyIC, formulated with or without loading onto NPs, following subcutaneous administration **(Figure 3.1)**. As anticipated, free OVA and polyIC very rapidly cleared the injection site (i.e., half-life ~1.5 h); polyIC is polydisperse (0.2-1 kbp; ~100-500 kDa) and is highly susceptible to nuclease degradation,[85] and though OVA (43 kDa) is of sufficient molecular weight to be absorbed via the lymphatics[119] it accumulates only

minimally within lymph nodes. By contrast, OVA and polyIC loaded onto NPs cleared the injection site slowly, with injection site half-lives of ~44 h and ~28 h, respectively. This can likely be attributed to the larger size of the OVA-NP/polyIC formulation as well as non-specific interactions with surrounding tissue at the injection site. Additionally, the retention profiles of OVA and polyIC were closely matched when integrated into NPs, an indication of co-transport on common nanocarrier.

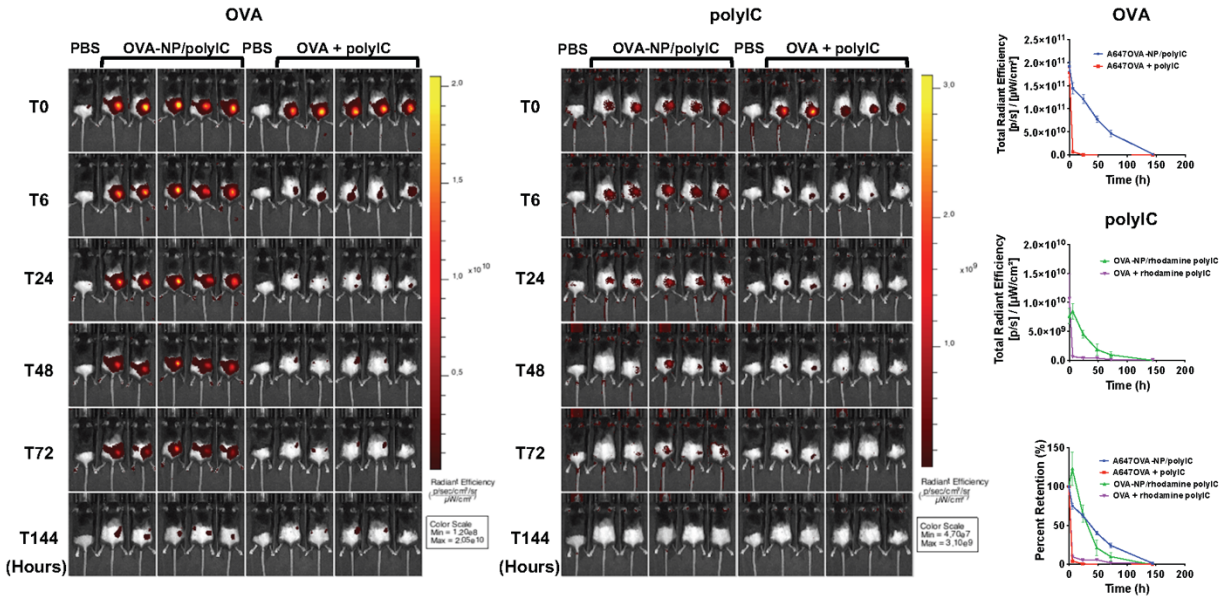

Figure 3.1: NP vaccines modulate antigen and polyIC clearance kinetics. Representative fluorescence IVIS images (left) of mice following subcutaneous administration of NP vaccine formulated with AF647-labeled OVA and rhodamine-polyIC or a soluble mixture of AF647-OVA and rhodamine-polyIC and (right) quantification of relative amounts of OVA and polyIC at the injection site as a function of time post-injection.

To evaluate the distribution of the NP vaccine components to the injection site LN, vaccine formulations containing fluorescently labeled OVA and polyIC were administered subcutaneously to allow for monitoring of carrier and cargo distribution to the draining LN – the inguinal LN **(Figure 3.2A)**. Intravital imaging of inguinal LNs isolated 48 h after injection demonstrated that

loading of antigen and polyIC onto NPs significantly increased their accumulation within the inguinal LN compared to soluble antigen and adjuvant. A slight increase in OVA accumulation was observed when mixed with NP/polyIC, potentially a result of weak non-covalent associations with OVA that affected its distribution behavior. Additionally, a significant increase in the expression of *Ifnb1*, *Cxcl10*, and *Tnfa* in the inguinal LN was observed 6 hours after administration, further demonstrating the ability of NP vaccine to enhance polyIC activity and delivery to the draining LN **(Figure 3.2B)**. Interestingly, and consistent with in vitro data, free polyIC stimulated significantly more Il6 expression than when complexed with the NP, further highlighting the potential to tune the cytokine profile elicited by polyIC via control of nanocarrier properties, with implications for improving vaccine efficacy as well as safety.[113] Collectively, these data demonstrate the ability of the NP vaccine platform to modulate the local pharmacokinetics of a protein antigen and polyIC and thereby enhance their delivery to vaccine site draining LNs.

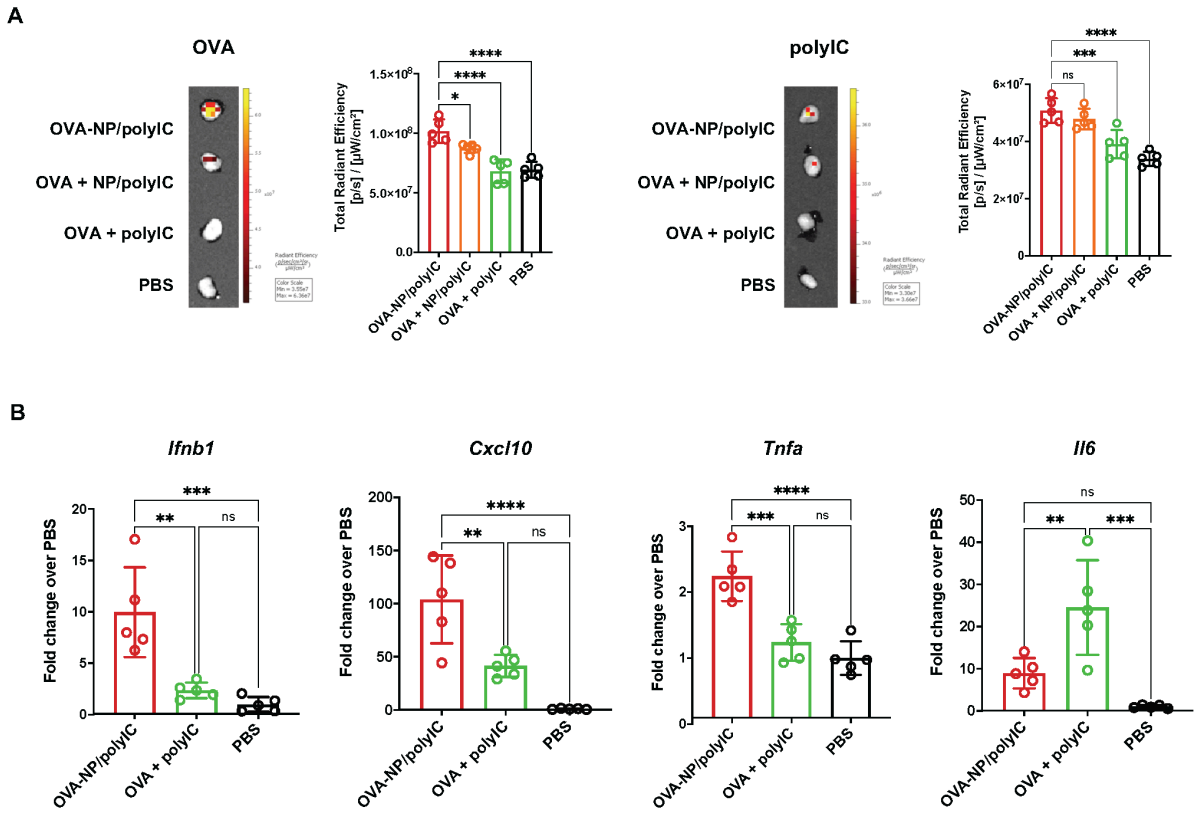

Figure 3.2: NP vaccines enhances OVA and polyIC dual-delivery to draining lymph nodes. **(A)** Representative images and IVIS quantification of fluorescence intensity of the vaccine site draining inguinal LN 48 h following subcutaneous administration of NP vaccine formulated with AF647-labeled OVA and rhodamine-polyIC or a soluble mixture of AF647-OVA and rhodamine-polyIC (mean ± SD; n = 5; statistical significance between OVA-NP/polyIC vs other indicated formulations are shown; *P <0.05, **P < 0.01, ***P < 0.001, ****P < 0.0001; one-way ANOVA with Dunnett's multiple comparisons test). **(B)** Ifnb1, Cxcl10, Tnf, and Il6 expression in the inguinal LN 6 h following administration of indicated vaccine formulation (mean ± SD; n = 5; statistical significance between formulations vs PBS are shown; *P <0.05, **P < 0.01, ***P < 0.001, ****P < 0.0001; one-way ANOVA with Tukey's multiple comparisons test).

Co-delivery of antigen and polyIC with endosomolytic NPs enhances the magnitude and functionality of the CD8$^+$ T cell response

We next evaluated the capacity of nanovaccines to enhance CD8$^+$ T cell responses to the H-2K^b-restricted OVA epitope, SIINFEKL (pOVA), after vaccination. Mice were administered OVA-NP/polyIC, OVA + NP/polyIC, OVA-NP, OVA + polyIC, OVA, or PBS (vehicle), and boosted on days 7 and 14 **(Figure 3.3A)**. On day 20, pOVA/H-2K^b tetramer staining was used to

monitor the magnitude of the SIINFEKL-specific $CD8^+$ T cell response in peripheral blood **(Figure 3.3B)**. OVA-NP/polyIC generated the highest antigen-specific $CD8^+$ T cell response of all of formulations tested, resulting in ~8% SIINFEKL-specific $CD8^+$ T cells in the blood. By contrast, free OVA and a soluble mixture of OVA and polyIC elicited responses undetectable beyond background. Similar to *in vitro* findings, a modest increase in the percentage of pOVA/H-$2K^b$ tetramer-positive $CD8^+$ T cells was observed for free OVA mixed with NPs complexed with polyIC. This likely reflects both the enhanced activity of polyIC when delivered using NPs as well as the slight increase in OVA accumulation associated with this formulation.

On day 21, mice were euthanized and spleens were harvested to track T cell responses with pOVA-H-$2K^b$ tetramer, ICCS, and ELISpot assay. In evaluating the magnitude of SIINFEKL-specific $CD8^+$ T cell response in the spleen by pOVA/H-$2K^b$ tetramer staining, we saw similar results as in the peripheral blood, where OVA-NP/polyIC generated the highest antigen-specific $CD8^+$ T cell response of all the formulations tested, resulting in ~6% SIINFEKL-specific $CD8^+$ T cells **(Figure 3.3C)**. The functionality of the OVA-specific T cell response was also evaluated via peptide restimulation of splenocytes followed by ICCS for TNFα and IFNγ **(Figure 3.3D)**. Vaccination with OVA-NP/polyIC increased the frequency of $TNF\alpha^+IFN\gamma^+$ polyfunctional antigen-specific $CD8^+$ T cells to a greater degree relative to all other formulations tested. A mixture of free OVA and NP complexed with polyIC (OVA+NP/polyIC) also resulted in an increase in the percentage of polyfunctional OVA-specific $CD8^+$ T cells compared OVA + polyIC (P=0.055), consistent with the strong enhancement in immunostimulatory potency achieved via delivery of polyIC with endosomolytic NPs. We further evaluated the frequency of cytokine-secreting $CD8^+$ T cells by IFNγ ELISpot assay after restimulation of splenocytes with the peptide SIINFEKL. Again, we found that OVA-NP/polyIC enhanced the number of IFNγ+ secreting antigen-specific

$CD8^+$ T cells relative to other groups **(Figure 3.3E)**. The improved adjuvant effects of NP/polyIC was further demonstrated via restimulation of splenocytes with the MHC-II H-$2A^b$-restricted OVA epitope ISQAVHAAHAEINEAGR followed by ICCS analysis, which demonstrated that OVA-NP/polyIC and OVA + NP/polyIC similarly enhanced the frequency of $IFN\gamma^+TNF\alpha^+$ $CD4^+$ T cells (i.e., helper type 1 $CD4^+$ T cell; Th1) compared to all other formulations **(Figure 3.3F)**. This is also consistent with the ability of NP/polyIC complexes to increase total IgG endpoint antibody titer against OVA **(Figure 3.3G)**. Hence, while a distinctive feature of endosomolytic NPs is their capacity to promote MHC-I presentation to enhance $CD8^+$ T cell responses, these data also corroborate our previous findings that they are also able to augment $CD4^+$ T cell responses, particularly when co-loaded with a Th1-directing adjuvant.[69,70] The capacity of the platform to promote a balanced $CD8^+/CD4^+$ Th1 response may also further enhance cancer vaccine efficacy given the important role that $CD4^+$ T cells play in supporting $CD8^+$ T cell effector function as well as the intrinsic roles of $CD4^+$ T cells in antitumor immunity.[120,121] Together, these data demonstrate that the adjuvant effects of polyIC, which is a relatively weak adjuvant when administered alone, are strongly augmented when delivered into the cytosol using endosomolytic polymer NPs, and that the $CD8^+$ T cell response can be further enhanced by dual-delivery of antigen and polyIC formulated together using the NP platform.

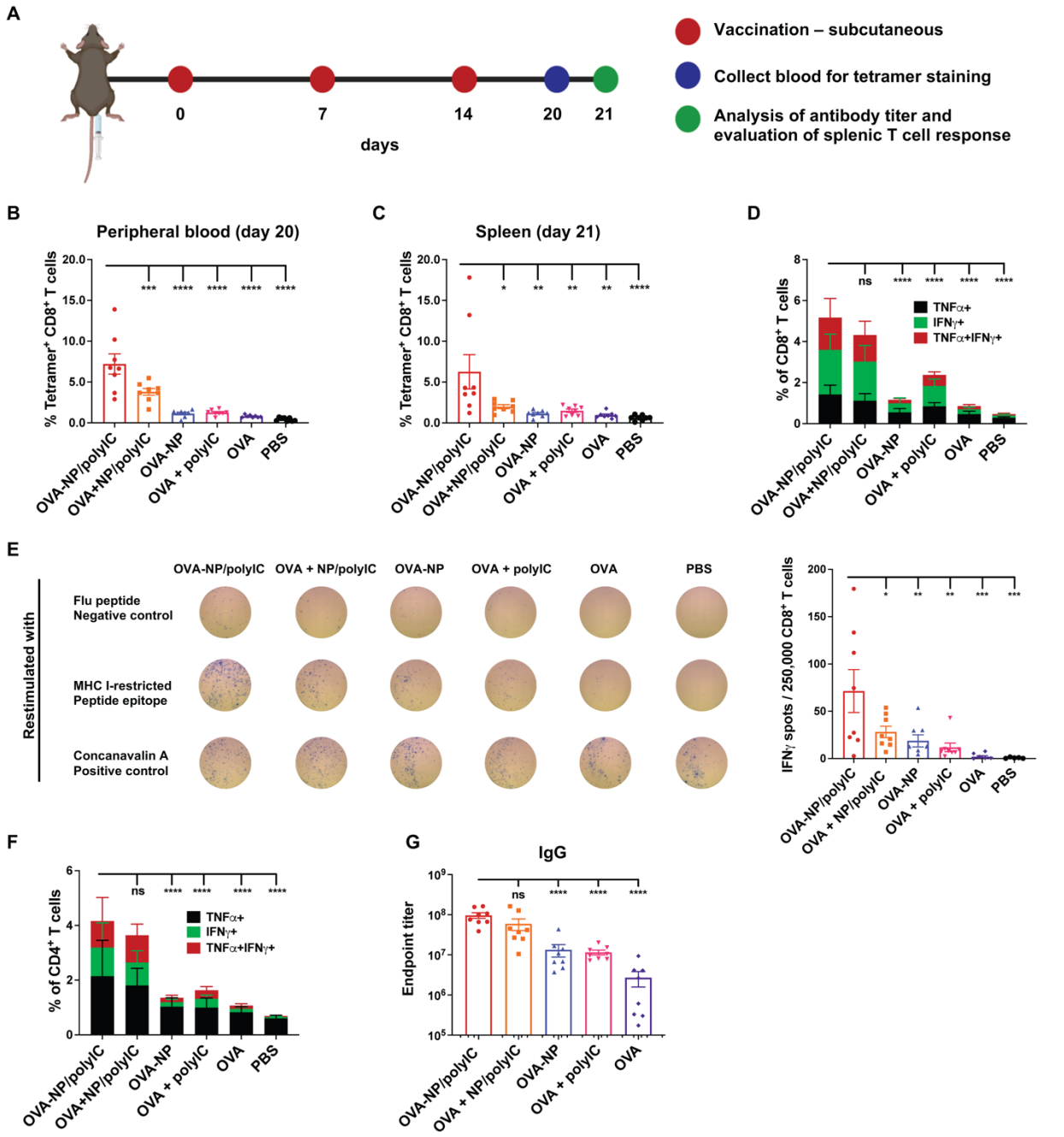

Figure 3.3: Dual-delivery of antigen and polyIC with NPs enhances the magnitude and functionality of CD8+ T cell response. (A) Administration and analysis scheme for mice vaccinated with OVA-NP/polyIC or indicated formulations containing OVA protein. **(B)** Quantification of the frequency of SIINFEKL-specific $CD8^+$ T cells in peripheral blood via peptide/MHC tetramer staining (mean ± SEM; n = 8 mice/group; statistical significance between OVA-NP/polyIC and all other formulations are shown; ***$P < 0.001$, ****$P < 0.0001$; two-way ANOVA with Dunnett's multiple comparison test). **(C)** Quantification of the frequency of SIINFEKL-specific $CD8^+$ T cells in the spleen via peptide/MHC tetramer staining (mean ± SEM; n = 8 mice/group; statistical significance between OVA-NP/polyIC and all other formulations are shown; *P <0.05, **$P < 0.01$, ***$P < 0.001$, ****$P < 0.0001$; two-way ANOVA with Dunnett's

multiple comparison test). **(D)** ICCS was used to determine the percentage of $CD8^+$ T cells positive for IFNγ and/or TNFα after *ex vivo* restimulation of splenocytes with SIINFEKL peptide (mean ± SD; n = 8 mice/group; statistical significance between OVA-NP/polyIC and all other formulations are shown; ****$P < 0.0001$; two-way ANOVA with Tukey's multiple comparison test). **(E)** Representative images of ELISPOT and quantification of $CD8^+$ IFN-γ^+ T cell response after *ex vivo* restimulation of splenocytes with SIINFEKL peptide (mean ± SEM; n = 8 mice/group; statistical significance between OVA-NP/polyIC and all other formulations are shown; *P <0.05, **$P < 0.01$, ***$P < 0.001$, ****$P < 0.0001$; two-way ANOVA with Tukey's multiple comparison test). **(F)** ICCS was used to determine the percentage of $CD4^+$ T cells positive for IFNγ and/or TNFα after *ex vivo* restimulation of splenocytes with ISQAVHAAHAEINEAGR peptide (mean ± SD; n = 8 mice/group; statistical significance between OVA-NP/polyIC and all other formulations are shown; ****$P < 0.0001$; two-way ANOVA with Tukey's multiple comparison test). **(G)** Serum IgG antibody titer at day 21 as measured by ELISA (mean ± SEM; n = 8 mice/group; statistical significance between OVA-NP/polyIC and all other formulations are shown; *P <0.05, **P < 0.01, ***$P < 0.001$, ****$P < 0.0001$; one-way ANOVA with Tukey's multiple comparison test).

Nanovaccine protects from tumor formation and inhibits tumor growth in mice

As a functional validation of the T cell response elicited by vaccination, we next evaluated the ability of NP vaccines to protect against tumor growth following challenge with a murine thymoma EL-4 cell line that expresses OVA as a model antigen (EG7.OVA). Mice were vaccinated subcutaneously and boosted on days 7 and 14 **(Figure 3.4A)**. On day 23, mice were challenged with a contralateral subcutaneous inoculation of EG7.OVA cells, and tumor growth and survival were measured **(Figure 3.4B-D)**. Consistent with the increased magnitude and polyfunctionality of the CD8+ T cell response, vaccination with OVA-NP/polyIC conferred the greatest degree of protection from tumor growth. The OVA + NP/polyIC formulation also afforded some protection from tumor formation. It is also notable that OVA-NP conjugates (i.e., in the absence of polyIC) also inhibited tumor growth to a limited degree but to a level similar to a mixture of OVA + polyIC, a finding consistent with our previous work demonstrating that conjugation of antigens to endosomolytic NPs can enhance cellular immunity even in the absence of an additional adjuvant.[70,122] We re-challenged complete responders ~103 days following the last vaccine treatment with EG7.OVA tumor cells on the opposite flank and monitored tumor volume.

Without any additional treatment, five out of seven (~70%) challenged mice completely resisted tumor growth through at least 50 days. Tumor growth in the remaining two mice was significantly slower relative to naïve controls.

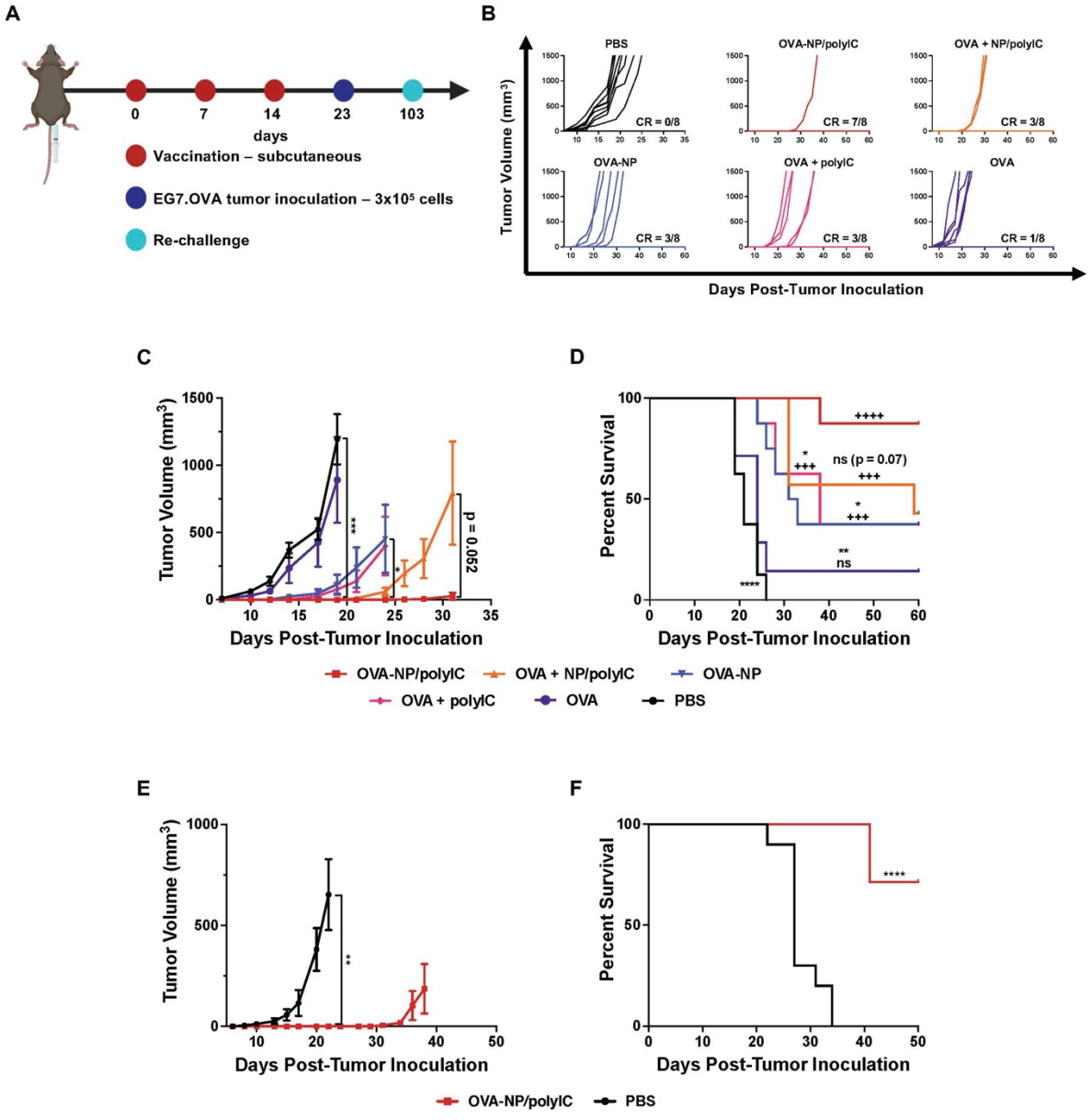

Figure 3.4: Dual-delivery of antigen and polyIC protects from tumor formation in a mouse tumor model. (A) Administration, analysis, and tumor challenge scheme for mice immunized with OVA-NP/polyIC or indicated formulations containing OVA protein. **(B)** Spider plots of individual tumor growth curves, with the numbers of mice exhibiting complete responses (CR) denoted. **(C)** Average tumor volume following challenge with EG7.OVA cells of mice immunized

with indicated vaccine formulations (mean ± SEM; n = 8 mice/group; P=0.052 for OVA-NP/polyIC vs. OVA + NP/polyIC on day 31 via unpaired t test). **(D)** Kaplan-Meier survival curves of mice growing EG7.OVA tumors treated with indicated formulations using 1500 mm^3 tumor volume as the end point (n = 8 mice/group; statistical significance between OVA-NP/polyIC and all other formulations are shown; *P <0.05, **P < 0.01, ***P < 0.001, ****P < 0.0001; Mantel-Cox log-rank test; statistical significance between PBS and all other formulations are shown; +P <0.05, ++P < 0.01, +++P < 0.001, ++++P < 0.0001; Mantel-Cox log-rank test). **(E)** Mice showing complete responses to indicated treatment groups were re-challenged with EG7.OVA cells on the contralateral flank 103 d after inoculation without any further treatment. **(F)** Kaplan-Meier survival curves of complete responders using 1500 mm^3 tumor volume as the end point.

Finally, we determined whether endosomolytic NPs improve the efficacy of therapeutic cancer vaccines in proof-of-concept experiments. Mice were treated beginning 5 days after subcutaneous inoculation of EG7.OVA cells and were boosted on days 12 and 19, and tumor growth was monitored **(Figure 3.5A)**. Therapeutic vaccination with the OVA-NP/polyIC formulation significantly inhibited tumor growth and extended mean survival time relative to mice vaccinated with OVA only, a mixture of polyIC and OVA, or OVA-NP conjugates, which had an insignificant effect on tumor growth **(Figure 3.5B-D)**. In accord with our other studies, immunization with OVA + NP/polyIC also inhibited tumor growth, though to a slightly lesser degree than when OVA was also covalently bound to the carrier.

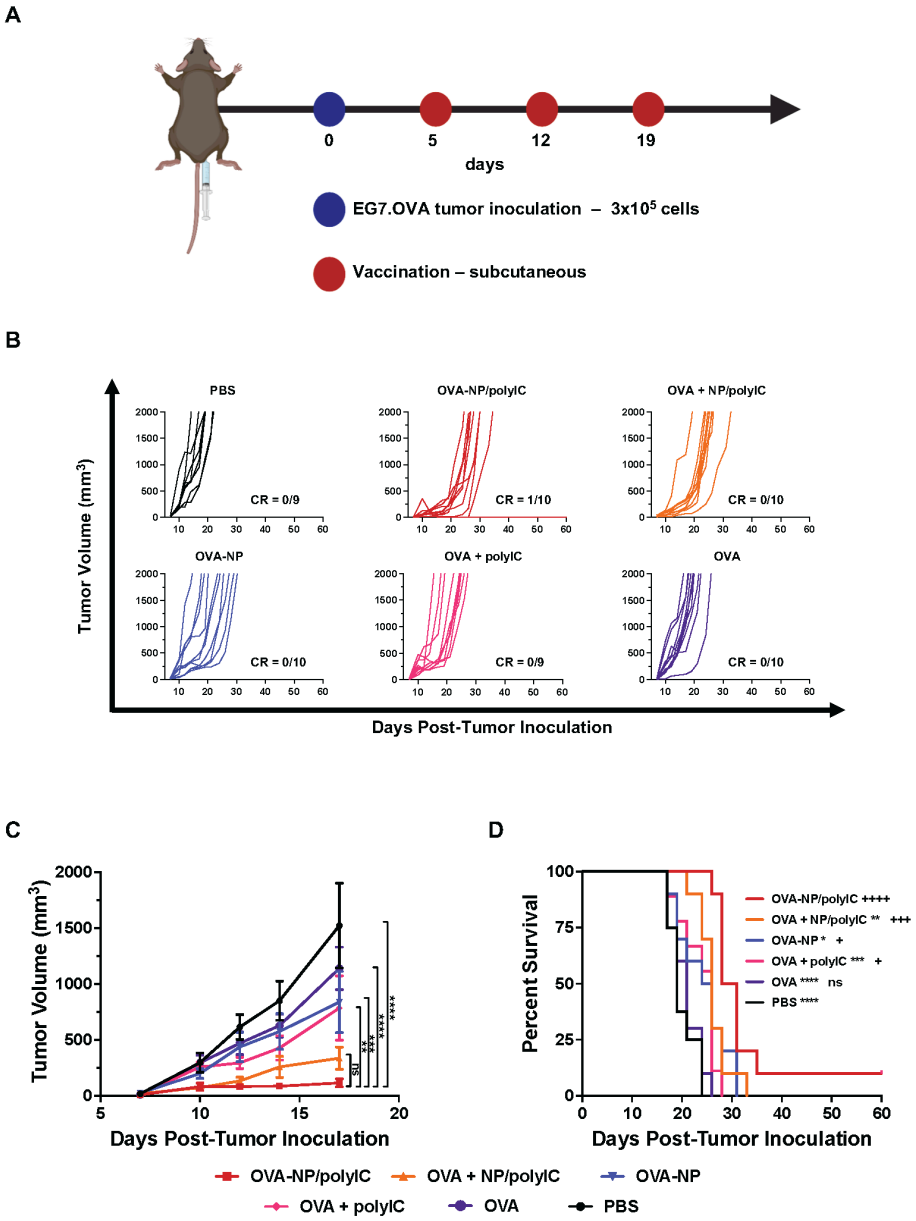

Figure 3.5: Dual-delivery of antigen and polyIC inhibits tumor growth in a mouse tumor model. (A) Tumor inoculation and therapeutic vaccination scheme for mice immunized with OVA-NP/polyIC or indicated formulations containing OVA protein. **(B)** Spider plots of individual tumor growth curves, with the numbers of complete responders (CR) denoted. **(C)** Average EG7.OVA tumor volume in response to indicated treatments (mean ± SEM; n = 8-10 mice/group; *P <0.05, **P < 0.01, ***P < 0.001, ****P < 0.0001; unpaired t test of OVA-NP/polyIC vs. all other formulations on day on day 17). **(D)** Kaplan-Meier survival curves of mice growing EG7.OVA tumors treated with indicated formulations using 2000 mm3 tumor volume as the end point (n=8-10 mice/group; statistical significance between OVA-NP/polyIC and all other formulations are shown; *P <0.05, **P < 0.01, ***P < 0.001, ****P < 0.0001; Mantel-Cox log-rank test; statistical significance between PBS and all other formulations are shown; +*P* <0.05, ++*P* < 0.01, +++*P* < 0.001, ++++*P* < 0.0001; Mantel-Cox log-rank test).

While these results are promising, future studies are necessary to validate the capacity of this nanovaccine platform to enhance the immunogenicity of bone fide tumor antigens, many of which may be less immunogenic than OVA. We anticipate that the platform would be directly amenable to covalent loading of tumor peptide antigens containing cysteine residues, though antigenic sequences can also be cloned into OVA or similar proteins (e.g., albumin),[123,124] a strategy that would allow for direct integration of diverse epitopes using the same fabrication and assembly process used here. Additionally, this cancer vaccine technology also remains to be tested in more aggressive and poorly immunogenic tumor models (e.g., B16 melanoma or MOC2 oral squamous cell carcinoma) and evaluated in combination with immune checkpoint blockade or other adjunctive therapies that address established barriers to T cell function and tumor infiltration.[125-127] Nonetheless, these studies validate proof-of-principle for a new cancer vaccine platform that significantly augments antitumor cellular immunity via cytosolic dual-delivery of antigen and adjuvant using the clinically advanced nucleic acid adjuvant, polyIC.

3.4 Conclusion

Cancer vaccines offer a promising strategy for bolstering the magnitude, breadth, and quality of the tumor antigen-specific T cell response and have emerged as important components of an expanding immunotherapeutic armamentarium. While there is clinical evidence that protein- and peptide-based cancer vaccines generate immune responses in patients, their clinical efficacy remains limited by an insufficient capacity to generate robust cytotoxic CD8+ T cell responses, the primary mediator of antitumor immunity in most cancers. To meet this challenge, we employ an optimized nanoparticle cancer vaccine platform for enhancing antitumor CD8+ T cell responses via cytosolic dual-delivery of antigen and polyIC – a clinically advanced nucleic acid vaccine adjuvant. Owing to its nanoscale dimensions, the NP vaccine platform extended the injection site

half-life of protein antigen and polyIC and increased their accumulation in vaccine site draining LNs. By overcoming these intracellular and physiological delivery barriers, NPs co-loaded with antigen and polyIC stimulated a strong, multifunctional CD8+ T cell response that conferred protection from tumor formation and inhibited the growth of established tumors in a mouse tumor model. In summary, the NP vaccine platform is a promising and versatile platform for cytosolic dual-delivery of antigen and nucleic acid adjuvants that potently augments antitumor cellular immunity.

3.5 Materials and Methods

Animal care and experimentation

Female C57BL/6 mice (6-8 weeks old) were purchased from the Jackson Laboratory (Bar Harbor, ME). All animal experiments were reviewed and approved by the Vanderbilt University Institutional Animal Care and Use Committee (IACUC), and all surgical and experimental procedures were performed in accordance with the regulations and guidelines of the Vanderbilt University IACUC.

Dose Finding Study

Female C57BL/6 mice were administered a single 100 μL subcutaneous injection at the base of tail with either PBS or NP vaccine formulated with different doses of polymer, OVA, and polyIC. Doses are as follows: high (400 μg of polymer, 60 μg of OVA, 40 μg polyIC), medium (400 μg of polymer, 60 μg of OVA, 40 μg polyIC), low (400 μg of polymer, 60 μg of OVA, 40 μg polyIC). NP antigen conjugates were prepared 24 h prior to injection, and polyIC was complexed to conjugates on the day of use, as described above. Animals were monitored for weight

loss and signs of lethargy and no adverse effects were observed with any formulation tested (**Figure 3.6**). The dose ultimately selected was in the range of physiologically relevant doses found in the literature.

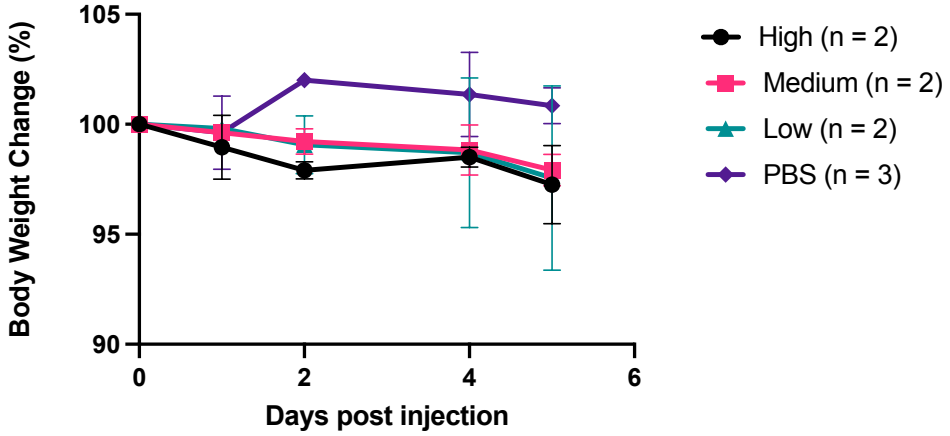

Figure 3.6: Subcutaneously injected NP vaccine is well-tolerated. Female C57BL/6 mice (6-8 weeks old) were administered a single 100 uL subcutaneous injection of either PBS or NP vaccine formulated with different doses of polymer, OVA, and polyIC at the base of tail. Doses are as follows: high (400 μg of polymer, 60 μg of OVA, 40 μg polyIC), medium (400 μg of polymer, 60 μg of OVA, 40 μg polyIC), low (400 μg of polymer, 60 μg of OVA, 40 μg polyIC). Conjugates were prepared 24 h prior to injection and polyIC was complexed to conjugates on the day of use, as described above. Animals were monitored for weight loss and signs of lethargy and no adverse effects were observed with any formulation tested. The medium dose was ultimately selected because it is in the range of physiologically relevant doses found in the literature.

Intravital fluorescent imaging of antigen and polyIC at injection site

Female C57BL/6 mice (6-8 weeks old) were injected subcutaneously in the right lower flank with formulations containing 58 μg Alexa Fluor 647-labeled OVA (labeling detailed in Section 2.3) and 32 μg rhodamine-labeled LMW polyIC (Invivogen). Experimental groups were as follows: PBS, polyIC complexed OVA-NP conjugates (OVA-NP/polyIC), or a soluble mixture of OVA and polyIC (OVA + polyIC). Injection site was longitudinally monitored for one week via intravital microscopy using the IVIS Lumina III (PerkinElmer). The levels of Alexa Fluor 647

and rhodamine were determined using an Ex 650 /Em 668 nm and Ex 571/ Em 591 filter set, respectively. Spectral unmixing, which is a tool provided by the IVIS software, was used to isolate and quantify each individual fluorescence source.

In vivo analysis of lymph node accumulation

Female C57BL/6 mice (6-8 weeks old) were injected subcutaneously at the base of tail with formulations containing 58 μg Alexa Fluor 647-labeled OVA and/or 32 μg rhodamine-labeled LMW polyIC (Invivogen). Experimental groups were as follows: PBS, OVA-NP/polyIC, or OVA + polyIC). After 48 h, inguinal (draining) LNs were harvested, and the AF647 and rhodamine fluorescence signal was imaged and measured with the IVIS Lumina III (PerkinElmer). The injection site retention half-life of fluorescently-labeled OVA and polyIC was estimated by fitting fluorescence intensity as a function of to an exponential decay model using non-linear regression.

qRT-PCR analysis of gene expression in lymph nodes

Female C57BL/6 mice (6-8 weeks old) were injected subcutaneously at the base of tail with formulations containing 58 μg Alexa Fluor 647-labeled OVA and/or 32 μg rhodamine-labeled LMW polyIC (Invivogen). Experimental groups were as follows: PBS, OVA-NP/polyIC, or OVA + polyIC). After 48 h, inguinal LNs were harvested and placed in RLT lysis buffer (Qiagen) supplemented with 2% β-mercaptoethanol (Sigma) in a gentleMACS M tube with mechanical disruption using an OctoMACS tissue dissociator (Miltenyi). LN RNA was isolated with a RNeasy RNA isolation kit (Qiagen) with the RNase-free DNase Set (Qiagen), used according to manufacturer's specifications. Complementary DNA (cDNA) was synthesized with

the Bio-Rad iScript cDNA kit and analyzed via qPCR using the appropriate TaqMan kits (Thermo Fisher Scientific). The TaqMan gene expression kits were: *Ifnb1* (Mm00439552_s1), *Cxcl10* (Mm00445235_m1), *Tnf* (Mm00443258_m1), Il6 (Mm00445235_m1), and *Hmbs* (Mm01143545_m1).

In vivo immunization

C57BL/6 mice (6−8 weeks old) were immunized via subcutaneous injection at the base of the tail on days 0, 7, and 14 with formulations containing 58 μg of OVA and/or 32 μg of polyIC with or without 400 μg of polymer in PBS. The groups were as follows: PBS, OVA-NP/polyIC, OVA + NP/polyIC, OVA-NP, OVA + polyIC, or OVA. On day 20, whole blood was collected for SIINFEKL (pOVA/H-$2K^b$) tetramer staining. On day 21, mice were euthanized to evaluate antibody titer and track $CD8^+$ T cell response by tetramer staining, as well as to determine T cell function by intracellular cytokine staining and ELISpot assay.

Analysis of OVA-specific CD8+ T cell responses in whole blood

On day 20 after immunizations, whole blood was collected in K2EDTA treated tubes (BD Biosciences), treated with ACK lysis buffer (KD Medical), washed, resuspended in cold FACS buffer (PBS supplemented with 2% FBS and 50 μM dasatinib), and plated in a 96-well U-bottom plate. Next, the cells were centrifuged for 5 min at 1,500 rpm and resuspended in FACS buffer and incubated with Fc-block (anti-CD16/CD32, clone 2.4G2; Tonbo) for 15 min at 4°C, and stained with antibodies CD45.2 (APC; clone 104; BioLegend), CD3ε (PE/Cy7; clone 145.2C11; BioLegend), and CD8α (APC/Cy7; clone 53-6.7; Tonbo) for 1 h at 4°C. Cells were then washed 3x in FACS buffer and then stained for 2 h with 1.5 μg/mL of PE-labeled $OVA_{257–264}$ pOVA/H-

$2K^b$ tetramer prepared according to a previously reported procedure.[128] Cells were then washed 3x in FACS buffer, resuspended using FACS buffer supplemented with 1 μg/mL DAPI, and analyzed using an Amnis CellStream Luminex flow cytometer. Representative flow cytometry data and gating strategies for determining the frequency of SIINFEKL-specific $CD8^+$ T cells are shown in **Figure 3.7**.

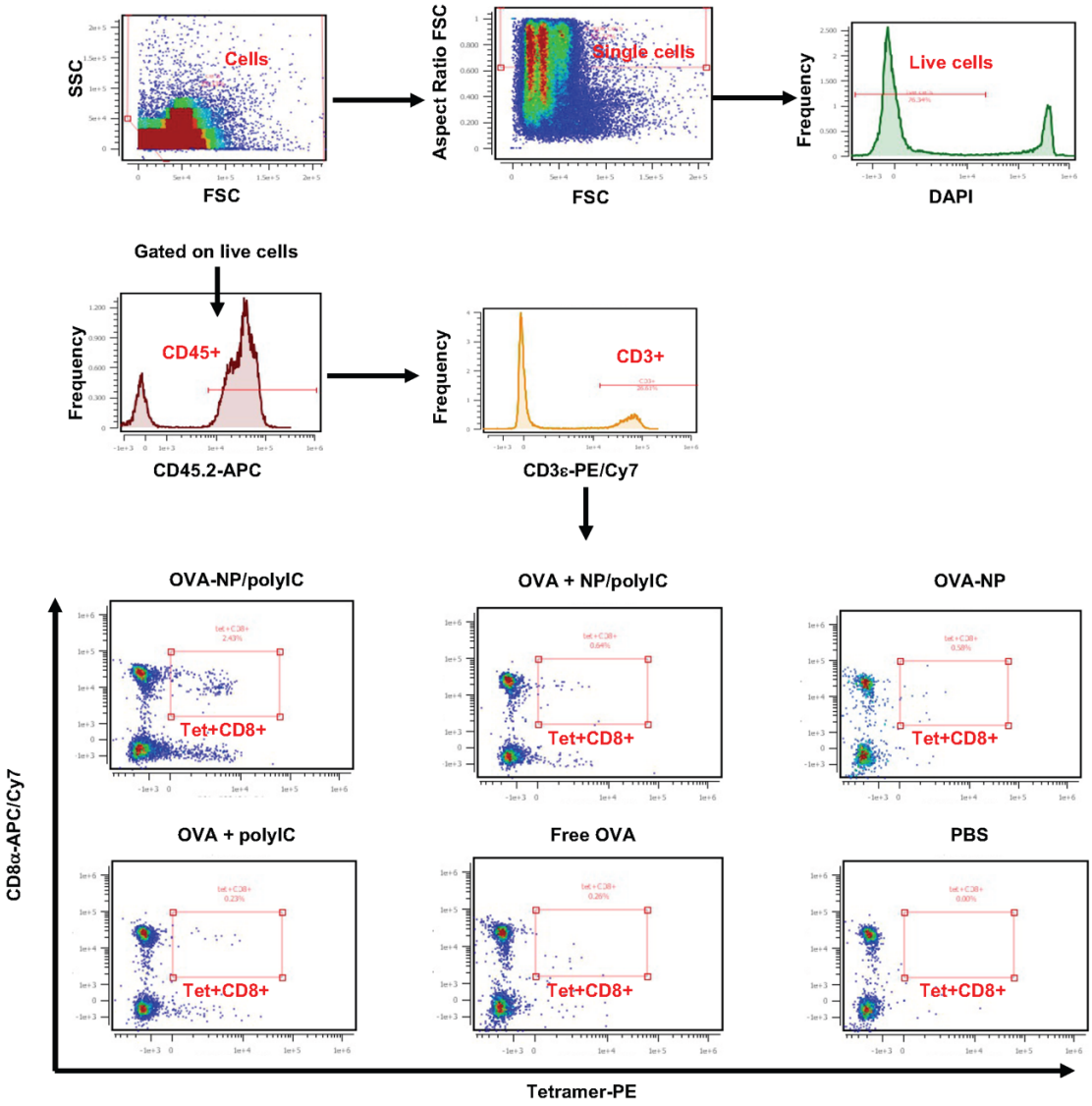

Figure 3.7: Gating strategy for flow cytometric analysis of antigen-specific $CD8^+$ T cell response in whole blood or spleen via staining with PE-labeled pOVA/MHC-I tetramer. Representative plots are from mice immunized with OVA-NP/polyIC. Events were first gated on lymphocytes (FSC vs. SSC), the single cells were isolated via gating FSC vs. aspect ratio (The aspect ratio feature allows for gating on single cell populations by drawing a gate around the single

cells using the FSC vs aspect ratio (minimum width/length) to remove doublets. Single, round cells have a higher aspect ratio while elongated cells, aggregates, or more than one cell in a frame have a lower aspect ratio). Single cells were gated on the DAPI negative populations to distinguish live cells from the dead. Histograms were used to gate on viable $CD45^+$ cells, followed by $CD3^+$ cells. CD3+ cells were then gated on tetramer vs. $CD8^+$ T cells to determine OVA-specific $CD8^+$ T cells.

Preparation of splenocytes

On day 21 after immunization, mice were euthanized and spleens harvested and mechanically disrupted into single-cell suspensions in complete RPMI 1640 (cRPMI; 10% FBS, 100 U/mL penicillin, 100 μg/mL streptomycin, 50 μM 2-mercaptoethanol, and 2 mM L-glutamine) by forcing them through a 70 μm cell strainer (FisherbrandTM; Thermo Fisher Scientific) using a sterile syringe plunger. Cells were passed through the strainer two more times to remove any residual tissue fragments. The cells were centrifuged for 5 min at 1,500 rpm and resuspended in ACK lysis buffer (KD Medical) to remove erythrocytes. After 5 min incubation, cRPMI was added to deactivate ACK lysis buffer. Finally, cells were centrifuged and resuspended in cRPMI.

Analysis of OVA-specific CD8+ T cell responses in the spleen

Splenocytes were plated at 3 x 10^6 cells/well in a 96-well U-bottom plate. Next, the cells were centrifuged for 5 min at 1,500 rpm and resuspended in FACS buffer and incubated with Fc-block (anti-CD16/CD32, clone 2.4G2; Tonbo) for 15 min at 4°C, and then stained with antibodies CD45.2 (APC; clone 104; BioLegend), CD3ε (PE/Cy7; clone 145.2C11; BioLegend), and CD8α (APC/Cy7; clone 53-6.7; Tonbo) for 1 h at 4°C. Cells were then washed 3x in FACS buffer and then stained for 2 h with 1.5 μg/mL of PE-labeled pOVA/H-$2K^b$ tetramer. Cells were then washed 3x in FACS buffer and analyzed as described above. Representative flow cytometry data and gating strategies for determining the frequency of SIINFEKL-specific $CD8^+$ T cells are also shown in **Figure 3.7**.

Intracellular cytokine staining of OVA-specific $CD8^+$ and $CD4^+$ T Cells

Splenocytes were plated in 96-well U-bottom plates at 2 x 10^6 cells/well in cRPMI and the appropriate stimulant or control was added: 10 μM of MHC-I H-$2K^b$ epitope SIINFEKL ($OVA_{257–264}$; Invivogen), 10 μM of MHC-II H-2Ab epitope ISQAVHAAHAEINEAGR ($OVA_{323-339}$; Invivogen), 1x cell stimulation cocktail (PMA and ionomycin; Thermo Fischer Scientific) as the positive control, and cRPMI as the negative control. Cells were incubated at 37°C in an atmosphere of 5% CO_2 for 1 h 30 min. BD GolgiPlug protein transport inhibitor (BD Biosciences) was then added to each well, and cells were incubated for an additional 5 h 30 min. Following incubation, cells were washed with PBS and stained with eFluor 450 fixable viability dye (eBioscience) for 30 min at 4°C. Cells were next washed with FACS buffer (PBS supplemented with 2% FBS) and incubated with Fc-block (anti-CD16/CD32, clone 2.4G2; Tonbo) for 15 min at 4°C, and then stained with antibodies for CD3ε (PE/Cy7; clone 145.2C11; Biolegend), CD8α (APC/Cy7; clone 53-6.7; Tonbo), and CD4 (AF488; clone RM4-5; Biolegend) for 1 h at 4°C. Cells were washed 2x in FACS buffer, then fixed and permeabilized by incubating for 10 min at 4°C with BD Cytofix/Cytoperm (BD Biosciences), according to manufacturer instructions. Cells were then washed 2x with 1x BD perm/wash buffer (BD Biosciences) and incubated for 1 h at 4°C with antibodies against intracellular cytokines: anti-IFNγ-APC (clone XMG1.2; BD Biosciences) and anti-TNFα-PE (clone MP6-XT22; BD Biosciences). Finally, cells were washed once with 1x perm/wash buffer, resuspended in FACS buffer supplemented with 50 nM dasatinib, and analyzed as described above. Data are reported as the percentage of $CD8\alpha^+$ cells that are $IFN\gamma^+$ and/or $TNF\alpha^+$ after subtraction of background values from unstimulated negative controls. Representative gating for ICCS analysis of splenocytes is presented in **Figure 3.8**.

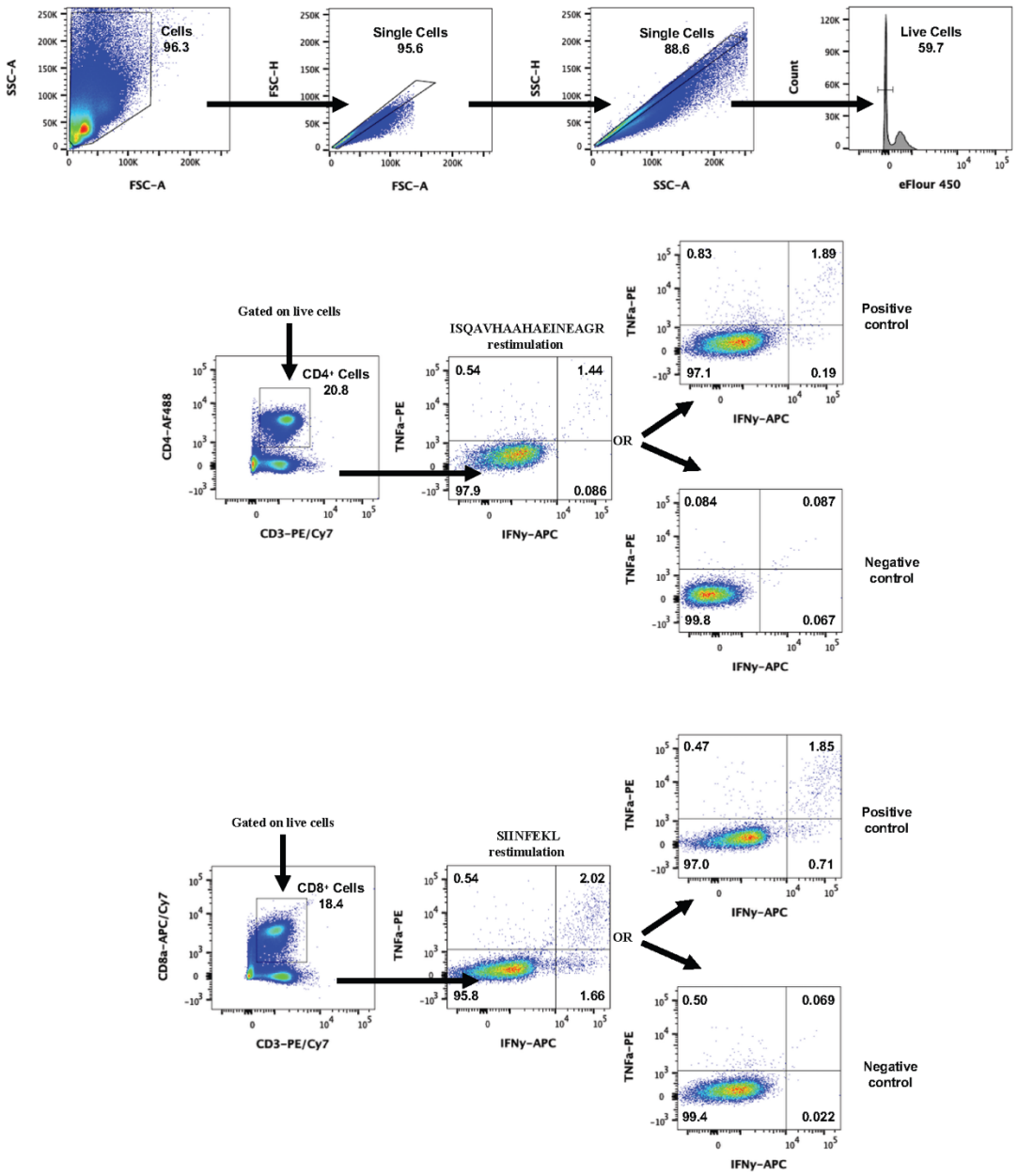

Figure 3.8: Gating strategy for flow cytometric analysis of intracellular cytokine production in CD8$^+$ T cells and CD4$^+$ T cells. Representative plots are from mice immunized with OVA-NP/polyIC. Events were first gated on lymphocytes (FSC-A vs. SSC-A), the single cells were isolated via gating FSC-A vs. FSC-H and SSC-A vs. SSC-H. Single cells were gated on the DAPI negative populations to distinguish live cells from the dead. Cells were restimulated with MHC-I H-2K^b epitope SIINFEKL, MHC-II H-2A^b epitope ISQAVHAAHAEINEAGR, PMA/ionomycin (positive control), and cRPMI (negative control). CD8$^+$ T cells and CD4$^+$ T Cells were gated on TNFα-PE and IFNγ-APC to assess cytokine production.

Enzyme-Linked Immunosorbent Spot assay (ELISpot)

Splenocytes from each vaccinated mouse were evaluated for antigen-specific IFN-γ production by ELISpot assay (Mouse IFN-gamma Single-Color ELISpot; ImmunoSpot) according to manufacturer's instructions with minor modifications. Microtiter 96-well plates pre-coated with anti-mouse IFN-γ monoclonal antibody (capture antibody) were washed 3x with sterile PBS and blocked with 200 µL of complete RPMI 1640 for 2 h at 37°C in an atmosphere of 5% CO_2. Medium was aspirated and the appropriate stimulant or control added: 10 µg/mL SIINFEKL peptide, 10 µM ISQAVHAAHAEINEAGR peptide, 10 µg/mL Concanavalin A (Invivogen) as the positive control, and 10 µg/mL Influenza A NP (366-374) (GenScript) alone as the negative control. Immediately thereafter, splenocytes were plated in quadruplicate at 2.5 x 10^5 cells/well and incubated for 48 h at 37°C in an atmosphere of 5% CO^2. Plates were washed 3x with wash buffer (PBS supplemented with 1% v/v FBS and 0.05% v/v Tween 20) and incubated for 2 h at room temperature with biotin-conjugated rat anti-mouse IFN-γ detection antibody (BDbiosciences). Plates were washed four times with wash buffer and incubated with 1 µg/mL of avidin-HRP for 45 min at room temperature. After three washes with wash buffer and two washes with PBS, 100 µL of Blue Developer Solution prepared according to (ImmunoSpot) was added to each well and left to develop for ~4 min at room temperature or when solution turns blue in the darkest wells. Plates were then washed 5x with water, dried overnight, and the number of spots was counted using an ImmunoSpot ELISpot reader and analysis software package (Cellular Technology Limited). The average number of spots counted upon incubation with cRPMI (i.e., background) was subtracted from the number of spots counted upon peptide stimulation, and data are reported as the number of IFN-γ spot forming cells (SFCs) normalized to 2 x 10^5 cells.

Antibody titer

Approximately 100 μL of blood was collected from each mouse via cardiac puncture, and sera were tested for OVA-specific IgG. Nunc MaxiSorp plates (high protein binding plates; Thermo Fisher Scientific) were coated with 10 μg/mL OVA in 1x PBS overnight at 4°C. Plates were then washed two times with PBS and blocked with PBS/0.01% tween 20 for 1 h at room temperature. Sera were added at a 1/100 dilution and subsequent 10-fold serial dilutions in PBS/0.01% tween 20 and incubated for 2 h at room temperature. Sera from one naïve mouse (negative control) and monoclonal anti-chicken OVA antibody (positive control; Sigma-Aldrich) were included in each plate to determine cutoff values. Following incubation, plates were washed 3x with PBS and incubated with secondary antibody (anti-IgG-HRP; EMD Millipore) at a 1:5000 dilution in PBS for 1 h at room temperature. Plates were again washed 3x with PBS and incubated with 100 μl of developing agent (1-step Ultra-TMB ELISA; Thermo Fisher Scientific). After 1 min, the enzymatic reaction was quenched with 100 μl of 0.18 M sulfuric acid and absorption of the colormetric reaction measured within 30 min at 450 nm using a plate reader (Synergy HTX). End point titers were determined from reciprocal dilutions using a sigmoidal fit (GraphPad Prism 5; GraphPad Software Inc.) to determine the dilution at which the $A_{450\ nm}$ value was equal to the mean + two standard deviations of that of naïve serum.

Tumor studies

For the prophylactic tumor challenge studies, C57BL/6 mice (6−8 weeks old) were immunized via the subcutaneous route at the base of the tail on days 0, 7, and 14 with formulations containing 58 μg of OVA and/or 32 μg of polyIC with or without 400 μg of polymer in PBS. The groups were as follows: PBS, OVA-NP/polyIC, OVA + NP/polyIC, OVA-NP, OVA + polyIC, or

OVA. Mice were challenged 7 days following the final vaccination by subcutaneous flank injection of 3 x 10^5 EG7.OVA cells (C57BL/6 mouse derived EL-4 thymoma line expressing OVA cDNA). Tumor volume was measured three times per week via caliper measurements using the formula $V = (L \times W \times W)/2$. Mice were euthanized at a tumor burden end point of 1500 mm^3.

For the EG7.OVA therapeutic vaccination model, C57BL/6 mice (6−8 weeks old) were inoculated via subcutaneous flank injection with 3 x 10^5 EG7.OVA cells. Mice were then vaccinated as described above on days 5, 12, and 19 with formulations containing 58 μg of OVA and/or 32 μg of polyIC with or without 400 μg of polymer in PBS. The groups were as follows: PBS, OVA-NP/polyIC, OVA + NP/polyIC, OVA-NP, OVA + polyIC, or OVA. Tumor growth was monitored as indicated above. Mice were euthanized at a tumor burden end point of 2000 mm^3.

Statistical analysis

Significance for each experiment was determined as indicated in the corresponding figure captions. All analyses were done using GraphPad Prism software, version 9.3.1. Plotted values represent experimental means, and error bars represent SD unless otherwise noted in the figure captions. **** $P < 0.0001$, *** $P < 0.005$, **$P < 0.01$, * $P < 0.05$.

CHAPTER 4

Conclusions

4.1 Chapter Summaries

In Aim 1 of this dissertation (chapter 2), it was hypothesized that the pH-responsive polymer platform can promote cytosolic delivery of protein antigen and polyIC providing a mechanism to maximize antigen presentation and DC activation. Accordingly, the objective of Aim 1 was to design a pH-responsive, endosomolytic NP that enables facile co-loading and cytosolic co-delivery of antigens and polyIC as the adjuvant. A NP was designed with a PEG-rich corona that displays pyridyl disulfide (PDS) groups for covalent conjugation of thiol-containing antigens via thiol-disulfide exchange reactions, and a pH-responsive, endosomolytic core for electrostatic loading of immunostimulatory nucleic acids that also facilitates cytosolic delivery of both antigen and adjuvants. Subsequently, we demonstrated that model antigen OVA and polyIC can both be loaded on the same NP, while maintaining particle size and colloidal stability. Next, we validated the endosomolytic activity of the NP using a red blood cell hemolysis assay and a Gal8-YFP reporter assay. Utilizing several reporter cells, the NP demonstrated its ability to enhance the immunostimulatory activity of polyIC. Also, using MDA-5 knockout cells it was revealed that the NPs facilitate delivery of polyIC to the cytosol and activates an MDA-5-dependent IFN-I response. Furthermore, NP vaccine platform increased antigen presentation on MHC-I molecules, while endosomal escape of polyIC strongly increased its immunostimulatory potency via the MDA-5 pathway, resulting in proinflammatory cytokine production, costimulatory molecule upregulation, and IFN-I secretion by dendritic cells.

The second central hypothesis of this work (Chapter 3) was that the NP vaccine could enhance antigen-specific T cell priming by DCs through increased uptake and cytosolic delivery

of cargo. Accordingly, the objective of Aim 2 was to evaluate the DC-mediate T cell response induced by the optimized NP vaccine *in vivo*. Owing to its nanoscale dimensions, the NP vaccine platform extended the injection site half-life of protein antigen and polyIC and increased their accumulation in vaccine site draining LNs. Additionally, a significant increase in the expression of *Ifnb1, Cxcl10*, and *Tnfa* in the inguinal LN was observed 6 hours after administration, further demonstrating the ability of NP vaccine to enhance polyIC activity and delivery to the draining LN. By overcoming intracellular and physiological delivery barriers, NPs co-loaded with antigen and polyIC stimulated a strong, multifunctional $CD8^+$ T cell response that conferred protection from tumor formation and inhibited the growth of established tumors in a mouse tumor model.

The work presented here established the use of a versatile NP platform for the co-delivery of antigens and nucleic acid adjuvants while also demonstrating its ability to stimulate optimal $CD8^+$ T cells against tumor cells.

4.2 Limitations and Future Work

Overall, this work has demonstrated the ability of a pH-responsive nanoparticle vaccine to generate CD8+ T cells and confer protection from tumor formation and inhibited the growth of established tumors in a murine thymoma EL-4 cell line that expresses OVA as a model antigen (EG7.OVA). While these studies have established an important proof-of-concept, this cancer vaccine technology remains to be tested using clinically relevant peptides in more aggressive and poorly immunogenic tumor models (e.g., B16 melanoma or MOC2 oral squamous cell carcinoma) and evaluated in combination with immune checkpoint blockade or other adjunctive therapies that address established barriers to T cell function and tumor infiltration. Numerous peptide formulation strategies have been developed to enhance antigen-specific CD8+ T cell

immunity,[129,130] however the diverse physicochemical properties of neoantigens that arise from amino-acid sequence variation may limit the translatability of such delivery systems.[125]

Future work associated with the research described in this dissertation will address these challenges by optimizing the NP platform to enable covalent conjugation of diverse cysteine-containing peptides that span the range of different charge and hydrophobicity. In preliminary studies, we synthesized amphiphilic co-polymers with different compositions to allow for direct integration of diverse epitopes using the same fabrication and assembly process described in Chapter 2. A summary of polymer properties can be found in **Table 4.1**. To investigate conjugation efficiency of cysteine-containing peptides listed in **Table 4.2**, we used SDS-polyacrylamide gel electrophoresis (SDS-PAGE) to monitor the band shift and disappearance of fluorescently-labeled peptides due to conjugation to NP. Conjugation efficiencies between 60%-100% was achieved for all three polymers at different polymer:peptide molar ratios (**Figure 4.1**) demonstrating the potential to load peptides with different physicochemical properties. The cationic moiety in the polymeric nanoparticle platform may also open new opportunities for exploring other emerging adjuvants to maximize their *in vivo* activity.

Table 4.1: Summary of polymer library.

Polymer	1st block (mCTA)	2nd block (mCTA)	3rd block (mCTA)	Di or tri block copolymer
1	10,000	19,400	34,000	63,400
2	15,700	16,500	N/A	32,200
3	15,700	24,200	N/A	39,900

1. PEG_{10kDa}-*b*-$[(PEGMA_{90}$-*co*-$PDSMA_{10})]_{19.4kDa}$-*b*-$[(DMAEMA_{50}$-*co*-$BMA_{50})]_{34kDa}$
(MW = 63.4kDa with 7.5 PDSMA groups/chain)

2. $[(PEGMA_{90}$-*co*-$PDSMA_{10})]_{15.7kDa}$-*b*-$[(DMAEMA_{50}$-*co*-$BMA_{50})]_{16.5kDa}$
(MW = 32.2kDa with 5 PDSMA groups/chain)

3. $[(PEGMA_{90}$-*co*-$PDSMA_{10})]_{15.7kDa}$-*b*-$[(DMAEMA_{50}$-*co*-$BMA_{50})]_{24.2kDa}$
(MW = 39.9kDa with 5 PDSMA groups/chain)

Table 4.2: Cysteine-containing peptides.

Sequence	Net Charge at pH 7	Gravy
CSSSIINFEK(Cy5)L	-0.1	0.03
CSG(TAMRA)LEQLESIINFEKL	-2.1	0.144

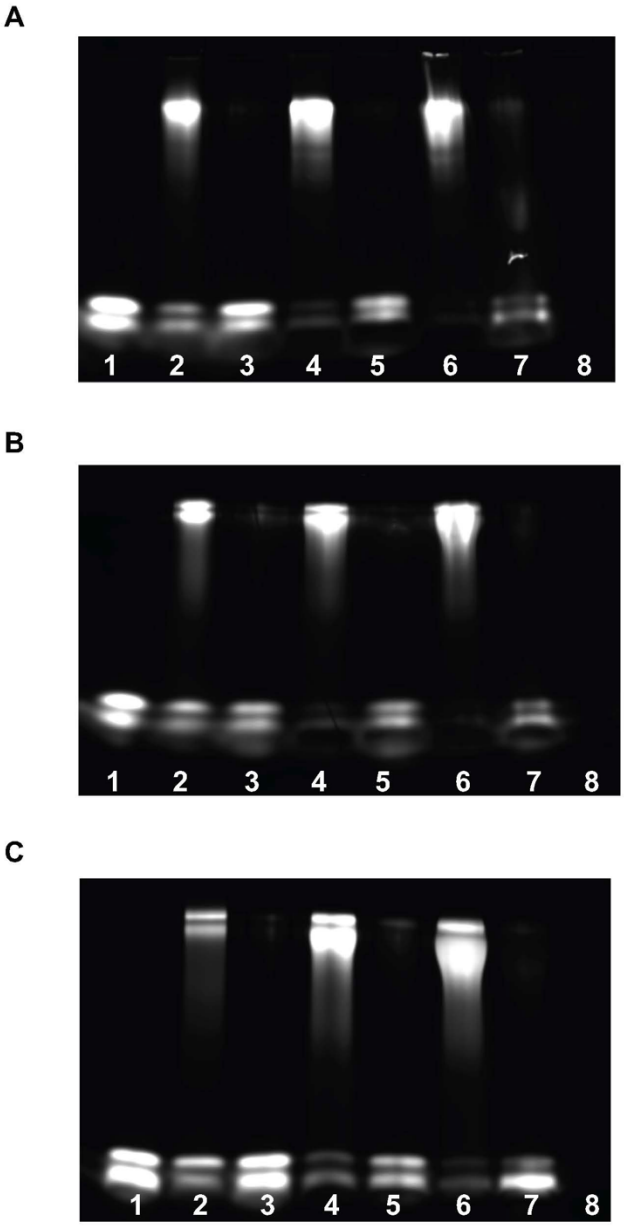

Figure 4.1: Peptide-nanoparticle conjugation. (A,B,C) Cystein-containing peptide labeled with TAMRA was reacted with NP to form conjugates at varying molar ratios of NP:peptide. SDS-PAGE was used to confirm antigen conjugation. Lane (1) free peptide; (2) pep-NP (1:5); (3) pep-NP (1:5) + TCEP; (4) pep-NP (1:1); (5) pep-NP (1:1) + TCEP; (6) pep-NP (5:1); (7) pep-NP (5:1) + TCEP; (8) NP. Material loaded into each lane was normalized to 1 μg peptide. The NP itself was not fluorescent (lane 8). **(A)** conjugates made using polymer 1. **(B)** conjugates made using polymer 2. **(C)** conjugates made using polymer 3.

We also demonstrated that the polymer can efficiently delivery polyIC to the cytosolic MDA-5 pathway by using an MDA-5 deficient reporter cell line. This warrants further investigation of the polymer-mediated endosomal and/or cytosolic delivery of polyIC and the relative downstream contributions of MDA-5 and TLR3 on innate immune activation. Future work should build on this by synthesizing a library of polymers with varying degrees of pH-responsiveness and using them to deliver polyIC to its endosomal or cytosolic receptor. The relative contributions of MDA-5 and TLR3 can be investigated using MDA-5-/-, TLR3-/-, and MDA-5-/-TLR3-/- mice. Showing a connection between varying the degree of pH-responsiveness and the ability to potentially skew polyIC activation towards either pathway would further support the notion that biomaterials can be used to modulate innate and adaptive immunity.

A distinctive feature of endosomolytic NPs is their capacity to promote MHC-I presentation to enhance $CD8^+$ T cell responses, the data in Chapter 3 shows that they are also able to augment $CD4^+$ T cell responses. The capacity of the platform to promote a balanced $CD8^+/CD4^+$ Th1 response may also further enhance cancer vaccine efficacy given the important role that $CD4^+$ T cells play in supporting $CD8^+$ T cell effector function as well as the intrinsic roles of $CD4^+$ T cells in antitumor immunity. Thus, it will be important to characterize this in the future to obtain a more complete picture of the cellular response generated.

4.3 Concluding Remarks

Technological advances in cancer genomics now enable the rapid identification of neoantigens for the development of personalized therapeutic cancer vaccines. Initial clinical trial studies of personalized neoantigen-based vaccines have shown the feasibility, safety, and potential immunotherapeutic benefits of targeting patient-specific tumor mutations.[55] With advances in vaccine technology and encouraging results from clinical trial studies of neoantigen-based

vaccines, there is ample reason to believe that neoantigens hold promise for developing novel personalized immunotherapeutic strategies for the treatment of various cancers.

In order to employ our nanovaccine platform in clinical trials, we would first use non-human primates to assess the immune response generated by the vaccine. During these pre-clinical studies, we would also monitor safety of the vaccine. Next, we would start Phase I vaccine trials to assess the vaccine in a small cohort of people. First, we would sequence each patient's tumor and germline DNA and tumor RNA. Following any standard cancer treatment such as surgery for solid tumors, patients would receive doses of our novel personalized vaccine. The goal of these studies would be to assess safety of the candidate vaccine and to determine the type and extent of immune response that the vaccine provokes. If phase I trials seem promising, we would progress to Phase II vaccine trials and assess the vaccine in a larger cohort of people. The goals of Phase II testing would be to study the vaccine's safety, immunogenicity, proposed doses, schedule of immunizations, and method of delivery. A successful Phase II study would allow us to progress to Phase III vaccine trials involving thousands of people. The goals of Phase III would be to assess vaccine safety and efficacy in a large group of people. After a successful Phase III trial, we would submit an application to the FDA and continue to test the vaccine for safety, efficacy, and other potential uses.

In conclusion, the work described in this dissertation has demonstrated that the nanovaccine platform is an effective delivery vehicle for antigens and polyIC, and likely other cytosolically active immunotherapeutics. As demonstrated by their prophylactic and therapeutic efficacy in a mouse tumor model, the nanovaccine is a powerful addition to the cancer immunotherapy toolbox and has the potential to synergize with the most promising clinically relevant immunotherapies. Although the nanovaccine described has exciting translational

potential, significant improvements in the technology can likely be made through future particle engineering as well as through further exploration of combination therapies. It is my hope that these results offer new insights into the rational design of the next generation nanoparticle vaccine for cytosolic dual-delivery of diverse peptide neoantigens and nucleic acid adjuvants that potently augments antitumor cellular immunity.

REFERENCES

1 Siegel, R. L., Miller, K. D., Fuchs, H. E. & Jemal, A. Cancer statistics, 2022. *CA: A Cancer Journal for Clinicians* **72**, 7-33, doi:10.3322/caac.21708 (2022).

2 Waldman, A. D., Fritz, J. M. & Lenardo, M. J. A guide to cancer immunotherapy: from T cell basic science to clinical practice. *Nature Reviews Immunology* **20**, 651-668, doi:10.1038/s41577-020-0306-5 (2020).

3 Tan, S., Li, D. & Zhu, X. Cancer immunotherapy: Pros, cons and beyond. *Biomedicine & Pharmacotherapy* **124**, 109821, doi:https://doi.org/10.1016/j.biopha.2020.109821 (2020).

4 Murciano-Goroff, Y. R., Warner, A. B. & Wolchok, J. D. The future of cancer immunotherapy: microenvironment-targeting combinations. *Cell Research* **30**, 507-519, doi:10.1038/s41422-020-0337-2 (2020).

5 Trujillo, J. A., Sweis, R. F., Bao, R. & Luke, J. J. T Cell-Inflamed versus Non-T Cell-Inflamed Tumors: A Conceptual Framework for Cancer Immunotherapy Drug Development and Combination Therapy Selection. *Cancer Immunol Res* **6**, 990-1000, doi:10.1158/2326-6066.CIR-18-0277 (2018).

6 Maibach, F., Sadozai, H., Seyed Jafari, S. M., Hunger, R. E. & Schenk, M. Tumor-Infiltrating Lymphocytes and Their Prognostic Value in Cutaneous Melanoma. *Frontiers in immunology* **11**, 2105-2105, doi:10.3389/fimmu.2020.02105 (2020).

7 Fridman, W. H., Zitvogel, L., Sautès–Fridman, C. & Kroemer, G. The immune contexture in cancer prognosis and treatment. *Nature Reviews Clinical Oncology* **14**, 717-734, doi:10.1038/nrclinonc.2017.101 (2017).

8 Tian, T., Olson, S., Whitacre, J. M. & Harding, A. The origins of cancer robustness and evolvability. *Integr Biol (Camb)* **3**, 17-30, doi:10.1039/c0ib00046a (2011).

9 Podlaha, O., Riester, M., De, S. & Michor, F. Evolution of the cancer genome. *Trends in Genetics* **28**, 155-163 (2012).

10 Stratton, M. R., Campbell, P. J. & Futreal, P. A. The cancer genome. *Nature* **458**, 719-724 (2009).

11 Lambert, A. W., Pattabiraman, D. R. & Weinberg, R. A. Emerging Biological Principles of Metastasis. *Cell* **168**, 670-691, doi:10.1016/j.cell.2016.11.037 (2017).

12 Anderson, R. L. *et al.* A framework for the development of effective anti-metastatic agents. *Nature Reviews Clinical Oncology* **16**, 185-204, doi:10.1038/s41571-018-0134-8 (2019).

13 Gonzalez, H., Hagerling, C. & Werb, Z. Roles of the immune system in cancer: from tumor initiation to metastatic progression. *Genes & Development* **32**, 1267-1284, doi:10.1101/gad.314617.118 (2018).

14 Vinay, D. S. *et al.* Immune evasion in cancer: Mechanistic basis and therapeutic strategies. *Seminars in Cancer Biology* **35**, S185-S198, doi:10.1016/j.semcancer.2015.03.004 (2015).

15 Vaddepally, R. K., Kharel, P., Pandey, R., Garje, R. & Chandra, A. B. Review of Indications of FDA-Approved Immune Checkpoint Inhibitors per NCCN Guidelines with the Level of Evidence. *Cancers (Basel)* **12**, 738, doi:10.3390/cancers12030738 (2020).

16 Kabacaoglu, D., Ciecielski, K. J., Ruess, D. A. & Algül, H. Immune Checkpoint Inhibition for Pancreatic Ductal Adenocarcinoma: Current Limitations and Future Options. *Frontiers in Immunology* **9**, doi:10.3389/fimmu.2018.01878 (2018).

17 Venkatachalam, S., McFarland, T. R., Agarwal, N. & Swami, U. Immune Checkpoint Inhibitors in Prostate Cancer. *Cancers (Basel)* **13**, 2187, doi:10.3390/cancers13092187 (2021).

18 Zhang, N., Wei, L., Ye, M., Kang, C. & You, H. Treatment Progress of Immune Checkpoint Blockade Therapy for Glioblastoma. *Frontiers in Immunology* **11**, doi:10.3389/fimmu.2020.592612 (2020).
19 Dammeijer, F., Lau, S. P., van Eijck, C. H. J., van der Burg, S. H. & Aerts, J. Rationally combining immunotherapies to improve efficacy of immune checkpoint blockade in solid tumors. *Cytokine Growth Factor Rev* **36**, 5-15, doi:10.1016/j.cytogfr.2017.06.011 (2017).
20 Vanneman, M. & Dranoff, G. Combining immunotherapy and targeted therapies in cancer treatment. *Nature Reviews Cancer* **12**, 237-251, doi:10.1038/nrc3237 (2012).
21 Berraondo, P. *et al.* Cytokines in clinical cancer immunotherapy. *British Journal of Cancer* **120**, 6-15, doi:10.1038/s41416-018-0328-y (2019).
22 Ramello, M. C., Haura, E. B. & Abate-Daga, D. CAR-T cells and combination therapies: What's next in the immunotherapy revolution? *Pharmacological Research* **129**, 194-203, doi:10.1016/j.phrs.2017.11.035 (2018).
23 Wagner, D. L. *et al.* Immunogenicity of CAR T cells in cancer therapy. *Nature Reviews Clinical Oncology* **18**, 379-393, doi:10.1038/s41571-021-00476-2 (2021).
24 Sterner, R. C. & Sterner, R. M. CAR-T cell therapy: current limitations and potential strategies. *Blood Cancer Journal* **11**, doi:10.1038/s41408-021-00459-7 (2021).
25 Grosser, R., Cherkassky, L., Chintala, N. & Adusumilli, P. S. Combination Immunotherapy with CAR T Cells and Checkpoint Blockade for the Treatment of Solid Tumors. *Cancer Cell* **36**, 471-482, doi:10.1016/j.ccell.2019.09.006 (2019).
26 Hosseinkhani, N. *et al.* Immune Checkpoints and CAR-T Cells: The Pioneers in Future Cancer Therapies? *International Journal of Molecular Sciences* **21**, 8305, doi:10.3390/ijms21218305 (2020).
27 He, X. & Xu, C. Immune checkpoint signaling and cancer immunotherapy. *Cell Research* **30**, 660-669, doi:10.1038/s41422-020-0343-4 (2020).
28 Marin-Acevedo, J. A., Kimbrough, E. O. & Lou, Y. Next generation of immune checkpoint inhibitors and beyond. *Journal of Hematology & Oncology* **14**, doi:10.1186/s13045-021-01056-8 (2021).
29 Ribas, A. & Wolchok, J. D. Cancer immunotherapy using checkpoint blockade. *Science (New York, N.Y.)* **359**, 1350-1355, doi:10.1126/science.aar4060 (2018).
30 Morad, G., Helmink, B. A., Sharma, P. & Wargo, J. A. Hallmarks of response, resistance, and toxicity to immune checkpoint blockade. *Cell* **184**, 5309-5337, doi:10.1016/j.cell.2021.09.020 (2021).
31 Wei, S. C., Duffy, C. R. & Allison, J. P. Fundamental Mechanisms of Immune Checkpoint Blockade Therapy. *Cancer Discovery* **8**, 1069-1086, doi:10.1158/2159-8290.cd-18-0367 (2018).
32 Esfahani, K. *et al.* A Review of Cancer Immunotherapy: From the Past, to the Present, to the Future. *Current Oncology* **27**, 87-97, doi:10.3747/co.27.5223 (2020).
33 Postow, M. A., Callahan, M. K. & Wolchok, J. D. Immune Checkpoint Blockade in Cancer Therapy. *Journal of Clinical Oncology* **33**, 1974-1982, doi:10.1200/jco.2014.59.4358 (2015).
34 Wolchok, J. D. *et al.* Nivolumab plus Ipilimumab in Advanced Melanoma. *New England Journal of Medicine* **369**, 122-133, doi:10.1056/nejmoa1302369 (2013).
35 Furue, M. *et al.* Melanoma and Immune Checkpoint Inhibitors. *Current Oncology Reports* **20**, doi:10.1007/s11912-018-0676-z (2018).

36 Antonia, S. J. *et al.* Nivolumab (anti-PD-1; BMS-936558, ONO-4538) and ipilimumab in first-line NSCLC: Interim phase I results. *Journal of Clinical Oncology* **32**, 8023-8023, doi:10.1200/jco.2014.32.15_suppl.8023 (2014).
37 Garon, E. B. *et al.* Pembrolizumab for the Treatment of Non–Small-Cell Lung Cancer. *New England Journal of Medicine* **372**, 2018-2028, doi:10.1056/nejmoa1501824 (2015).
38 Thomas, R., Al-Khadairi, G. & Decock, J. Immune Checkpoint Inhibitors in Triple Negative Breast Cancer Treatment: Promising Future Prospects. *Frontiers in Oncology* **10**, doi:10.3389/fonc.2020.600573 (2021).
39 Tumeh, P. C. *et al.* PD-1 blockade induces responses by inhibiting adaptive immune resistance. *Nature* **515**, 568-571, doi:10.1038/nature13954 (2014).
40 Thommen, D. S. *et al.* A transcriptionally and functionally distinct PD-1+ CD8+ T cell pool with predictive potential in non-small-cell lung cancer treated with PD-1 blockade. *Nature medicine* **24**, 994-1004 (2018).
41 Loi, S. *et al.* Relationship between tumor infiltrating lymphocyte (TIL) levels and response to pembrolizumab (pembro) in metastatic triple-negative breast cancer (mTNBC): results from KEYNOTE-086. *Annals of Oncology* **28**, v608 (2017).
42 Darvin, P., Toor, S. M., Sasidharan Nair, V. & Elkord, E. Immune checkpoint inhibitors: recent progress and potential biomarkers. *Exp Mol Med* **50**, 1-11, doi:10.1038/s12276-018-0191-1 (2018).
43 Linette, G. P. & Carreno, B. M. Tumor-Infiltrating Lymphocytes in the Checkpoint Inhibitor Era. *Current Hematologic Malignancy Reports* **14**, 286-291, doi:10.1007/s11899-019-00523-x (2019).
44 Daud, A. I. *et al.* Tumor immune profiling predicts response to anti-PD-1 therapy in human melanoma. *J Clin Invest* **126**, 3447-3452, doi:10.1172/JCI87324 (2016).
45 Sarnaik, A. A. *et al.* Lifileucel, a Tumor-Infiltrating Lymphocyte Therapy, in Metastatic Melanoma. *Journal of Clinical Oncology* **39**, 2656-2666, doi:10.1200/jco.21.00612 (2021).
46 Bai, R., Lv, Z., Xu, D. & Cui, J. Predictive biomarkers for cancer immunotherapy with immune checkpoint inhibitors. *Biomarker Research* **8**, doi:10.1186/s40364-020-00209-0 (2020).
47 Havel, J. J., Chowell, D. & Chan, T. A. The evolving landscape of biomarkers for checkpoint inhibitor immunotherapy. *Nat Rev Cancer* **19**, 133-150, doi:10.1038/s41568-019-0116-x (2019).
48 Jacquelot, N. *et al.* Predictors of responses to immune checkpoint blockade in advanced melanoma. *Nature Communications* **8**, doi:10.1038/s41467-017-00608-2 (2017).
49 Ott, P. A. & Wu, C. J. Cancer Vaccines: Steering T Cells Down the Right Path to Eradicate Tumors. *Cancer Discov* **9**, 476-481, doi:10.1158/2159-8290.CD-18-1357 (2019).
50 Saxena, M., Van Der Burg, S. H., Melief, C. J. M. & Bhardwaj, N. Therapeutic cancer vaccines. *Nature Reviews Cancer* **21**, 360-378, doi:10.1038/s41568-021-00346-0 (2021).
51 Hollingsworth, R. E. & Jansen, K. Turning the corner on therapeutic cancer vaccines. *NPJ Vaccines* **4**, 7, doi:10.1038/s41541-019-0103-y (2019).
52 Garcia-Garijo, A., Fajardo, C. A. & Gros, A. Determinants for Neoantigen Identification. *Frontiers in Immunology* **10**, doi:10.3389/fimmu.2019.01392 (2019).
53 Blass, E. & Ott, P. A. Advances in the development of personalized neoantigen-based therapeutic cancer vaccines. *Nature Reviews Clinical Oncology* **18**, 215-229, doi:10.1038/s41571-020-00460-2 (2021).

54 Sahin, U. & Türeci, Ö. Personalized vaccines for cancer immunotherapy. *Science* **359**, 1355-1360, doi:10.1126/science.aar7112 (2018).
55 Zhang, Z. *et al.* Neoantigen: A New Breakthrough in Tumor Immunotherapy. *Frontiers in Immunology* **12**, doi:10.3389/fimmu.2021.672356 (2021).
56 Bezu, L. *et al.* Trial watch: Peptide-based vaccines in anticancer therapy. *OncoImmunology* **7**, e1511506, doi:10.1080/2162402x.2018.1511506 (2018).
57 Ott, P. A. *et al.* An immunogenic personal neoantigen vaccine for patients with melanoma. *Nature* **547**, 217-221 (2017).
58 Sahin, U. *et al.* Personalized RNA mutanome vaccines mobilize poly-specific therapeutic immunity against cancer. *Nature* **547**, 222-226 (2017).
59 Hilf, N. *et al.* Actively personalized vaccination trial for newly diagnosed glioblastoma. *Nature* **565**, 240-245 (2019).
60 Vermeulen, L. M. P., De Smedt, S. C., Remaut, K. & Braeckmans, K. The proton sponge hypothesis: Fable or fact? *European Journal of Pharmaceutics and Biopharmaceutics* **129**, 184-190, doi:10.1016/j.ejpb.2018.05.034 (2018).
61 Jackson, M. A. *et al.* Zwitterionic Nanocarrier Surface Chemistry Improves siRNA Tumor Delivery and Silencing Activity Relative to Polyethylene Glycol. *ACS Nano* **11**, 5680-5696, doi:10.1021/acsnano.7b01110 (2017).
62 Jackson, M. A. *et al.* Dual carrier-cargo hydrophobization and charge ratio optimization improve the systemic circulation and safety of zwitterionic nano-polyplexes. *Biomaterials* **192**, 245-259, doi:10.1016/j.biomaterials.2018.11.010 (2019).
63 Werfel, T. A. *et al.* Combinatorial optimization of PEG architecture and hydrophobic content improves ternary siRNA polyplex stability, pharmacokinetics, and potency in vivo. *Journal of Controlled Release* **255**, 12-26, doi:10.1016/j.jconrel.2017.03.389 (2017).
64 Wilson, J. T. *et al.* pH-Responsive Nanoparticle Vaccines for Dual-Delivery of Antigens and Immunostimulatory Oligonucleotides. *ACS Nano* **7**, 3912-3925, doi:10.1021/nn305466z (2013).
65 Lynn, G. M. *et al.* Peptide-TLR-7/8a conjugate vaccines chemically programmed for nanoparticle self-assembly enhance CD8 T-cell immunity to tumor antigens. *Nat Biotechnol* **38**, 320-332, doi:10.1038/s41587-019-0390-x (2020).
66 Thomas, S. N. & Schudel, A. Overcoming transport barriers for interstitial-, lymphatic-, and lymph node-targeted drug delivery. *Curr Opin Chem Eng* **7**, 65-74, doi:10.1016/j.coche.2014.11.003 (2015).
67 Liu, H. *et al.* Structure-based programming of lymph-node targeting in molecular vaccines. *Nature* **507**, 519-522, doi:10.1038/nature12978 (2014).
68 Reddy, S. T., Rehor, A., Schmoekel, H. G., Hubbell, J. A. & Swartz, M. A. In vivo targeting of dendritic cells in lymph nodes with poly(propylene sulfide) nanoparticles. *Journal of Controlled Release* **112**, 26-34, doi:10.1016/j.jconrel.2006.01.006 (2006).
69 Shae, D. *et al.* Co-delivery of Peptide Neoantigens and Stimulator of Interferon Genes Agonists Enhances Response to Cancer Vaccines. *ACS Nano* **14**, 9904-9916, doi:10.1021/acsnano.0c02765 (2020).
70 Knight, F. C. *et al.* Mucosal Immunization with a pH-Responsive Nanoparticle Vaccine Induces Protective CD8(+) Lung-Resident Memory T Cells. *ACS Nano* **13**, 10939-10960, doi:10.1021/acsnano.9b00326 (2019).

71 Koerner, J. *et al.* PLGA-particle vaccine carrying TLR3/RIG-I ligand Riboxxim synergizes with immune checkpoint blockade for effective anti-cancer immunotherapy. *Nature Communications* **12**, doi:10.1038/s41467-021-23244-3 (2021).
72 Peeler, D. J., Yen, A., Luera, N., Stayton, P. S. & Pun, S. H. Lytic Polyplex Vaccines Enhance Antigen-Specific Cytotoxic T Cell Response through Induction of Local Cell Death. *Advanced Therapeutics* **4**, doi:10.1002/adtp.202100005 (2021).
73 Luo, M. *et al.* A STING-activating nanovaccine for cancer immunotherapy. *Nature Nanotechnology* **12**, 648-654, doi:10.1038/nnano.2017.52 (2017).
74 Liu, Q. *et al.* pH-Responsive Poly(d,l-lactic-co-glycolic acid) Nanoparticles with Rapid Antigen Release Behavior Promote Immune Response. *ACS Nano* **9**, 4925-4938, doi:10.1021/nn5066793 (2015).
75 Vanpouille-Box, C., Hoffmann, J. A. & Galluzzi, L. Pharmacological modulation of nucleic acid sensors - therapeutic potential and persisting obstacles. *Nat Rev Drug Discov* **18**, 845-867, doi:10.1038/s41573-019-0043-2 (2019).
76 van den Boorn, J. G., Barchet, W. & Hartmann, G. Nucleic acid adjuvants: toward an educated vaccine. *Adv Immunol* **114**, 1-32, doi:10.1016/B978-0-12-396548-6.00001-9 (2012).
77 Iurescia, S., Fioretti, D. & Rinaldi, M. Targeting Cytosolic Nucleic Acid-Sensing Pathways for Cancer Immunotherapies. *Front Immunol* **9**, 711, doi:10.3389/fimmu.2018.00711 (2018).
78 McWhirter, S. M. & Jefferies, C. A. Nucleic Acid Sensors as Therapeutic Targets for Human Disease. *Immunity* **53**, 78-97, doi:10.1016/j.immuni.2020.04.004 (2020).
79 Dubensky, T. W., Jr. & Reed, S. G. Adjuvants for cancer vaccines. *Semin Immunol* **22**, 155-161, doi:10.1016/j.smim.2010.04.007 (2010).
80 Junt, T. & Barchet, W. Translating nucleic acid-sensing pathways into therapies. *Nat Rev Immunol* **15**, 529-544, doi:10.1038/nri3875 (2015).
81 Zitvogel, L., Galluzzi, L., Kepp, O., Smyth, M. J. & Kroemer, G. Type I interferons in anticancer immunity. *Nature Reviews Immunology* **15**, 405-414, doi:10.1038/nri3845 (2015).
82 Pack, D. W., Hoffman, A. S., Pun, S. & Stayton, P. S. Design and development of polymers for gene delivery. *Nature Reviews Drug Discovery* **4**, 581-593, doi:10.1038/nrd1775 (2005).
83 Afonin, K. A., Dobrovolskaia, M. A., Church, G. & Bathe, M. Opportunities, Barriers, and a Strategy for Overcoming Translational Challenges to Therapeutic Nucleic Acid Nanotechnology. *ACS Nano* **14**, 9221-9227, doi:10.1021/acsnano.0c04753 (2020).
84 Ammi, R. *et al.* Poly(I:C) as cancer vaccine adjuvant: knocking on the door of medical breakthroughs. *Pharmacol Ther* **146**, 120-131, doi:10.1016/j.pharmthera.2014.09.010 (2015).
85 Palchetti, S. *et al.* Transfected poly(I:C) activates different dsRNA receptors, leading to apoptosis or immunoadjuvant response in androgen-independent prostate cancer cells. *J Biol Chem* **290**, 5470-5483, doi:10.1074/jbc.M114.601625 (2015).
86 Wang, Y., Cella, M., Gilfillan, S. & Colonna, M. Cutting edge: polyinosinic:polycytidylic acid boosts the generation of memory CD8 T cells through melanoma differentiation-associated protein 5 expressed in stromal cells. *J Immunol* **184**, 2751-2755, doi:10.4049/jimmunol.0903201 (2010).

87 Sultan, H., Salazar, A. M. & Celis, E. Poly-ICLC, a multi-functional immune modulator for treating cancer. *Seminars in Immunology* **49**, 101414, doi:10.1016/j.smim.2020.101414 (2020).
88 Tormo, D. *et al.* Targeted Activation of Innate Immunity for Therapeutic Induction of Autophagy and Apoptosis in Melanoma Cells. *Cancer Cell* **16**, 103-114, doi:10.1016/j.ccr.2009.07.004 (2009).
89 Mehrotra, S. *et al.* Vaccination with poly(IC:LC) and peptide-pulsed autologous dendritic cells in patients with pancreatic cancer. *J Hematol Oncol* **10**, 82, doi:10.1186/s13045-017-0459-2 (2017).
90 Pollack, I. F. *et al.* Immune responses and outcome after vaccination with glioma-associated antigen peptides and poly-ICLC in a pilot study for pediatric recurrent low-grade gliomas. *Neuro Oncol* **18**, 1157-1168, doi:10.1093/neuonc/now026 (2016).
91 Najafabadi, A. H. *et al.* Vaccine nanodiscs plus polyICLC elicit robust CD8+ T cell responses in mice and non-human primates. *J Control Release* **337**, 168-178, doi:10.1016/j.jconrel.2021.07.026 (2021).
92 Ott, P. A. *et al.* An immunogenic personal neoantigen vaccine for patients with melanoma. *Nature* **547**, 217-221, doi:10.1038/nature22991 (2017).
93 Hu, Z. *et al.* Personal neoantigen vaccines induce persistent memory T cell responses and epitope spreading in patients with melanoma. *Nature Medicine* **27**, 515-525, doi:10.1038/s41591-020-01206-4 (2021).
94 Sultan, H., Wu, J., Kumai, T., Salazar, A. M. & Celis, E. Role of MDA5 and interferon-I in dendritic cells for T cell expansion by anti-tumor peptide vaccines in mice. *Cancer Immunol Immunother* **67**, 1091-1103, doi:10.1007/s00262-018-2164-6 (2018).
95 Gale, E. C. *et al.* A Nanoparticle Platform for Improved Potency, Stability, and Adjuvanticity of Poly(I:C). *Advanced Therapeutics* **3**, doi:10.1002/adtp.201900174 (2019).
96 Hammerich, L. *et al.* Systemic clinical tumor regressions and potentiation of PD1 blockade with in situ vaccination. *Nat Med* **25**, 814-824, doi:10.1038/s41591-019-0410-x (2019).
97 Pollack, I. F. *et al.* Antigen-specific immunoreactivity and clinical outcome following vaccination with glioma-associated antigen peptides in children with recurrent high-grade gliomas: results of a pilot study. *J Neurooncol* **130**, 517-527, doi:10.1007/s11060-016-2245-3 (2016).
98 Da Silva, C. G. *et al.* Co-delivery of immunomodulators in biodegradable nanoparticles improves therapeutic efficacy of cancer vaccines. *Biomaterials* **220**, 119417, doi:10.1016/j.biomaterials.2019.119417 (2019).
99 Kapadia, C. H., Tian, S., Perry, J. L., Luft, J. C. & DeSimone, J. M. Reduction Sensitive PEG Hydrogels for Codelivery of Antigen and Adjuvant To Induce Potent CTLs. *Mol Pharm* **13**, 3381-3394, doi:10.1021/acs.molpharmaceut.6b00288 (2016).
100 Kuai, R. *et al.* Dual TLR agonist nanodiscs as a strong adjuvant system for vaccines and immunotherapy. *Journal of Controlled Release* **282**, 131-139, doi:10.1016/j.jconrel.2018.04.041 (2018).
101 Tom, J. K. *et al.* Modulation of Innate Immune Responses via Covalently Linked TLR Agonists. *ACS Central Science* **1**, 439-448, doi:10.1021/acscentsci.5b00274 (2015).
102 Irvine, D. J., Swartz, M. A. & Szeto, G. L. Engineering synthetic vaccines using cues from natural immunity. *Nature Materials* **12**, 978-990, doi:10.1038/nmat3775 (2013).

103 Audiger, C., Rahman, M. J., Yun, T. J., Tarbell, K. V. & Lesage, S. The Importance of Dendritic Cells in Maintaining Immune Tolerance. *J Immunol* **198**, 2223-2231, doi:10.4049/jimmunol.1601629 (2017).

104 Jacobson, M. E. *et al.* Structural Optimization of Polymeric Carriers to Enhance the Immunostimulatory Activity of Molecularly Defined RIG-I Agonists. *ACS Cent Sci* **6**, 2008-2022, doi:10.1021/acscentsci.0c00568 (2020).

105 Nelson, C. E. *et al.* Balancing Cationic and Hydrophobic Content of PEGylated siRNA Polyplexes Enhances Endosome Escape, Stability, Blood Circulation Time, and Bioactivity in Vivo. *ACS Nano* **7**, 8870-8880, doi:10.1021/nn403325f (2013).

106 Evans, B. C. *et al.* Ex vivo red blood cell hemolysis assay for the evaluation of pH-responsive endosomolytic agents for cytosolic delivery of biomacromolecular drugs. *J Vis Exp*, e50166, doi:10.3791/50166 (2013).

107 Kilchrist, K. V. *et al.* Gal8 Visualization of Endosome Disruption Predicts Carrier-Mediated Biologic Drug Intracellular Bioavailability. *ACS Nano* **13**, 1136-1152, doi:10.1021/acsnano.8b05482 (2019).

108 Munson, M. J. *et al.* A high-throughput Galectin-9 imaging assay for quantifying nanoparticle uptake, endosomal escape and functional RNA delivery. *Communications Biology* **4**, doi:10.1038/s42003-021-01728-8 (2021).

109 Jacobson, M. E., Wang-Bishop, L., Becker, K. W. & Wilson, J. T. Delivery of 5'-triphosphate RNA with endosomolytic nanoparticles potently activates RIG-I to improve cancer immunotherapy. *Biomater Sci* **7**, 547-559, doi:10.1039/c8bm01064a (2019).

110 Garland, K. M. *et al.* Pharmacological Activation of cGAS for Cancer Immunotherapy. *Front Immunol* **12**, 753472, doi:10.3389/fimmu.2021.753472 (2021).

111 Hervas-Stubbs, S. *et al.* Direct Effects of Type I Interferons on Cells of the Immune System. *Clinical Cancer Research* **17**, 2619-2627, doi:10.1158/1078-0432.ccr-10-1114 (2011).

112 Caskey, M. *et al.* Synthetic double-stranded RNA induces innate immune responses similar to a live viral vaccine in humans. *Journal of Experimental Medicine* **208**, 2357-2366, doi:10.1084/jem.20111171 (2011).

113 Moser, B. A. *et al.* Increased vaccine tolerability and protection via NF-κB modulation. *Science Advances* **6**, eaaz8700, doi:10.1126/sciadv.aaz8700 (2020).

114 Christian, L. M., Porter, K., Karlsson, E. & Schultz-Cherry, S. Proinflammatory cytokine responses correspond with subjective side effects after influenza virus vaccination. *Vaccine* **33**, 3360-3366, doi:10.1016/j.vaccine.2015.05.008 (2015).

115 Schlich, M. *et al.* Cytosolic delivery of nucleic acids: The case of ionizable lipid nanoparticles. *Bioengineering & Translational Medicine* **6**, doi:10.1002/btm2.10213 (2021).

116 Smith, S. A., Selby, L. I., Johnston, A. P. R. & Such, G. K. The Endosomal Escape of Nanoparticles: Toward More Efficient Cellular Delivery. *Bioconjugate Chemistry* **30**, 263-272, doi:10.1021/acs.bioconjchem.8b00732 (2019).

117 Sultan, H., Salazar, A. M. & Celis, E. Poly-ICLC, a multi-functional immune modulator for treating cancer. *Semin Immunol* **49**, 101414, doi:10.1016/j.smim.2020.101414 (2020).

118 Sharma, J., Carson, C. S., Douglas, T., Wilson, J. T. & Joyce, S. in *Vaccine Design: Methods and Protocols, Volume 3. Resources for Vaccine Development* (ed Sunil Thomas) 367-398 (Springer US, 2022).

119 McLennan, D. N., Porter, C. J. H. & Charman, S. A. Subcutaneous drug delivery and the role of the lymphatics. *Drug Discovery Today: Technologies* **2**, 89-96, doi:10.1016/j.ddtec.2005.05.006 (2005).
120 Kreiter, S. *et al.* Mutant MHC class II epitopes drive therapeutic immune responses to cancer. *Nature* **520**, 692-696, doi:10.1038/nature14426 (2015).
121 Alspach, E. *et al.* MHC-II neoantigens shape tumour immunity and response to immunotherapy. *Nature* **574**, 696-701, doi:10.1038/s41586-019-1671-8 (2019).
122 Qiu, F. *et al.* Poly(propylacrylic acid)-peptide nanoplexes as a platform for enhancing the immunogenicity of neoantigen cancer vaccines. *Biomaterials* **182**, 82-91, doi:10.1016/j.biomaterials.2018.07.052 (2018).
123 Mehta, N. K. *et al.* Pharmacokinetic tuning of protein–antigen fusions enhances the immunogenicity of T-cell vaccines. *Nature Biomedical Engineering* **4**, 636-648, doi:10.1038/s41551-020-0563-4 (2020).
124 Kumar, A. *et al.* Heterotypic immunity against vaccinia virus in an HLA-B*07:02 transgenic mousepox infection model. *Scientific Reports* **10**, doi:10.1038/s41598-020-69897-w (2020).
125 Scheetz, L. *et al.* Engineering patient-specific cancer immunotherapies. *Nature Biomedical Engineering* **3**, 768-782, doi:10.1038/s41551-019-0436-x (2019).
126 Moynihan, K. D. *et al.* Eradication of large established tumors in mice by combination immunotherapy that engages innate and adaptive immune responses. *Nature Medicine* **22**, 1402-1410, doi:10.1038/nm.4200 (2016).
127 Binnewies, M. *et al.* Understanding the tumor immune microenvironment (TIME) for effective therapy. *Nature Medicine* **24**, 541-550, doi:10.1038/s41591-018-0014-x (2018).
128 Gilchuk, P. *et al.* Discovering naturally processed antigenic determinants that confer protective T cell immunity. *J Clin Invest* **123**, 1976-1987, doi:10.1172/JCI67388 (2013).
129 Mehta, N. K., Moynihan, K. D. & Irvine, D. J. Engineering New Approaches to Cancer Vaccines. *Cancer Immunol Res* **3**, 836-843, doi:10.1158/2326-6066.CIR-15-0112 (2015).
130 Bookstaver, M. L., Tsai, S. J., Bromberg, J. S. & Jewell, C. M. Improving Vaccine and Immunotherapy Design Using Biomaterials. *Trends Immunol* **39**, 135-150, doi:10.1016/j.it.2017.10.002 (2018).